UNIVERSITY OF CALIFORNIA, SAN DIEGO
SAN DIEGO STATE UNIVERSITY

Structure and Biochemistry of IKappaB Zeta: A Nuclear IKappaB Protein

A dissertation submitted in partial satisfaction of the requirements for the degree

Doctor of Philosophy

in

Chemistry

by

Norman L. Zhu

Committee in charge:

San Diego State University

Professor Tom Huxford, Chair
Professor John J. Love
Professor Roland Wolkowicz

University of California, San Diego

Professor Nathan C. Gianneschi
Professor Alexander Hoffmann
Professor Katherine A. Jones
Professor Hector Viadiu-Ilarraza

2013

The dissertation of Norman L. Zhu is approved, and it is acceptable in quality and form for publication on microfilm and electronically:

_____

_____

_____

_____

_____

_____

_____

Chair

University of California, San Diego

San Diego State University

2013

Dedication

I dedicate this dissertation to the following people:

My Lord, Jesus Christ, who supported me in more ways than I can put into words.

My parents, Mingde and Alice Zhu who always believed in me and would have given me the shirts off their backs had I asked for it.

And to all the people from the lab, especially Hux. Thanks for making the last six years seem not long enough.

Table of Contents

List of Abbreviations

ALS	Advance Light Source
AR	Ankyrin repeat
BSA	Bovine serum albumin
BDNF	Brain-derived neurotrophic factor
βME	β-Mercaptoethanol
CamK II	Ca2+/calmodulin-dependent protein kinases II
CD	Circular dichroism
CD28RE	CD28 response element
CRE	cAMP responsive element
CTD	C-terminus domain
CV	Column volume
DD	Dimerization domain
DOC	Desoxycholate
DTT	Dithiothreito
EDTA	Ethylenediaminetetraacetic acid
EGF	Epidermal growth factor
EMSA	Electrophoretic Mobility Shift Assay
GST	Glutathione S-transferase
GTF	General transcription factor
HAT	Histone acetyl transferase

HDAC	Histone deacetylase
IκB	Inhibitor of NF-κB
IKK	IκB kinase complex
IPTG	Isopropylthio-β-D-galactoside
IRE	Interferon response element
LPS	Lipopolysaccharide
MAPK	Mitogen-activated protein kinases
MHC	Major histocompatibility complex
MNK	MAPK-interacting kinase
MPD	2-methyl-2,4-pentanediol
MR	Molecular replacement
NGAL	Neutrophil gelatinase-associated lipocalin
NF-κB	Nuclear factor -κB
NSLS	National Synchrotron Light Source
NLS	Nuclear localization sequence
NTD	N-terminus domain
PAGE	Polyacrylamide gel electrophoresis
PCR	Polymerase chain reaction
PEG	Polyethylene glycol
PIC	Pre-initiation complex
PKAc	Cyclic AMP-dependent protein kinase
PMSF	Phenylmethylsulfonylfluoride

RHR	Rel homology region
RMSD	Root-mean-squared deviation
SDS	Sodium dodecyl sulfate
SPR	Surface plasmon resonance
STAT	Signal transducer and activator of transcription
TAD	Transactivation domain
TBP	TATA box polypeptide
TF	Transcription factor
TNF-α	Tumor necrosis factor alpha

List of Figures

List of Tables

Acknowledgements

Looking back at the last six years that led me to this point of my career I can't help but to feel blessed. I am blessed by the educational system I am privileged to be a part of and by the people I came to know. The SDSU-UCSD Joint Doctoral Program granted me access to a full array of biochemical instruments available at SDSU while allowing me access to the resources of a large research institution of UCSD. Through the program I had the pleasure to study under Dr. Tom Huxford who mentored me every step of the way. I can honestly say that everything I know about crystallography, protein purification, and just about everything research related I learned from him. There is not a single day that goes by that I am not amazed by his wealth of knowledge he commands while remain grounded and approachable. It is his easygoing demeanor and friendly way of interacting with others that lend to the welcoming environment that our lab is best known for. I know the uniqueness of this place won't be fully appreciated until I look back on it one day through the lense of nostalgia.

Then there are my parents who were never too far away. I know whether is in financial, emotional, or even scientific support they are just a phone call away. It is that sense of security that allowed me to focus wholeheartedly on the research without any distractions. My father also helped me directly with my research by providing the access and technical support to a SPR instrument through his company, BioRad

Laboratories. The data we obtained from that instrument contributed a great deal to the completion of this dissertation.

The next few people I want to acknowledge on this amazing journey are my two PhD compadres Art and James, the two people who went the whole way with me. I am indebted to Art for always being willing to join me on any crazy adventures we came up with. Whether was riding to Oregon on our bicycles or singing "Brown Eyed Girl" at a karaoke bar, he was always been there right next to me. To James—the one guy I have met in the whole world who never seems to have had a bad day—thanks for making the last few years such a blast and for your assistance in helping me format this dissertation.

I also want to thank Dr. Gourisankar Ghosh for his invaluable insights and laying the foundation for much of my own work. I thank Dr. David Heidary for his work on CD experiments. Those results proved pivotal in our understanding of the capping helix and its role on IκBζ stability. I want to thank a small army of undergraduate research assistants that have worked with me over the years, especially Kyle Grant for the DNA purification he did which was used in the crystallization process and Madison for setting up crystallization trays in her unique way which led to the p50:IκBζ complex co-crystal. And to everyone else from the lab, previous and current: you guys rock.

And finally, I thank God who made all this possible. Amen.

Vita

2002	B.S., University of California, San Diego
2013	Ph.D., University of California, San Diego San Diego State University

Publications

Wojciak JM, Zhu N, Schuerenberg KT, Moreno K, Shestowsky WS, Hiraiwa M, Sabbadini R, Huxford T. (2009). The crystal structure of sphingosine-1-phosphate in complex with a Fab fragment reveals metal bridging of an antibody and its antigen. *Proc Natl Acad Sci U S A.* 106(42):17717-22.

Trinh DV, Zhu N, Farhang G, Kim BJ, Huxford T. (2008). The nuclear I kappaB protein I kappaB zeta specifically binds NF-kappaB p50 homodimers and forms a ternary complex on kappaB DNA. *J Mol Biol.* 379(1):122-35.

ABSTRACT OF THE DISSERTATION

Structure and Biochemistry of IkappaB Zeta: A Nuclear IkappaB Protein

by

Norman L. Zhu

Doctor of Philosophy in Chemistry

University of California, San Diego, 2013
San Diego State University, 2013

Professor Tom Huxford, Chair

The NF-κB pathway is one of the hallmark signal transduction pathways associated with inflammation, innate and adaptive immunity, and regulation of apoptosis. Ever since its discovery in 1986, a plethora of studies have led us to a solid understanding of its function and regulation. One group of proteins that are at the center of its regulation is the IκB family of transcriptional inhibitory proteins. Of the nine gene products classified as functioning IκB proteins, five reside mainly in the cytosol, four localize in the nucleus. These nuclear IκB proteins associate with the NF-κB inside the nucleus and exert additional regulation over the gene expression profile of NF-κB. This current study is focused on the nuclear IκBζ protein. IκBζ is

an NF-κB-dependent transiently expressed protein that has been linked to the regulation of Csf2, Lcn2, IL-12, IL-18, IL-6, and NGAL genes. In the cases of IL-6 and NGAL, the presence of IκBζ proved to be indispensable. Mechanistically, IκBζ preferentially binds to NF-κB p50 homo-dimers. This preference is directly contrary to the classical cytoplasmic IκB proteins that favors p65/RelA subunit. In this study, using X-ray crystallography accompanied by *in vitro* biochemical assays, we have gained insights into the structure/function relationships of IκBζand p50. The 2.0 Å crystal structure of IκBζ in complex with the dimerization domains of the NF-κB p50 homo-dimer reveals that it adopts a structure and binding interactions that is similar to that of the classical IκBα and IκBβ complexes with p65-containing NF-κB dimers. However, the IκBζ ankyrin repeats domain contains an amino-terminal helix that caps the top of the ankyrin repeat stack. Circular dichroism (CD) and surface plasmon resonance (SPR) analysis indicate that this capping helix has a stabilizing effect on the folding of the rest of the AR structure. Without it, IκBζ adopts a disordered conformation, which disrupts its ability to bind to p50. The crystal structure also revealed IκBζ contains elongated ankyrin repeat 4 that is unique among the IκBproteins. It is not clear whether or not this plays any role in specific functions of IκBζ. A close examination of the protein-protein interface showed a cluster of salt bridge contacts focused at the nuclear localization sequence (NLS) region of the p50. GST-pull down and SPR experiments revealed that the removal NLS knocked out the interaction entirely. A closer examination of the region with site directed mutagenesis demonstrated a binding "hot spot" composed of Arg359, Lys360, and Arg361.

Simultaneous mutations of these residues to alanine resulted in complete loss of interaction. Furthermore, we established that NLS region contributes majority of protein-protein recognition between the two proteins, so much so that the transfer of the p50 NLS region to p65 is sufficient to cause p65:IκBζ interaction. In a separate but related project we also solved two structures of p50 homo-dimer bound to IL-6 and NGAL promoters. This allowed us to model IκBζ onto the p50:DNA structure and give us a theoretical ternary complex structure. In the model the carboxy-terminus of IκBζ can be seen to collide with the DNA backbone of the promoter. The consequence of this would be collision was examined with SPR and EMSA. Both techniques detected the formation of stable ternary complex on DNA promoters. The result also showed the binding of IκBζ on p50 does not alter its rate of dissociation by any detectable amount. From these finding we conclude that the stable ankyrin repeat domain of IκBζ interacts specifically with p50:DNA complexes in the nucleus through a relatively focused portion of the overall interface. This suggests that small molecule that inhibitors this interaction could be developed as potential therapeutics.

Chapter I

Introduction

1. Overview of Signal Transduction

Every living organism requires an ability to sense and respond to its environment in an appropriate way in order to improve its chances of survival in a constantly changing world. At the cellular level, varied responses to diverse environmental stimuli often involve fundamental processes such as metabolic modifications, cell cycle alterations, and/or immune reactions that are governed by a particular cell's gene expression profile. Thus it is critical for organisms to correctly relay information from the cell surface into the interior of the cell and, ultimately, into the nucleus where the information encoding all potential cellular responses is stored. To accomplish this cells utilize a sophisticated network of signal transduction pathways made up of a diverse array of signaling molecules. These molecules act on one another in a hierarchical manner, perpetuating the initial signal down a complicated branching network of paths that can lead to various effects. One of the typical outcomes of diverse signaling pathways is the recruitment and activation of transcription factors. Members of this superfamily of signal transduction effector molecules bind to DNA regulatory elements in the nucleus and alter the expression of target genes. Thus, it is through the signal transduction pathways and the subsequent activity of transcription factors that organisms enlist the appropriate cellular responses to diverse environmental stimuli.

2. The Different Roles of Transcription Factors

Transcription factors can be separated into two main classifications: The general transcription factors and the specific transcription factors. The general transcription factors are highly conserved and used by virtually by all organisms to transcribe most every gene. General transcription factors that recruit and facilitate RNA Polymerase II, for example, include the TATA binding protein (TBP), transcription factor (TF) II-A, -B, -D, E, -F and -H as well as TBP associated factors (TAFs) (Roeder, 1996). Together these macromolecules assemble into the pre-initiation complex (PIC) at the initiation site within a gene prior to transcription. The basic role and mechanism of these factors are shared from yeast to human, hence the term general transcription factors.

Specific transcription factors, on the other hand, are much more specialized and particular in the roles they play. Rather than taking part in the initiation of every gene, they alter basal gene expression levels of one or a small subset of genes. Their role can be that of a suppressor or activator accomplished by binding to the proximal or distal gene promoter elements in the DNA. By either residing within the cell in a dormant state or awaiting new synthesis, these transcription factors can be induced or activated in response to specific signals. That signal can be initiated by extracellular stimuli or come from within the cell. An example of extracellular stimulus activation can be seen in the case of cAMP response element-binding protein (CREB). A mitogen such as epidermal growth factor (EGF) binds to the EGF receptor (EGFR) on the cell surface. This causes Ras, a small GTPase, to swap its bound GDP nucleotide

for GTP. In its GTP-bound state, Ras can switch on RAF kinase (Avruch et al., 2001). RAF, in turn, phosphorylates MEK1 and MEK2 which activate Mitogen-activated protein kinases (MAPKs). Of the many signaling molecules downstream of MAPK one of them is MAPK-interacting kinase (MNK). Upon phosphorylation by MAPK, MNK enters the nucleus and interacts with transcription factor, cAMP response element-binding protein (CREB). CREB contains a leucine zipper motif is able to bind to the cAMP responsive element (CRE) and regulates downstream genes such as c-fos, the neurotrophin brain-derived neurotrophic factor (BDNF), tyrosine hydroxylase, and many neuropeptides such as somatostatin, enkephalin, VGF, and corticotropin-releasing hormone (Purves, 2008).

For an example of intercellular activation, one can be seen in the case of Ca^{2+}/calmodulin-dependent protein kinases II (CamK II). CamK II is dormant in its unphosphorylated form and resides in the cytosol of a resting cell. Upon the elevated concentrations of Ca^{2+} and calmodulin, CamK II forms a complex with both of them and auto-phosphorylates itself on Threonine-286 (Yamauchi, 2005). This activates CamK II and causes it phosphorylation of a broad number of downstream substrate proteins. One of these is a transcription factor c/EBPβ (Braun and Schulman, 1995), which regulates the expression of such cytokines as IL-6 (Natsuka et al., 1992), IL-4 (Davydov et al., 1995), IL-5 (van Dijk et al., 1999), and TNF-α (Greenwel et al., 2000). Several other well known inducible transcription factors include: p300 in G-protein signaling (Goodman and Smolik, 2000), Signal Transducer and Activator of

Transcription (STAT) in interferon stimulated gene regulation (Yan et al., 1995), and the immune response modulator NF-κB (Gilmore, 2006).

3. The NF-κB family

3.1 The Discovery of NF-κB

NF-κB was first discovered by Dr. David Baltimore's group in the mid-1980s as they searched for factors that are involved in the B cell maturation cycle. NF-κB was identified as a nuclear factor bound to the enhancer region of immunoglobulin kappa light chain in B lymphocytes (Sen and Baltimore, 1986a). The sequence it recognizes is a decameric double-stranded DNA, 5'-GGGACTTTCC-3', located within an intronic enhancer element of the kappa light chain gene. Binding of NF-κB to this site was confirmed to be essential for the activation of kappa light chain gene expression in B cells (Kawakami et al., 1988). Subsequent experiments with translation inhibitors showed that induction of NF-κB transcriptional activity does not require *de novo* protein synthesis and that an inactive version of the factor is present in cytoplasm of resting cells (Sen and Baltimore, 1986b). Ultra-centrifugation of the cell lysate showed that in uninduced cells virtually all NF-κB DNA binding activity was localized to the cytosolic fraction. Upon induction through treatment of cells with bacterial LPS or phorbol esters, NF-κB could be detected inside of the nucleus at the expense of the cytosolic fraction. The NF-κB found outside of the nucleus in resting cells fails to bind target DNA. However, this could be remedied *in vitro* by the treatment of mild dissociation agents, such as formamide or sodium dexycholate

(Baeuerle and Baltimore, 1988a). Taken together, these early experiments revealed NF-κB as an inducible sequence specific DNA binding activity that resides in the cytosol in dormant form through noncovalent associate with an inhibitor. Upon induction a dissociation reaction takes place, which releases NF-κB from its inhibitor. This allows both its translocation into the nucleus and its ability to bind with high affinity and specificity to its target DNA (Baeuerle, 1991).

This model for induction of NF-κB activity has stood the test of time and is consistent with what has been observed in many other cell types as well. However, what early researchers could not have predicted was the farreaching ramifications of this inducible transcription factor and its simple mechanism of activation. Though it was initially thought to be only present in B lymphocytes, NF-κB has since been shown to be present in practically all cell types where regulates such diverse physiological functions as immunological and inflammatory responses, developmental processes, cellular growth, and important modulating effects on apoptosis. In addition, NF-κB is activated in number of diseases, including cancer, arthritis, acute and chronic inflammatory states, asthma, as well as neurodegenerative and heart diseases. Because of its involvement in so many cellular functions, NF-κB has found itself at the center of numerous investigations. To date, there have been over 4,700 articles written on its regulatory pathway alone. After twenty-seven years of investigation, the NF-κB signaling pathway is firmly established as one of the main hubs of inducible gene regulation.

3.2 Members of the NF-κB Family

For its initial discovery, NF-κB was purified using affinity column with kappa gene enhancer target DNA covalently attached. The factor purified was found to contain two distinct subunits. One exhibited a approximate molecular mass of 65 kDa and the other 50 kDa, hence the names p65 and p50, respectively (Baeuerle and Baltimore, 1989). Subsequent cloning of gene encoding the p50 subunit revealed that the protein is first expressed as a much large construct, composed of 968 amino acids that is referred to as p105. This precursor protein was found to possess a large amino-terminal region that resembled the *rel* oncogene and the *dorsal* morphogen from *Drosophila.* Its carboxyl-terminal was found to share sequence homology with the oncogene BCL-3 and other ankyrin repeat-containing proteins (Bours et al., 1990). In contrast, the p65 was not found to encode a precursor and is expressed in its fully mature form. It also shares homology with p50 in its amino-terminal region (Schmitz and Baeuerle, 1991). The conserved region expands roughly 300 peptides and makes up roughly 75% of p50 and 50% of p65. This region is termed the Rel homology region (RHR) because of its sequence homology to the proto-oncogene c-Rel (Lee et al., 1991).

Using this as the standard, to date there are total of five RHR-containing genes identified to constitute the entire mammalian family of NF-κB. These five genes encode the following polypeptides: p50, p65 (also referred to as "RelA"), c-Rel, p52, and RelB (Figure I.1). The individual polypeptide subunits are capable of associating in different combinations to form functioning homo- and heterodimers in solution.

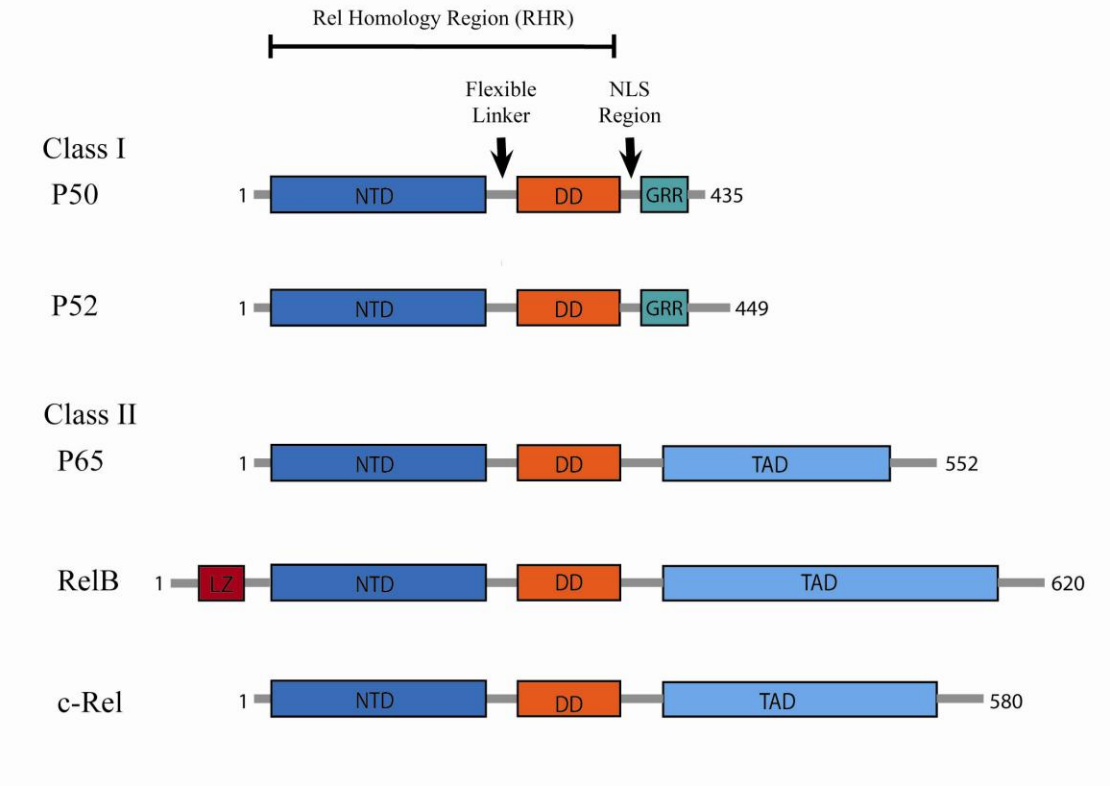

Figure I.1 Members of the NFkB family illustrated by their domains. The five members are separated into two classes based on the presence of the transactivation domain (TAD). Members of class I subunits, P50 and P52 without the TAD, are the proteolytic products of P105 and p100, respectively.

Through this combinatorial match pairing, different NF-κB dimers form an array of related but distinct transcription factors that collectively carry out the functions ascribed to NF-κB. Dimerization is mediated through the final 100 amino acids of the RHR. Interestingly, not all possible dimer combinations have been detected in nature (Ryseck et al., 1995). Dimerization is also required for members of the NF-κB family to bind target DNA and interact with members of inhibitors. Finally, the nuclear localization potential, in the form of a Type I nuclear localization signal (NLS) is also contained within the RHR at its extreme carboxy-terminus.

Beyond the RHR, three members of the NF-κB family, p65, c-Rel, and RelB, contain a potent transactivation domain (TAD) at their C-terminus. This sets them apart from p50 and p52, which are both produced by post-translational partial degradation of p105 and p100, respectively, and lack any potential to activate target gene transcription. The NF-κB family subunits can therefore be categorized into two classes with p50 and p52 being Class I and p65, c-Rel, and RelB as Class II. Homo- and heterodimers of Class I proteins have been shown to act as repressors of gene transcription (Franzoso et al., 1992a; Plaksin et al., 1993). This is not surprising as both p50 and p52 possess in their RHR all the features necessary for dimerization, nuclear localization, and sequence-specific DNA binding. By contrast, dimers with one or more Class II family members act as potent activators of transcription by virtue of their C-terminal TAD. Within class II, RelB sets itself further apart because it is the only member that contains a leucine zipper motif at its N-terminus. Moreover,

RelB does not easily form homodimers or or heterodimers with p65 or c-Rel (Ryseck et al., 1995)

3.3 Functions of NF-κB

The five members in the NF-κB family, each of which is capable forming dimers with itself or with another member of the family, can give rise to a variety of distinct functional complexes. Each dimer is capable of recognizing a distinct but overlapping set of genes and exert regulatory control unilaterally. Additional layers of regulation are introduced as they associate with other co-factors, either directly or in the context of an enhanceosome. In addition, post-translational modification, such as phosphorylation or acetylation, on the subunits have been linked to effect the function, stability, subcellular and sub-nuclear localization, DNA binding, and co-factor binding of NF-κB. In light of all this, NF-κB is viewed at the center of a complex regulatory system that controls and influences an incredibly broad range of genes.

The link between NF-κB and transcription regulation is its recruitment of co-factors to the pre-initiation complex (PIC). Under the classical model of eukaryotic transcription, activation of gene expression begins at the core promoter sequence (Kornberg, 2007). Recognition of the core promoter is thought to be the primary role of NF-κB. Recruitment of TATA box binding protein (TBP), TFIID, TFIIA, and RNA polymerase II, along with the other general transcription factors, TFIIB, TFIIE, TFIIF, and TFIIH completes the PIC and is sufficient for transcription to begin.

However, *in vivo*, additional modifications to the PIC are still needed after its assembly to sustain the activation. These modifications include chromatin alteration, release of paused Pol II, and that involvement of transcriptional elongation factors. While NF-κB is traditionally thought to be primary affiliated with the assembly of PIC, recent data have shown it to play a role post-PIC regulation as well (Barboric et al., 2001). The trouble with our current understanding of NF-κB is that it is difficult to distinguish pre-PIC regulation from post-PIC regulation. This is partially due to our poor understanding of co-regulator recruitment by the NF-κB dimers.

The few co-regulators that are known to be recruited by NF-κB to the promoter include PCAF, CBP, and p300, of the histone acetyl transferase (HAT) family, as well as HDAC1 and HDAC2 of the histone deacetylase (HDAC) family (Zhong et al., 2002a). The HAT proteins promote opening of the chromatin structure and allow PIC assembly and transcription while the HDACs reverse this effect. Each NF-κB subunit has its own distinct binding profile for HATs and HDACs and, therefore, different capacity for induction or repression. For example, in the case of the NF-κB p50 homodimer, its association with HDACs leads to the removal of acetyl groups from histones. This serves to keep genes repressed in resting cells (Zhong et al., 2002a). In the case of p65, phosphorylation of S276 by cyclic AMP-dependent protein kinase (PKAc) leads to its recruitment of p300/CBP resulting in activation of transcription (Zhong et al., 2002a; Zhong et al., 1998).

3.4 NF-κB DNA Recognition

Another level of gene regulation happens at the level of DNA recognition. In 1992, a study reported the first systematic screening of NF-κB binding to diverse double stranded DNA sequences (Kunsch et al., 1992a). The study identified DNA sequences with high affinity for binding to p50, c-Rel, or p65 homodimers from a random oligonucleotide pool. 18 sequences for each homodimer were reported and used to generate a consensus. For p50 the consensus is 5'-GGGGATYCCC-3' (Y=T or C). For p65 and c-Rel the consensus was similar: 5'-GGGRNTTTCC-3' (R=A or G) and 5'-NGGNNATTTCC-3', respectively. The distinct differences between the p50 consensus and that of p65 and c-Rel suggest they may preferentially bind and, consequently, regulate different types of genes. And yet these differences are small enough to allow p50 homodimer to compete with many of the p65 or c-Rel targeted genes. This model is consistent with the idea p50 homodimer can escape IκB inhibitor binding in the cytosol and migrate to the nucleus where it functions as a repressor for a subset of NF-κB genes in resting cells by its recruitment of HDACs to the promoter. Upon induction, p50 is replaced by other NF-κB dimers that activate transcription (Zhong et al., 2002a). A strong p50 half site, 5'-GGGGA, has been found overlapping many of the interferon response element (IRE) promoters (Cheng et al., 2011). They seem to increase the stimuli specificity in uninduced macrophages.

The differences between the p65 consensus and that of c-Rel are subtle and difficult to interpret. The c-Rel homodimer appeared to be less strict in its recognition requirement than p65. Electrophoretic mobility shift assay (EMSA) experiments

performed with these two proteins revealed that c-Rel can bind to all of DNA that is also recognized p65. However, the converse is not true (Kunsch et al., 1992b). This inherent flexibility in c-Rel recognition is best demonstrated in IL-2 CD28 response element (CD28RE). The DNA sequence which c-Rel binds to is 5'-GGAATTTCT-3', which does not conform to the consensus for p65 or c-Rel. Yet it clearly preferentially binds to c-Rel and is essential for the activation of IL-2 gene (Shapiro et al., 1997). However, this raises an interesting question. If c-Rel can bind to everything p65 recognizes and its transactivation domain has shown to be interchangeable with that of p65, so why there are genes can only be activated by p65? One of the possibilities is that p65 specific transcription requires the recruitment of co-activators with which c-Rel cannot interact, such as CBP/p300 (Wang et al., 2007).

3.5 NF-κB Structures

To date, four out of five members of the NF-κB family have been crystalized and its structure determined by X-ray crystallography. The four include, p50 (Chen et al., 1998a) Ghosh et al., 1995; Müller et al., 1995), p52 (Cramer et al., 1997), p65 (Chen et al., 1998a) (Chen et al., 1998b); Chen et al., 2000), and c-Rel (Huang et al., 2001). Each of these homodimers as well as the p50:p65 heterodimer were crystallized in complex with target DNA, suggesting that the RHR structure is stabilized by the complex formation. Inherent flexibility in the RHA is probably due to the flexible linker connecting the amino-terminal and dimerization domains. This

linker permits a great deal of inter-domain movement which can be seen in the comparison of the solved structures (Müller and Harrison, 1995). This is likely the reason why there has not been a DNA-free structure of NF-κB out there.

All of the NF-κB structures share an overall shape that resembles a butterfly as it is docked on the DNA (Figure I.2). The C-terminal dimerization domains (DD) from each monomer make up the two forewings of the creature and the two N-terminal domains (NTD) make up the two hind wings. The two domains within each monomer are joined together by the aforementioned ten amino acid linker. Both domains exhibit different variations of the immunoglobulin-like fold. The NTD, composed of roughly 200 amino acids, can be classified as an I-type Ig domain (Figure I.3). Three anti-parallel β-sheets and two alpha-helices make up the bulk of the domain. Two of the larger β-sheets make up the walls of the barrel with the remaining sheet hovering over at the opening of the barrel like a lid. The two alpha-helices form a bundle that sits next to the barrel. This alpha-helical region differs significantly in size between the RHR of the different NF-κB subunits. From the crystal structures the two groups look like they could be independent from one another. However, no conformational change within the domain has been detected in any of the x-ray structures. Taken alone, the NTD from all four structures overlap one another perfectly, showing it moves as a rigid single entity (Figure I.4A).

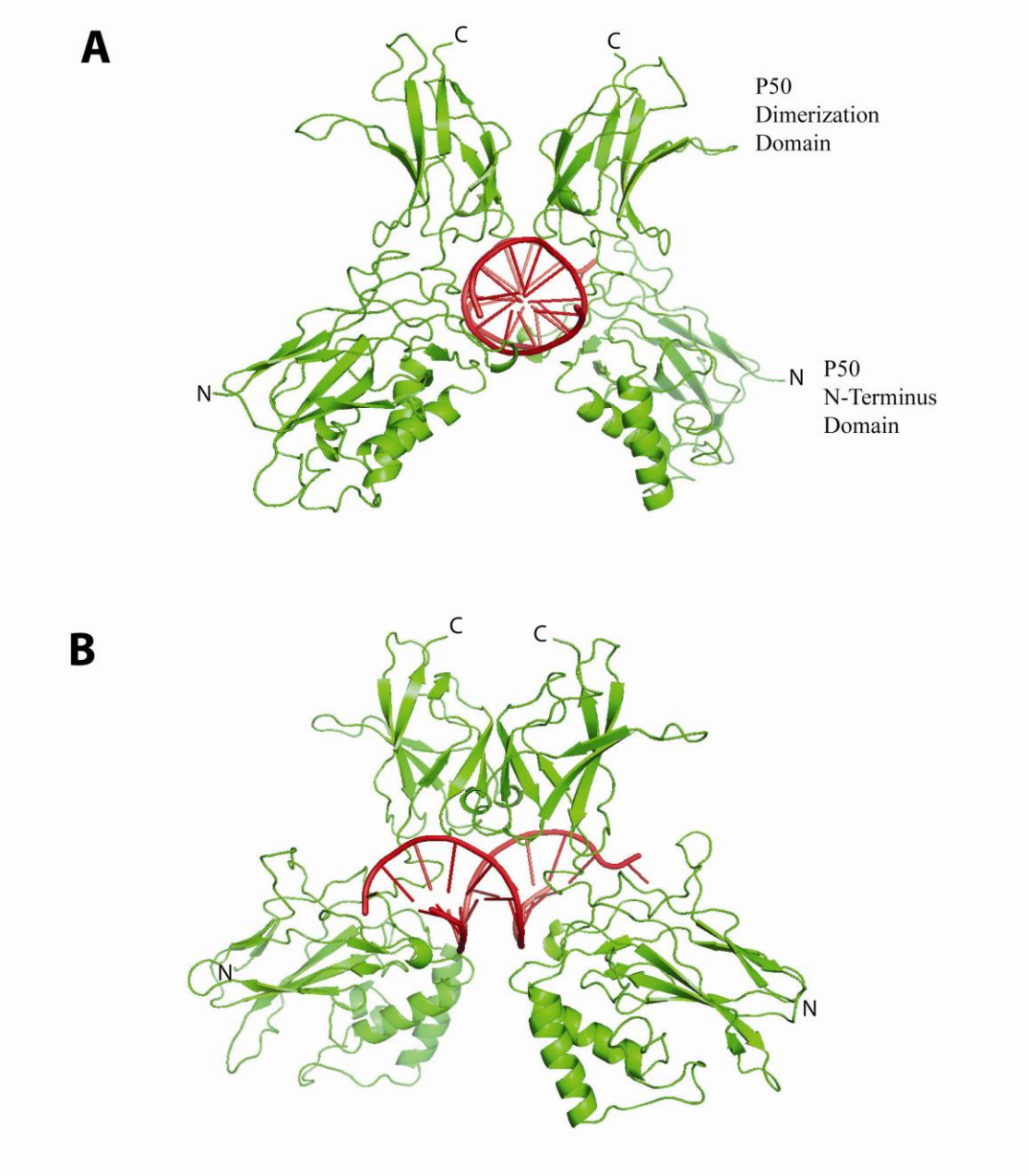

Figure I.2 Crystal structure of P50 homo-dimer bound to kB DNA (Gouri et al., 1995). The structure depicts the classical "butterfly" conformation seen in NF-κB DNA structures. A. The two-fold symmetry of the two p50 subunits seen along the DNA axis. B. The view turned approximately 75 degree to the side. From here the recognition loop can seen wedged in the major groove of the DNA.

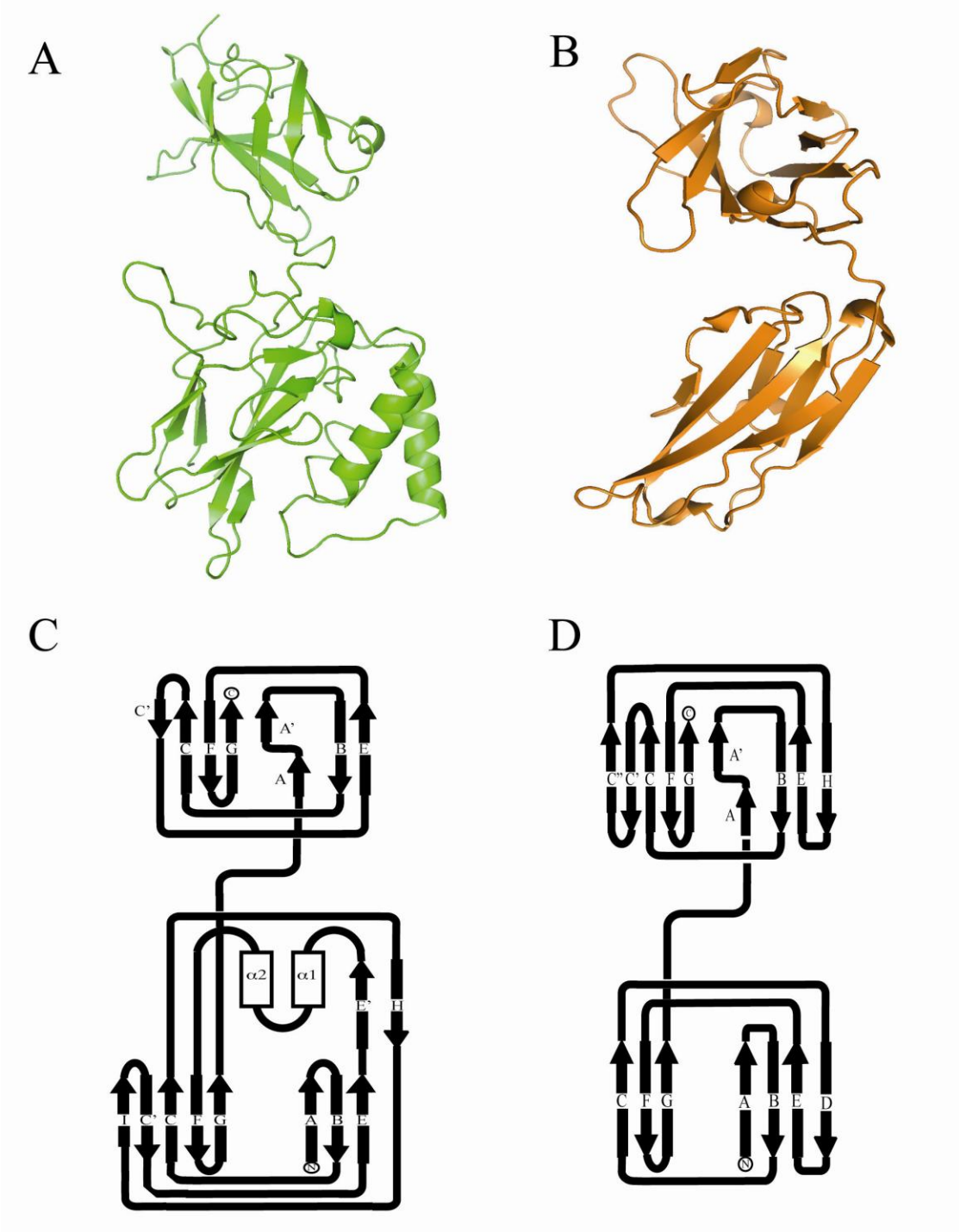

Figure I.3 A. Ribbon diagram of a single P50 subunit taken from the kB P50 structure (Gouri et al. 1995). This is compared with that of B. ribbon diagram of Ig light chain from the

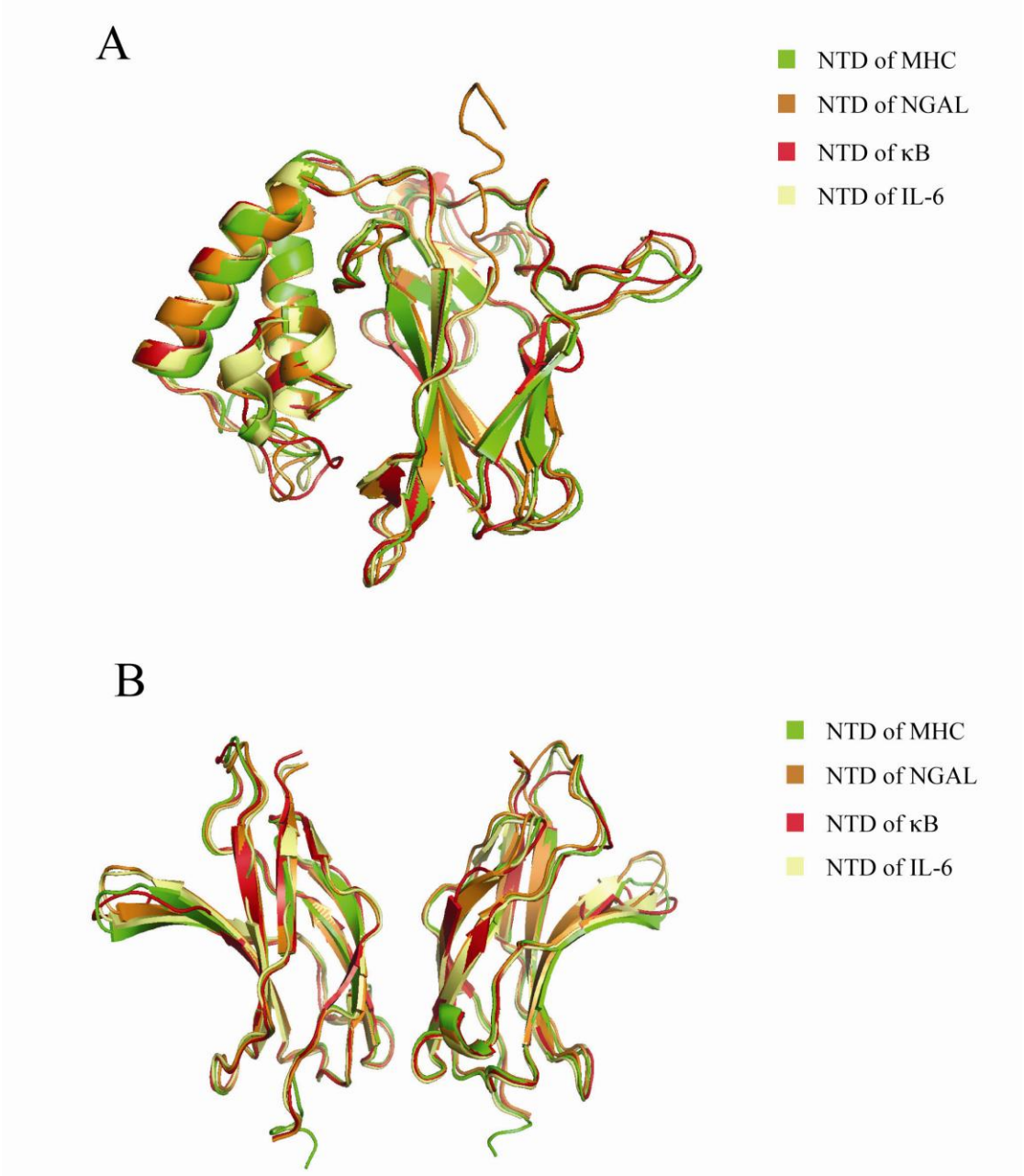

Figure I.4 A. Overlapping of the N-terminus domains (NTD) from four p50 crystal structures using the secondary structure match (SSM) function from COOT. The uniformity between all the structures show there is very little conformation variance between the β-barrel and α-helices within the NTD. B. Overlapping of the dimerization domains from the four p50 crystal structures. The DDs interact with one another in same fashion for all four structures with very little variance. This is especially true for the interface region of the structures.

The C-terminal domain, also called the dimerization domain (DD), is wholly responsible for the dimer formation observed in NF-κB. The DD, which is composed of roughly 100 amino acids. The domain is that of a C-type Ig barrel with two β-sheets forming the wall of the barrel. Dimerization occurs through the hydrophobic and hydrogen bonding interactions in the middle of the interface and salt bridge contacts on the periphery. The surface buried by the interaction is about 1500 $Å^2$ (Ghosh et al., 1995). The two subunits share a 180-degree rotational symmetry with one another along the vertical axis (when viewed from one end of the bound double-helical DNA) at the interface. This interaction results in a stable dimerization region that is seen in all of the p50 structures adopting the same conformation (Figure I.4B).

3.6 NF-κB DNA Contacts

DNA contacts made by NF-κB can be separated into two groups: base-specific contacts or nonspecific phosphate backbone contacts. All except one of the base-specific contacts are mediated by residues from the "recognition loop", a region made up of residues 57-67 of p50 (numbering according to mouse genome). The sequence of the loop is highly conserved among all members of NF-κB family (Müller and Harrison, 1995) (Figure I.5). The most striking set of protein:DNA interactions involve Arg 54, Arg56, and Glu 60 which make direct DNA base contact in all of the NF-κB:DNA structures (Müller et al., 1995; Escalante et al., 2002; Huang et al., 2001; Cramer et al., 1997) (Figure I.6). The conservation of these residues is not limited to

the NF-κB family. They are also conserved in NF-κB homologues in virus (c-Rel) and *Drosopholia* (Dorsal, Dif, Relish). More interestingly, the bases they contact are almost always consecutive guanines, which is the hallmark of the NF-κB consensus binding site (Sen and Baltimore, 1986c). The only other base-specific contact made outside of the recognition loop is at position 241 (Figure I.7). This residue is part of the flexible linker connecting DD with the NTD and is either an arginine or lysine. The base it contacts can be a guanine (in p50 and p52), or a thymine (in p65 and c-Rel).

The nonspecific contacts on the phosphate backbone are carried out by residues from NTD and DD as well as the flexible linker. They are mostly mediated by positively charged residues such as arginine or lysine but tyrosine, glutamine, and asparagine residues also participate in DNA contacts (Chen et al., 1998a); Ghosh et al., 1995; Müller et al., 1995), p52 (Cramer et al., 1997), p65 (Chen et al., 1998a); (Chen et al., 1998b); Chen et al., 2000), and c-Rel (Huang et al., 2001). The role for non-specific contacts is most likely to position NF-κB in such a way so that the recognition loops can be situated in the vicinity to make the gene specific contacts. One more possibility for these base non-specific contacts is to allow NF-κB to dock on DNA in a superficial way and allow it to glide up and down the DNA until it comes across a binding site where the high affinity interaction can be realized.

4. The IκB Family

4.1 The Discovery of IκB Proteins

Early research reported that, after induction, NF-κB has the ability to translocate into the nucleus where it interacts with target (also known as "κB") DNA. However, this DNA binding activity was observed only in the fraction of NF-κB found inside of the nucleus. NF-κB extracted directly from the cytosol failed to shift κB DNA probes by EMSA (Baeuerle and Baltimore, 1988b). However, this inhibitory affect could be abrogated by the addition of sodium deoxycholate (DOC), a bile salt and mild dissociation reagent. This observation strongly suggested that NF-κB inactivation was dependent upon its non-covalent association with some inhibitory factor. After passing DOC treated cytoplasmic fractions through DNA cellulose and size exclusion columns, a 67 kDa protein was discovered to be IκB, the inhibitor of NF-κB (Baeuerle and Baltimore, 1988c).

Upon discovery of IκB, research was quickly focused upon the mechanism under which its dissociation was regulated in the cell. One of the first observations involved the phosphorylation state of the inhibitor protein. It was found that *in vitro* phosphorylation on IκB by various purified kinases can cause the release of NF-κB (Ghosh and Baltimore, 1990; Naumann and Scheidereit, 1994). The exact phosphorylation sites were later identified as serines 32 and 36 on IκBα (Brown et al., 1995). After extensive work, it was discovered that the kinase activity responsible for phosphorylating these sites it was a kinase complex that has been dubbed the IκB

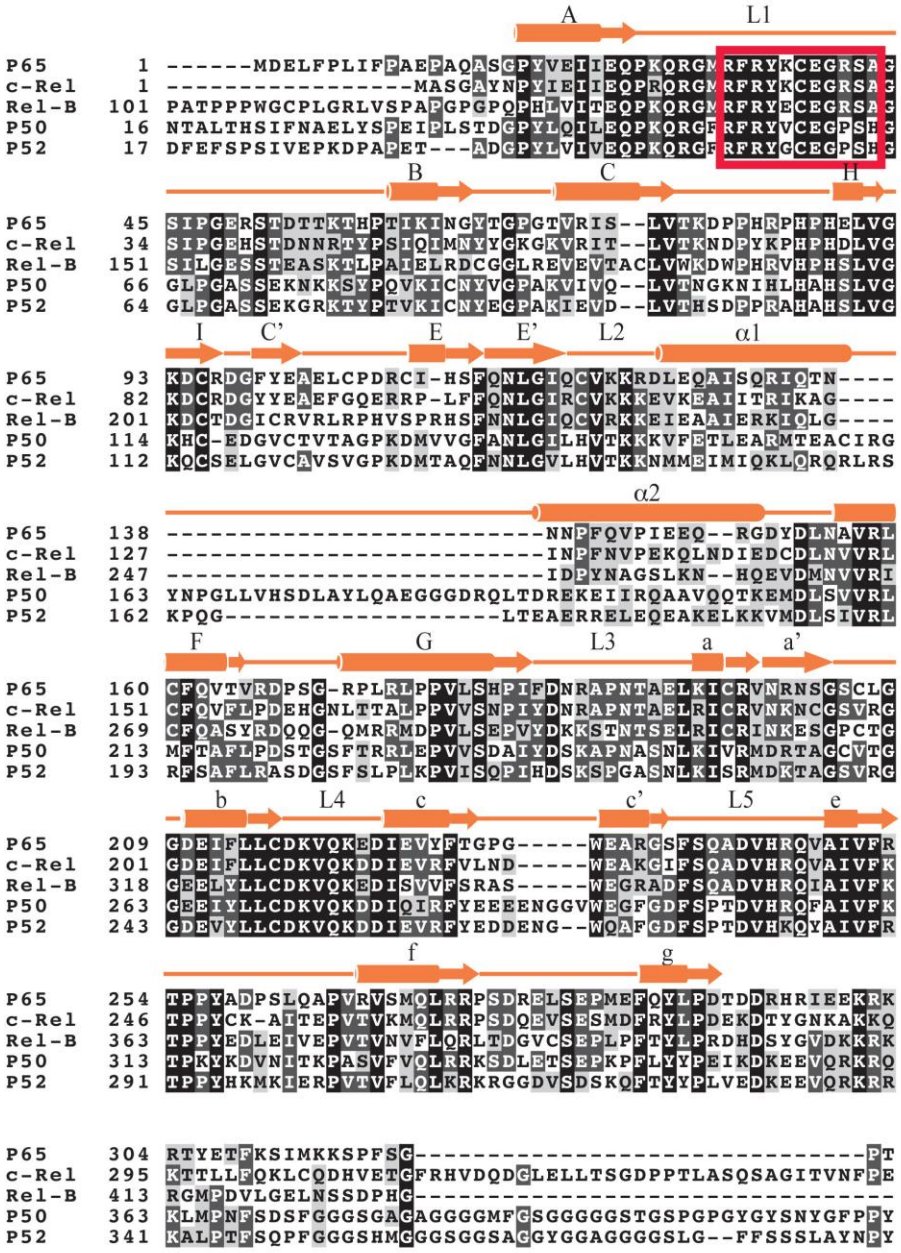

Figure I.5 Sequence alignment of Rel homology region of NF-kB proteins. Block boxes represent identical positions, dark grey represent positions of homology, and light grey boxes indicate conservative changes. Secondary structures within the region are labeled according to their alphabetical order given in figure 1.3. Highly conserved region of the recognition loop is boxed in red.

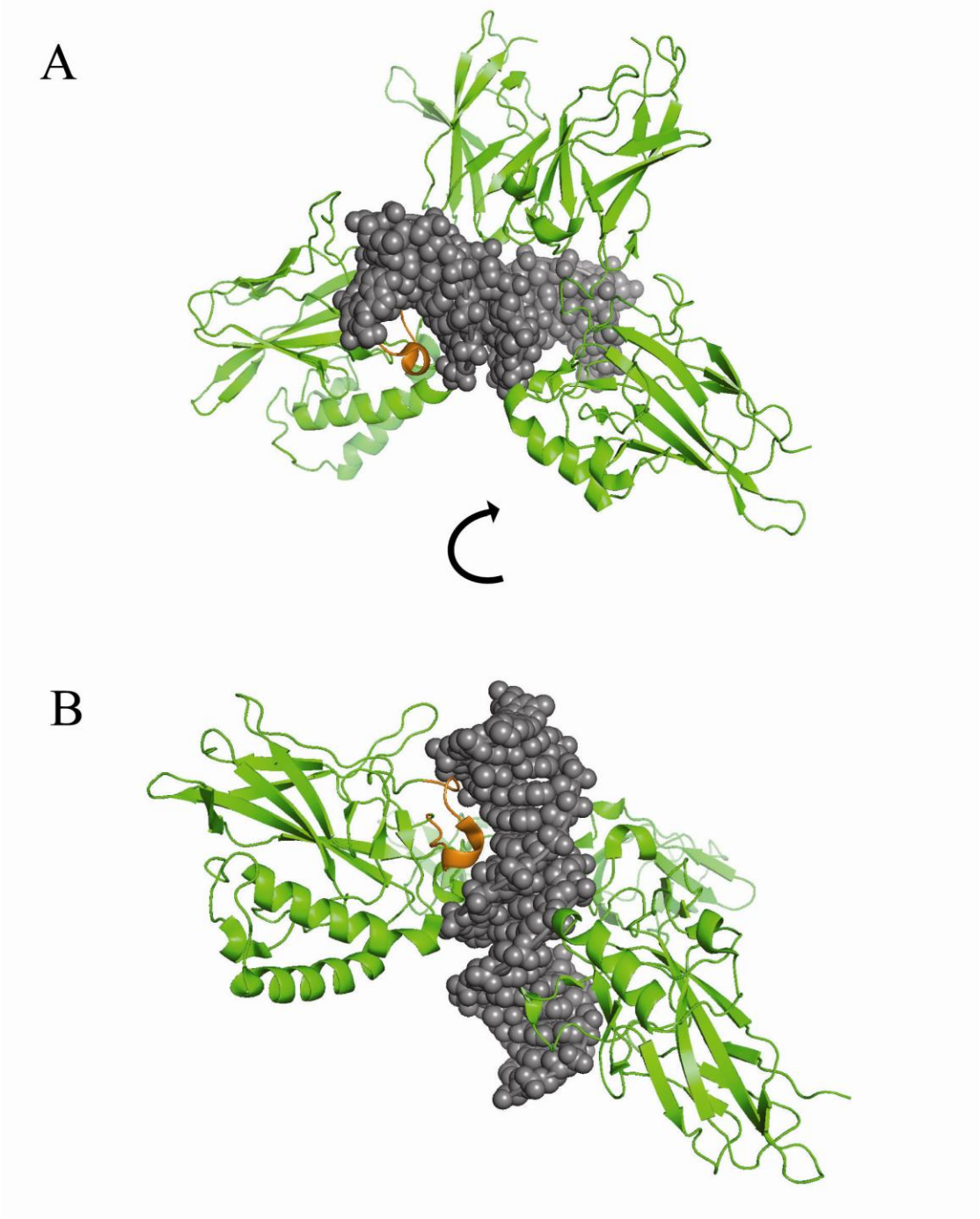

Figure I.6 A. Structure of P50/p65 bound to interferon-b promoter (Aggarwal et al. 2002). Recognition loop, colored in gold, can be seen embedded in the major groove of the DNA. B. The same structure turned clockwise 80 degrees.

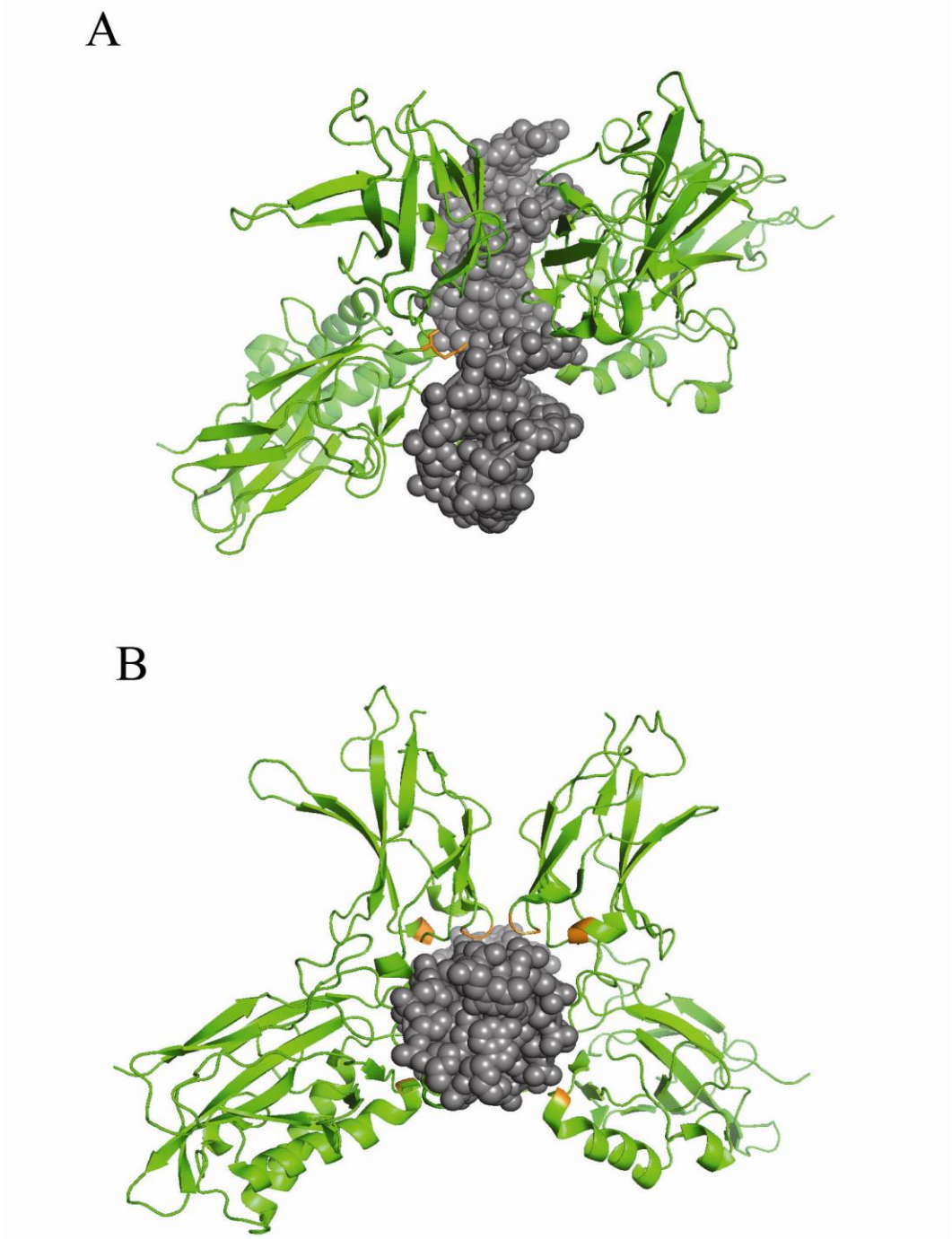

Figure I.7 A. The base specific contact of DNA made by the flexible linker of NF-κB. This highly conserved position, #241, on the linker is either occupied by a lysine or an arginine (shown in gold). B. Contacts made to the phosphate backbone of the DNA shown in gold.

kinase (IKK). IKK consists of three subunits: IKKα, IKKβ and IKKγ/NEMO (Mercurio et al., 1997; Rothwarf et al., 1998; [Wrong citation-Baeuerle and Baltimore, 1988c]; Yamaoka et al., 1998). However, dissociation of NF-κB from IκB does not result directly from phosphorylation of the latter. Rather, it was found that the newly phosphorylated IκB protein is marked for poly-ubiquitination via a specific SCF-type E3 ubiquitin-protein ligase enzyme known as $E3RS^{\beta\text{-}TrCP}$ and subsequent degradation by the 26 S proteasome (Chen et al., 1995; Palombella et al., 1994; Alkalay et al., 1995) (Figure I.8). Freed from its inhibitor, NF-κB migrates into the nucleus via its nuclear localization signals and regulates transcription. Notably, the NF-κB:IκB regulatory system is one of the signaling pathways that first demonstrated the use of ubiquitination as part of its proteolysis mechanism (Kanarek et al., 2010).

In the 1991 the first IκB was cloned (Haskill et al., 1991) and named IκBα. It contains six consecutive ankyrin repeats flanked on the N-terminal side with its phosphorylation sites and the C-terminal side with an acidic PEST region. IκBβ was cloned and identified soon after and added to the family (Thompson et al., 1995; Zabel and Baeuerle, 1990). IκBε was the next to join the family (Li and Nabel, 1997). These proteins constitute the proto-typical cytoplasmic IκB proteins. They behave like the classic inhibitor of NF-κB made famous by IκBα in such that they all undergo stimulus-dependent phosphorylation, ubquitination, proteasomal degradation, and re-synthesis. Along with these prototypical IκB proteins, p105 and p100 function in the cytoplasm to control NF-κB activity and sub-cellular localization either through their

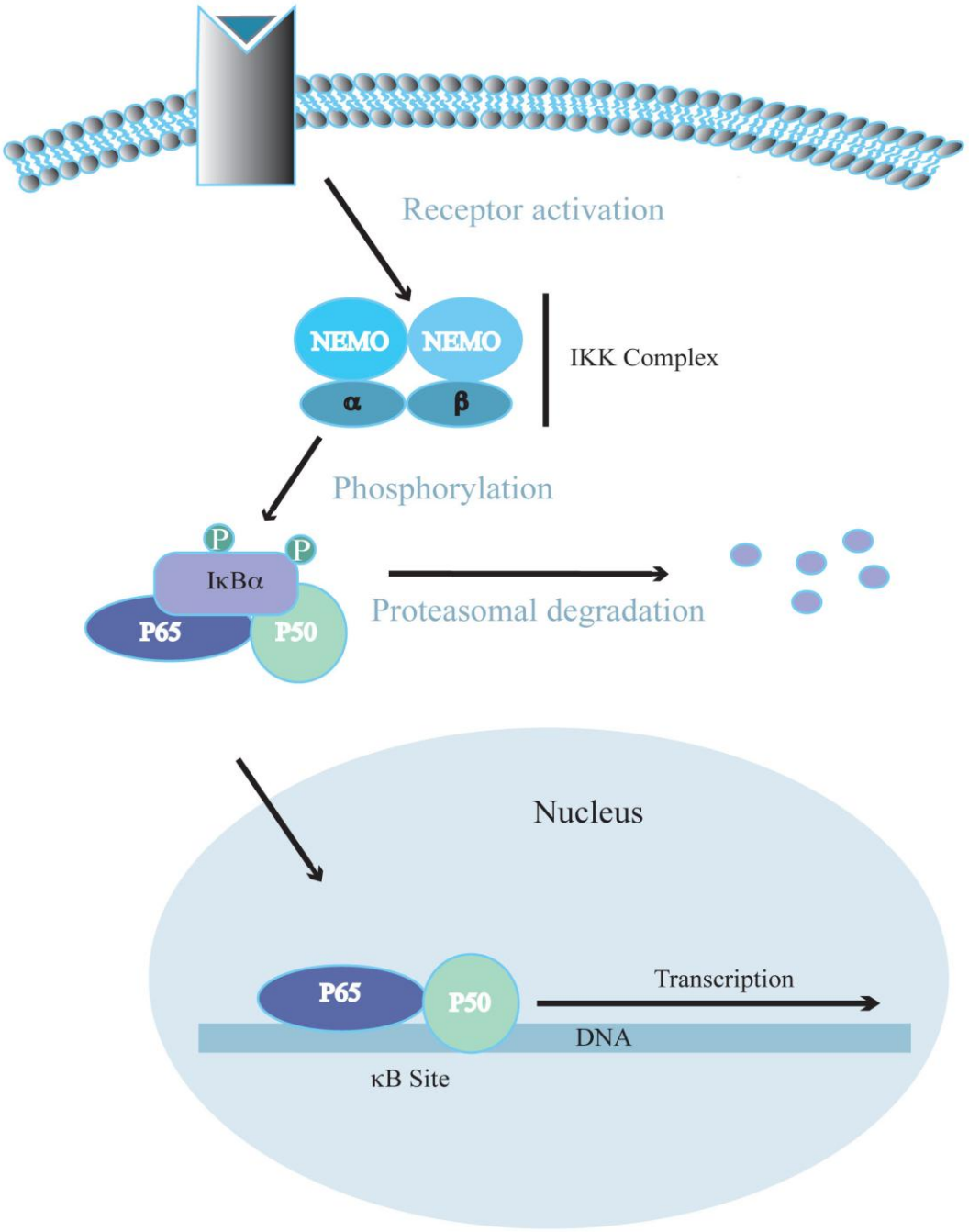

Figure I.8 Schematic representation of the canonical NF-κB pathway. Note in the pathway NF-κB is represented by P65/P50 heterodimer but is not limited to that. Other members of NF-κB family also take part in the pathway but P65/P50 heterodimer is the most abundant one.

own partial proteolysis to yield mature p50 and p52 subunits, or through the masking of noncovalently associated NF-κB subunits (Bours et al., 1992).

In addition to the prototypical IκB proteins and the NF-κB precursors, four additional IκB-like proteins have since been discovered. These include Bcl-3 (Fujita et al., 1993), IκBζ (Yamazaki et al., 2001), IκBNS (Fiorini et al., 2002a), and the recently discovered IκBη (Yamauchi et al., 2010a). This third group are not typically found in the resting cells. Rather, their expression requires cellular stimulation. After their translation, the atypical IκB proteins translocate into the nucleus where they can act as transcriptional co-activators of NF-κB-driven transcription. Collectively, these four atypical IκB proteins are referred to as "Nuclear IκB" (Figure I.9).

4.2 Prototypical Cytoplasmic IκB Proteins

Each of the three proto-typical cytoplasmic IκB proteins contains six ankyrin repeats within their structures(Huxford et al., 1998) (Zheng et al., 2011). They are expressed in a wide range of cell types include spleen (IκBα and IκBε), testis (IκBβ and IκBε), thymus (IκBα), and lung (IκBε). Because of their structural similarity and overlapping appearance in many cell types, extensive studies have gone into isolating their distinctive roles.

In IκBα$^{-/-}$ knockout mouse studies, the double mutants die within 7-8 days after birth. Severe granulopoiesis and dermatitis lesions were found on their skin (Beg and Baltimore, 1996; Klement et al., 1996). Cultured fibroblasts derived from these mice

revealed sustained NF-κB activation after lipopolysaccharide (LPS) and tumor necrosis factor alpha (TNF-α) induction. This also caused the upregulation of IκBε and defective NF-κB signaling in B-cells (Beg and Baltimore, 1996; Klement et al., 1996).

In IκBβ and IκBε knockout studies the mouse showed no developmental defects and minimal changes to their overall health. The few subtle abnormalities include increased expression of specific Ig isotypes and cytokines (Hoffmann et al., 2002; Mémet et al., 1999; Rao et al., 2010). IκBβ deficient mice developed high resistance to LPS-induced septic shock and collagen-induced arthritis (Rao et al., 2010). In one knockin experiment, IκBβ was placed in the coding region of IκBα. This effectively placed IκBβ in the role of IκBα. Mice with this mutation were relatively healthy and had the same NF-κB related responses as the wild type mice. This result indicates the two proteins function in very similar ways and have overlapping roles which can compensate for one another. This phenomenon was further supported by the upregulation of IκBε in IκBα$^{-/-}$ knockout mice (Beg and Baltimore, 1996; Klement et al., 1996) and the rare occurrence of IκB mutation related illness (Courtois and Gilmore, 2006). This apparent compensation effect makes for a very robust regulatory system. However, is also makes it incredibly difficult to pinpoint the distinct role for each cytosolic IκB.

One possible manner in which nature selects for this seemly redundant regulatory system is the creation of an interaction equilibrium caused by competitive binding of two IκB proteins with the one NF-κB dimer. To explore this idea, serveral

different studies have systematically mapped out the binding pattern between all the cytosolic IκB proteins and the different NF-κB binding partners. IκBα has been shown to preferentially bind to the NF-κB p50:p65 or p50:c-Rel heterodimers (Zabel and Baeuerle, 1990; (Hatada et al., 1992); Beg et al., 1992; Nolan et al., 1991). Its function in the cell seems stress removing NF-κB proteins from DNA promoters and inhibiting stimulus-dependent activation of transcription (Simeonidis et al., 1997; Malek et al., 2001; Tran et al., 1997a). IκBβ also preferentially binds to p65 and c-Rel containing heterodimers and also removes NF-κB from DNA, but to a lesser degree than IκBα (Thompson et al., 1995; Simeonidis et al., 1997; Malek et al., 2001; Tran et al., 1997b; Hirano et al., 1998). IκBε showed preferential binding for NF-κB proteins containing p65 or c-Rel subunits. It has also been shown to remove p65/p50 heterodimer from κB DNA, which is consistent with its inhibitory effect on TNF-α or phorbol myristate acetate (PMA) induced transcription (Li and Nabel, 1997; Simeonidis et al., 1997; Whiteside et al., 1997). Although it is evident each cytosolic IκB has its own binding preference, it is still not clear what does that mean for the NF-κB:IκB regulatory system as a whole.

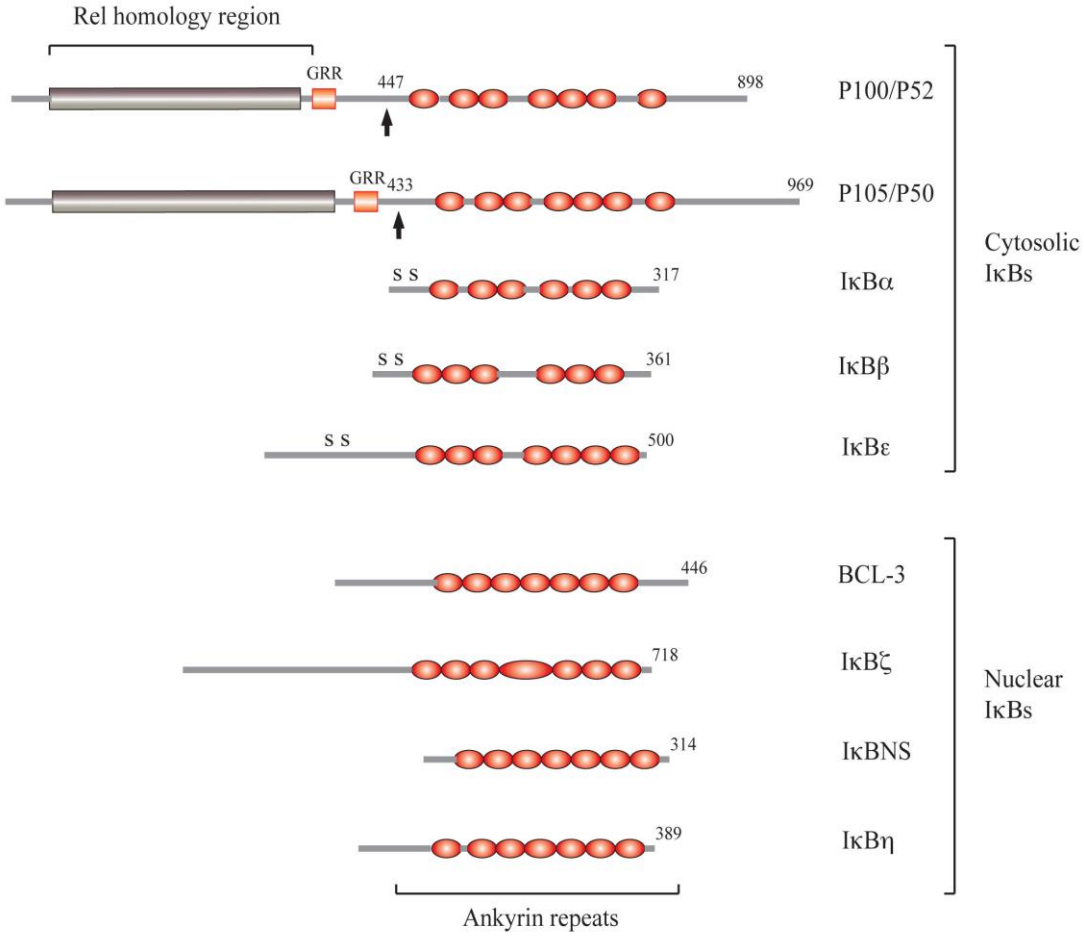

Figure I.9 Domain representation of the IκB family. P100 and P105 are proteolytically processed into the mature P52 and P50, respectively, at the position marked by the black arrows. The phosphorylation sites on IκBα, IκBβ and IκBε are marked by S, correlating to the serines where the phosphates are added which lead to the degradation of the protein.

4.3 Nuclear IκB Proteins

The atypical nuclear IκB group is made up of Bcl-3, IκBζ, IκBNS, and IκBη. With the exception of IκBη, none is present in resting cells but transiently expressed upon cellular stimuulation. This induction process is typically mediated by the NF-κB regulatory pathway. This indicates that nuclear IκB proteins are transcriptionally regulated by NF-κB. Once expressed, nuclear IκB proteins reside predominantly inside the nucleus where they engage in a number of regulatory functions. In one case, the interaction of nuclear IκB with DNA-bound NF-κB proteins was shown to retard the NF-κB turnover rate. This may be done through the formation of an IκB:NF-κB:DNA complex, which serves to retain the NF-κB where is safe from proteolysis. Another study reported that a similar ternary complex might serve as a platform for other cofactors to bind (Ghosh and Hayden, 2008). An important role that the nuclear IκB proteins may serve is to compete with cytosolic IκB proteins for the binding of DNA-bound NF-κB proteins. This competition creates binding equilibrium, which could serve as the basis for the NF-κB regulation inside the nucleus.

4.4 Bcl-3

Bcl-3 was originally identified as a rearranged proto-oncogene in chronic lymphocytic leukemia (CML). It was originally suggested to function in cell cycle control and lineage determination (Ohno et al., 1990). A wide variety of cancers have reported elevated levels of Bcl-3 (Courtois and Gilmore, 2006). Structurally, Bcl-3

contains seven ARs, which share high homology with that of the AR domain in the C-terminal portions of p100 and p105 (Figure I.10). It is not surprising, therefore, that Bcl-3 has shown a preference for binding to p52 and p50 homodimers, the mature proteolytic products of p100 and p105, respectively (Franzoso et al., 1992b; Wulczyn et al., 1992; Nolan et al., 1993). Early reports suggested that Bcl-3 removes p50 and p52 homodimers from DNA, thus terminating their repressor function (Hatada et al., 1992b; Naumann et al., 1993; Franzoso et al., 1993). However, subsequent findings have shown that Bcl-3 can also activate transcription in complex with p50, which shows the duel capacities of Bcl-3. More interestingly, one of the promoters this was demonstrated on was IL-6, a gene closely associated with IκBζ (Wulczyn et al., 1992; Yamamoto et al., 2004), the protein this study is focusing on. This overlapping of regulation by two closely related proteins mirrors what was seen in the case of IκBα and IκBβ (Beg and Baltimore, 1996; Klement et al., 1996).

Another study aimed at exploring whether Bcl-3 can interact with p105 outside of the nucleus because of its close resemblance to the ARD of p105. To test this, Bcl-3 was expressed ectopically in the cytoplasm of pro B-cells. Bcl-3 expression resulted in cytoplasmic transition of p50/p105 complex to nuclear p50 homodimers (Watanabe et al., 1997). As Bcl-3 is predominantly located in the nucleus, the observed interaction was suspected of having been carried out by the *de novo* protein as it is first being synthesized. This demonstrated Bcl-3 can interact with p105 and expedite its proteolysis into the mature p50 protein.

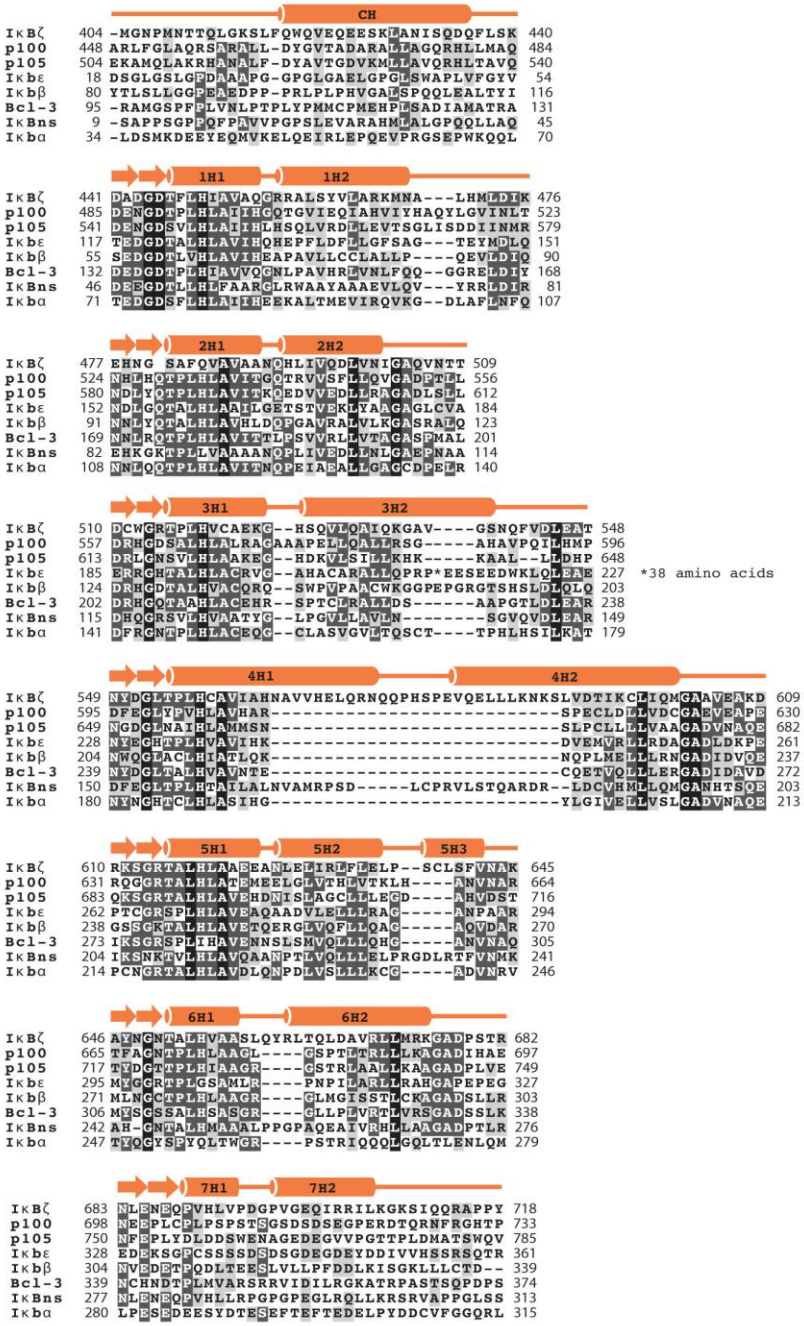

Figure I.10 Sequence alignment of the ankyrin repeats region of IκB proteins. The two α–helices within each ankyrin repeats are indicated by the orange rods with their designation. The seventh ankyrin repeat may not be present in proteins but is confirmed for BCL-3 and IκBζ. Black boxes represent identical positions, dark grey positions of homology, and light grey boxes represent position of conservative changes.

Other studies showed Bcl-3 can be phosphorylated, but the significance of Bcl-3 phosphorylation on transcriptional regulation is poorly understood (Nolan et al., 1993; Bundy and McKeithan, 1997). Bcl-3 has been further identified to interact with histone acetyl-transferase Tip60, corepressor CtBp, E3 ligase TBLR1, and Pirin (Dechend et al., 1999; Keutgens et al., 2010).

Various mouse knockout studies were used to explore the physiological role of Bcl-3. Mice missing both copies of their BCL-3 gene developed defects in splenic microarchitecture and had problems with T-cell differentiation and protective humoral immune responses (Franzoso et al., 1997a; Franzoso et al., 1997b; Pène et al., 2011; Schwarz et al., 1997). Another study credited Bcl-3 with prevention of granulocyte formation in acute inflammatory lung injuries (Kreisel et al., 2011). Double knockout of Bcl-3 and p52 caused impaired medullary thymic epithelial cells in mice, which led to breakdown of central tolerance. That led to multi-organ inflammation which killed 77% of the double knockouts (Zhang et al., 2007).

4.5 IκBNS

IκBNS was first characterized as a gene expressed during negative selection process of thymocytes (Fiorini et al., 2002b). After the initial induction, IκBNS enters the nucleus where it preferentially interacts with p50 and functions as repressor of NF-κB. The genes that are affiliated with this protein include IL-6, IL-12 p40, and IL-18 (Kuwata et al., 2006; Hirotani et al., 2005). The IL-6 promoter, in particular, was

affected by the transient overexpression of IκBNS, which caused p50 to bind to the DNA more readily and resulted in the suppression of IL-6 production (Hirotani et al., 2005). This is interesting because this is exactly the opposite to what has been reported for IκBζ (Yamamoto et al., 2004). This suggests IκBNS and IκBζ function as antagonists of each other competing for the binding of nuclear p50. This delicate balance between the two proteins may regulate the production of the important IL-6 pro-inflammatory cytokine.

Mouse knockout studies further support this antagonist theory. IκBNS deficient mice had increased production of IL-6, IL-12 p40, and IL-18 (Kuwata et al., 2006; Hirotani et al., 2005). Elevation of pro-inflammatory cytokines correlated with intestinal inflammation and high sensitivity to LPS induced endotoxin shock (Kuwata et al., 2006). However, not all of the cytokines responded the same to the absence of IκBNS. IL-2 production was decreased, which reduced T-cell proliferation. Thus it is not easy to consign IκBNS as a transcriptional activator or inhibitor. The presence of the IκBNS alone is not enough to dictate the matter.

4.6 IκBη

IκBη is unique among nuclear IκB proteins in that it is constitutively expressed. It resides predominantly in the nucleus and shares the highest degree of sequence homology with IκBβ (Yamauchi et al., 2010b). IκBη preferentially binds to p50 and responds minimally to TLR mediated induction. Gene silencing experiments

performed with RNAi showed that reduction of IκBη caused decreased levels of IL-1β, IL-6, and G-CSF during LPS induction. Thus, preliminary data suggests IκBη functions as a positive regulator for a subset of pro-inflammatory cytokines in conjunction with nuclear NF-κB proteins, p50 in particular.

4.7 IκBζ

IκBζ is a nuclear IκB protein that is the focus of this dissertation research.

4.7.1 The Discovery of IκBζ

IκBζ was first discovered in the early 2000's by two Japanese groups who published their results within one month of each other. The Saito group from Hokkaido University was investigating genes that were activated downstream of the NF-κB pathway as a result of murine macrophage stimulation by bacterial LPS. Of the 1500 mouse genes they analyzed, eleven showed significantly elevated levels of expression. Among this group was the gene encoding IκBζ. The researchers recognized this to be a previously uncharacterized gene with an open reading frame of 2187 base pairs, which translates into polypeptide of 728 amino acids (Kitamura et al., 2000). Cursory analysis predicted it to contain six Ankyrin repeats (AR) within its carboxy-terminal half. Consequently, the group named the protein MAIL, which is an acronym for Molecule possessing Ankyrin-repeats Induced by LPS. Around the same

time, 650 miles away in the city of Ibaraki, researchers in the Todokoro group discovered a new nuclear protein while looking at the expression pattern of OP9 stromal cells as they were being exposed to the inflammatory cytokine IL-1α. The researchers reported a new gene identified to be in chromosome 3 and containing two alternatively spliced variations, one isoform of 718 residues and a second isoform with 618 residues. The longer isoform appeared to be expressed more predominantly in cells (Haruta et al., 2001). The group named the protein INAP after IL-1-inducible Nuclear Ankyrin repeat Protein.

Though at the time they referred to it by different names, both groups reported IκBζ to be an inducible protein that is not expressed in resting cells. Upon induction by NF-κB-inducing stimuli such as LPS or IL-1, IκBζ is transiently expressed and localizes to the nucleus (Kitamura et al., 2000; Haruta et al., 2001). Ecotopically expressed IκBζ significantly increased the amount of IL-6 produced by the cell in response to LPS induction (Kitamura et al., 2000). At the primary sequence level, the new protein shared the highest sequence homology with Bcl-3 and other IκB proteins (Haruta et al., 2001).

4.7.2 Activation of IκBζ

An array of pro-inflammatory stimuli is known to induce IκBζ expression. The list include LPS, IL-1, peptidoglycan, bacterial and mycoplasmal lipopeptides, flagellin, R-848 (an imidazoquindine derivative) as well as CpG oligonucleotides and

ligands for TLR2, -5, -7, and -9 (Kitamura et al., 2000; Haruta et al., 2001; Yamamoto et al., 2004). Among these inducers, LPS is most often used to study the mechanism behind the elevated expression of IκBζ. LPS levels as low as 0.1ng/ml are sufficient to cause rapid production of IκBζ which peaks at one hour post-induction and is sustained for another 48 hours. This process does not require the synthesis of new protein as its unaffected by cycloheximide, an inhibitor of translation. Intraperitoneal administration of LPS in mice resulted in elevated expression of IκBζ in lung, heart, liver, kidney, testis, spleen, lymphnode, and thymus (Kitamura et al., 2000).

Mechanistically, IκBζ induction has been traced to assortment of TLRs on the cell surface, which signal either through the MyD88 or the TRAF6 pathways or both. Both signal pathways leads to the eventual activation of NF-κB and the subsequent transcriptional activation of target genes (Eto et al., 2003). Of three potential κB sites identified in the proximal promoter of IκBζ, two have been shown to be essential for its elevated expression (Yamazaki et al., 2005).

Interestingly, not all pro-inflammatory cytokines that induce NF-κB activity lead to elevated expression levels of IκBζ. Tumor necrosis factor-alpha (TNF-α), for example, is a potent inducer of NF-κB that does not lead directly of elevated expression of IκBζ. The TNF Receptors are unique from IL-1R and TLRS in their immediate signaling effects, but inside the cell there is convergence of all three receptor signaling pathways at TRAF2 and TRAF6. This leads to the activation of NF-κB and MAP kinases (Li and Verma, 2002; Kracht and Saklatvala, 2002). Furthermore, many of the genes targeted by these cytokines are the same ones that

lead to similar biological effects such as inflammation, coagulation, and pyrexia. One study suggested the reason as why LPS, but not TNF-α, can induce the production of IκBζ is because of the differential post-transcription stability of IκBζ mRNA. In an expression reporter experiment, IκBζ gene was shown to be transcribed in response to TNF-α just as if though it was induced by LPS or IL-1. However, whereas the mRNA product induced by TNF-α was quickly degraded, the IκBζ transcription product in response to LPS or IL-1 persisted long enough for efficient translation to occur, indicating that the difference in its expression was not at the transcriptional level but at the translational level. Northern blot analysis of mRNA levels in cells continuously expressing IκBζ showed LPS and IL-1 induction stabilized the mRNA product while TNF-α induction did not. The cause of this inherent fragility of the mRNA has been associated to a *cis* element in the N-terminal region of the open reading frame. This spontaneous breakdown of the product can be halted by the induction of another cytokine, IL-17. Consequently, accompanied by IL-17, TNF-α can too induce the expression of IκBζ. These experiments demonstrate the importance of post-transcriptional regulation in the activation of IκBζ.

4.7.3 IκBζ and Gene Regulation

Because all of the IκB proteins interact with members of NF-κB family, one of the first thing that were being looked at was the effect of IκBζ has on the activation of NF-κB. In cell lines transfected with IκBζ, their NF-κB responses to the LPS

induction is significantly lower than that of un-transfected cell lines (Yamazaki et al., 2001). This inhibition was also seen in cells induced by IL-1. Overexpression of p65 and IKKβ did not overcome this inhibitory effect indicating IκBζ act on NF-κB itself rather than its signaling pathway. The lowered expression levels of the NF-κB related genes and the nuclear localization of NF-κB showed IκBζ inhibits on a transcriptional level and is not through the disruption of NF-κB nuclear shuttling system (Yamazaki et al., 2001).

However what complicate the matter is IκBζ has also been shown to be a positive regulator of genes. In the case of forced expression of IκBζ in macrophages or fibroblast, the IL-6 response to LPS was dramatically augmented (Motoyama et al., 2005) (Kitamura et al., 2000). Besides IL-6 IκBζ also regulate such genes as colony-stimulating factor (Csf2), IL-12p40 (IL-12b), and Lipocalin-2 (Lcn2) (Yamamoto et al., 2004) (Yamazaki et al., 2008), neutrophil gelatinase-associated lipocalin (NGAL) (Cowland et al., 2006) as well as IL-12 and IL-18 mediated interferon –ϒ (Kannan et al., 2011). Of these perhaps IL-6 activation is most closely study. Upon stimulation by IL-1 IκBζ form a complex with p50 homo-dimer and is recruited to the promoter site of IL-6 gene. Because IκBζ is itself regulated by NF-κB and is made *de novo* only after the induction, it is considered to be a regulatory cofactor for the second wave of NF-κB responsive genes. Due to this delay, the IL-6 expression does not peak until four hours after its initial induction (Yamamoto et al., 2004).

Mechanistically, IκBζ have shown to preferentially bind to p50 over p65 (Yamazaki et al., 2001) (Yamamoto et al., 2004). This association was also confirmed

by *in vivo* electrophoresis mobility shift assay (EMSA) where IκBζ inhibited DNA binding of p65/p50 as well as p50 homo-dimer. GAL4 reporter assay carried out in HEK293 cells showed IκBζ contains a transaction domain close to its N-terminus but is kept in an inactive state by its own ARs structure in the C-terminus. This inhibitory affect can be removed by its binding to p50 subunit, possibly through a binding induced conformational change (Motoyama et al., 2005). The collaborative property of p50 and IκBζ is further supported by the evidence that p50 deficient mice exhibit similar symptoms as the IκBζ deficient mice which are the impairment of IL-6 production and prolonged inflammation responses (Yamamoto et al., 2004). Thus, IκBζ seem to be a transcriptional cofactor with latent transcriptional activation capability but is masked by its own C-terminus in the free protein. This activity may be triggered by a p50 interaction induced conformational change that releases the transactivation domain. Additionally, IκBζ has also shown to mediate the recruitment of NF-κB and other gene regulators, such as C/ebpβ and chromatin remodeling factor Brg1 to the promoter of lipocalin2 gene (Yamazaki et al., 2008). These other cofactors would no doubt add additional intricacy to this already complex regulatory system.

4.7.4 Physiological Roles of IκBζ

Initial attempts in creating IκBζ-deficient mice by intercrossing heterozygous knockout were met with difficulties. The numbers of homozygous knockout mice

were far below one in four littermate predicated by standard Mendelian ratios. It turned out 90% of the IκBζ-deficient embryo dies *in utero* (Shiina et al., 2004). The surviving pups develop normally to 4-5weeks of age. By 10 weeks, all IκBζ-deficient mice exhibit atopic dermatitis-like lesions on the surface of their skin. Acanthosis and lichenoid changes can be seen in the inflamed areas (Yamamoto et al., 2004; Shiina et al., 2004). The IκBζ knockout mice also express chronic inflammation in their ocular surface. Histological analysis of the diseased tissue showed high concentration of lymphocytes in the submucosa of the conjunctiva epithelia cells. The inflammation also destroyed most of the goblet cells in that area (Ueta et al., 2005; Yamamoto et al., 2004). This is very close to what has been documented for human ocular surface disorder seen in Stevens-Johnson Syndrome patients and ocular cicatricial pemphigoid cases (Faraj and Hoang-Xuan, 2001). In wild type mice only a few types of tissues that are known to express IκBζ constitutively. These include the keratinocytes on the outer surface of the skin and a variety of mucosal tissue (Shiina et al., 2004; Ueta et al., 2005). Thus, these evidences suggest IκBζ is needed in parts of the body that contact microbiota and assist with downregulation of prolonged inflammation.

4.7.5 Sequence Analysis of IκBζ

Initial sequence analysis of the IκBζ gene turned up an ankyrin repeat (AR) domain within the C-terminus of the protein. This region was predicted to contain seven ARs with an undefined loop insertion within its fourth AR (Figure I.10). The

analysis of its N-terminus did not identify any sequences known to correlate with a specific structure or function. Because this N-terminal region makes up more than half the total IκBζ protein, a great deal of effort was spent on understanding its function. A bipartite NLS with a sequence of K-R-X_{12}-K-R was identified between amino acids 163-178 in the human IκBζ sequence (Motoyama et al., 2005). An artificial expression system was next used to assess whether it has transactivation capability. To this end, the N-terminus region of IκBζ was fused to transcriptional factor GAL4. The resulting fusion protein was shown to activate reporter gene expression in yeast cells. Further dissection of the region pinpointed the transactivation domain to be within residues 329-402. Interestingly, this activation capability was not detected in another fusion protein composed of the full length IκBζ. This suggests the transaction ability of the full length protein is kept at bay by the C-terminus portion of the protein (Motoyama et al., 2005).

The C-terminal region of IκBζ exhibits highest similarity with BCL-3 (Franzoso et al., 1992b) and IκBNS (Fiorini et al., 2002a). This region was predicted to contain seven ARs with an undefined loop in its fourth AR (Figure I.10). Interestingly, all three of these proteins reside within the nucleus and preferentially bind to NF-κB p50 over homodimers of p65 (Wulczyn et al., 1992; Nolan et al., 1993; Kuwata et al., 2006; Hirotani et al., 2005). Transfection experiments performed with the AR region alone of IκBζ revealed it resides exclusively in the cytosol and inhibits NF-κB very much like IκBα (Yamazaki et al., 2005).

Chapter II

Material and Methods

1. Expression and Purification of Recombinant Proteins

1.1 Expression and Purification of Recombinant p50 Homo-dimers

Throughout this study, four different truncated versions of murine p50 were expressed and purified. Two are p50(39-363) and p50(39-376), which contain their entire RHR and, therefore, possess the ability to interact with κB DNA. The other two constructs, p50(245-350) and p50(245-376), lack their NTD and, consequently, can still dimerize and interact with IκB proteins, but cannot bind to DNA. The purification schemes for all four constructs are more or less the same except for the extra DNA precipitation step required for NTD-containing p50 proteins.

All recombinant NF-κB p50 proteins were cloned into T7 promoter-driven pET vector systems (Novagene). The expression vectors were transformed into chemically competent *E coli.* BL21 (DE3) cells by the heat shock method. Transformed cells were cultured in 2 liters LB media with either 25μg/ml of kanamycin or 50μg/ml of ampicillin. After three to four hours of cell growth at 37°C the culture was cool to room temperature (~20°C) by taking it out of the incubator and placed on top of the turn plate with constant agitation. The cell density was monitored by spectrophotometer absorbance at 600nm. Once the reading reached 1.0 they were induced with 0.1mM of isopropyl-β-D-thiogalactopyranoside (IPTG). The cells were harvested 16-18 hours after induction of by centrifugation at 2927 rcf for 10min at 4°C.

The collected bacterial cell pellets were resuspended in 140mL of lysis buffer composed of 25mM MES pH 6.5, 50mM NaCl, 0.5mM ethylenediaminetetraacetic acid (EDTA), 10mM β-mercaptoethanol (βME) and 0.5mM phenylmethane-sulphonylfluoride (PMSF) (added just prior to lysis). The mixture was lysed with two passages through a microfluidizer (Microfluidic). The lysate was separated into supernatant and cellular debris fractions by 50 minutes spinning at 24,318 rcf. For p50 constructs that retain the ability to bind to DNA, the supernatant was placed in a glass beaker and stirring rod. With gentle stirring, 10% streptomycin sulfate solution was added at a rate of roughly 1mL/minute. Addition of streptomycin sulfate was halted once the solution became turbid. After stirring for an additional hour, the precipitate was separated centrifugation again at 24,318 rcf for 50 minutes. The final solution was filtered through a 0.8μm filter.

The resulting soluble protein fraction was next loaded onto a pre-equilibrated 15-20 mL SP Sepharose column (GE Biosciences) by gravity at a rate of roughly 1 mL/minute. The bound protein was then washed with ten column volumes of lysis buffer. After that, the sample was eluted with NaCl gradient from 50mM to 500mM in lysis buffer over roughly 20 column volumes. The fractions were analyzed by SDS PAGE and Coomassie protein stain (Figure II.1A). The sample fractions containing the p50 protein were pooled and concentrated down with CentriPrep-10 (Millipore) to about 2mL. Concentrated product was passed through a 0.2μm syringe-tip filter and loaded onto a pre-equilibrated Superdex200 26/60 size exclusion column (Figure II.1C). The running buffer used for the isocratic separation contained 25mM Tris-HCl

pH 7.4, 50mM NaCl, and 1mM Dithiothreitol (DTT). The fractions under the peaks were collected and concentrated down with a new set of CentriPrep-10 centrifugal concentrators. The concentration of the protein was monitored by absorbance at 280nm. Concentration was halted when the protein reaches about 13mg/mL. The samples were either aliquotted, flash frozen in liquid nitrogen, stored in -80°C freezer or left at 4°C overnight to be used in complex formation with IκBζ.

1.2 Expression and Purification of Recombinant His-tagged IκBζ

The original DNA sequence for the full length human IκBζ was obtained from Dr. Tatsushi Muta of Kyushu University, Japan. Various constructs of the same protein were cloned in pGEX4T-2 and pHIS8 vectors. In the end, the one that gave us the diffracting crystal is IκBζ(404-718)pHIS8. First, the pHIS8 vector carrying the insert was transformed into chemically competent *E. Coli* BL21 bacteria cells. The transformed cells were plated on selective LB agar substrate and cultured in to 2 liter LB bacteria media culture containing 25μg/ml of kanamycin. With vigorous agitation at 37°C the culture was allowed to grow for about three and half hours. The exact time was determined by the density of the bacteria which gave a spectrophotometer reading of 0.6 @ 600nm. At that point, the culture was taken out of the incubator and placed on a magnetic stir plate at room temperature (~20°C). With stirring at about 600rpm, the bacteria culture was allowed to cool down for about 30 minutes. At that

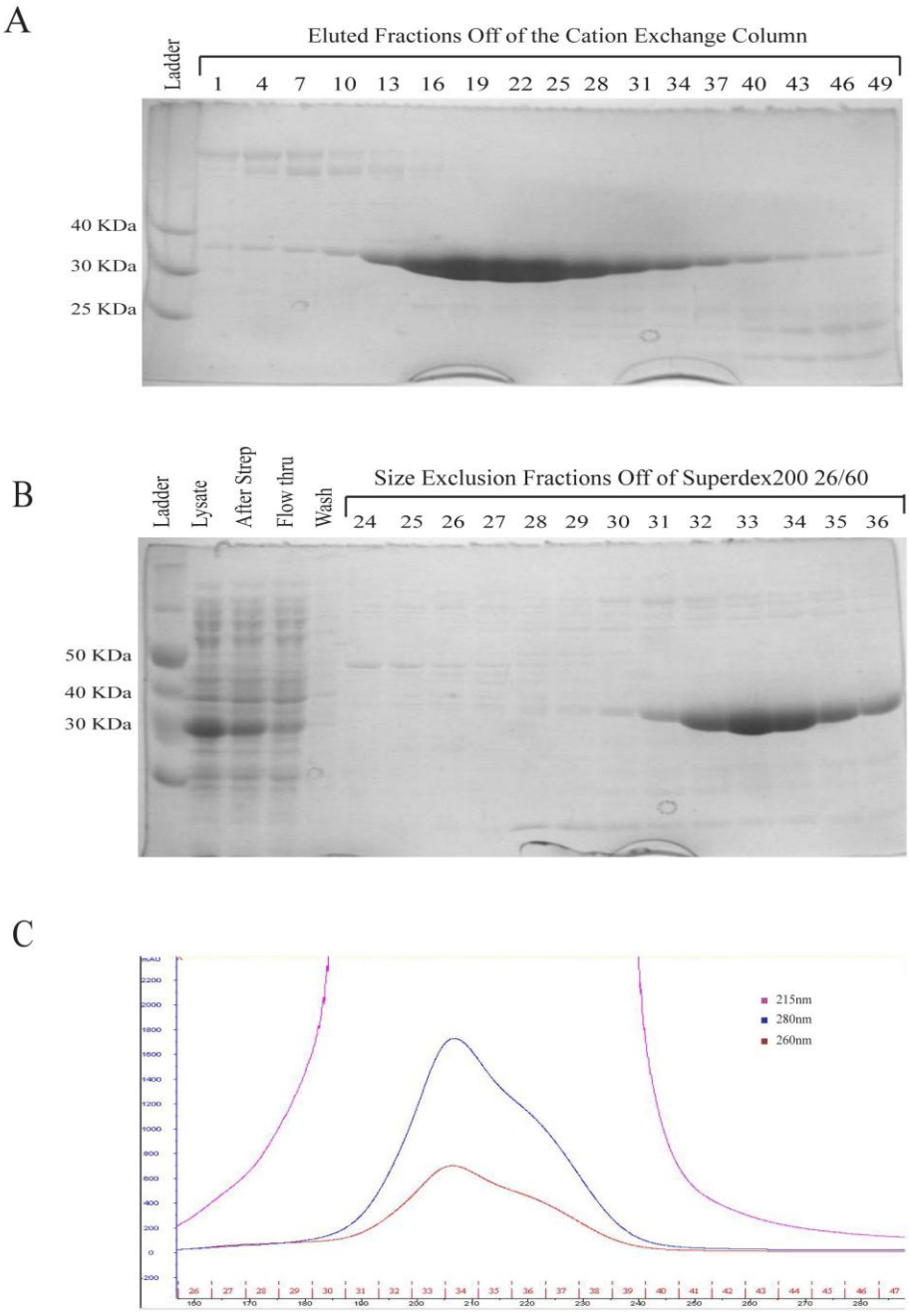

Figure II.1 A. Eluted fractions of P50(39-363) as it came off of the cation exchange column. The elution was done with a NaCl gradient that ranged from 50mM to 500mM. B. Samples were taken at different stage of the purification and analyzed by the SDS PAGE. C. Size exclusion chromatograph of P50(39-363) as it came off of the Superdex200 26/60 column.

Point the bacteria were induced with 0.1mM of isopropyl-β-D-thiogalactopyranoside (IPTG). The cells were left stirring for 16-18 hours on the to express the protein. The next day the bacteria were poured into six-500mL NALGENE centrifuge bottles and spun at 2979 × g for 10 minutes. The resulting supernatant was decanted and pellets were resuspended in 140mL of ice cold lysis buffer. The lysis buffer is made up of 25mM Tris-HCl pH7.4, 500mM NaCl, 10mM β-mercaptoethanol (βME), 10mM imidazole, and 0.5mM ethylenediamine tetraacetic acid (EDTA). 350μL of 200mM phenylmethylsulfonyl fluoride (PMSF) in isopropyl alcohol was added to the mixture right before the lysis. This is because PMSF has a short life span in water but it is very affective at disabling serine proteases while active. With the PMSF added the solution was twice passed through the pre-chilled, pre-equilibrated microfluidizer. The lysate was then divided into four 50mL round bottom centrifuge tubes and spun at 24,318 × g for 50minutes in the ss-34 rotor kept at 4°C. The supernatant collected from after the spin was put through a 0.8μm filter and 20μL sample was saved for later analysis.

The filtered lysate was passed through a pre-equilibrated 1cm × 1cm × 6cm gravity column with 2mL of Ni Sepharose Fast Flow resin (GE Biosciences). From this point on everything was done inside the cold room to ensure minimum denaturation and/or proteolysis of the protein. After the flow through, the column was washed with 20mL of wash buffer, which is composed of 25mM Tris-HCl pH 7.4, 500mM NaCl and 25mM imdazole. A 20μL of the flow through was taken at this point for later analysis. Following the wash IκBζ was eluted from the affinity column

with the elution solution, which was made from adding solid imidazole into the lysis buffer to give a final concentration of 250mM imidazole. (Note: desolving that much imidazole in the lysis buffer changes its pH to about 8.9. This will lead to the crashing out of IκBζ soon after elution. That is why the pH has to be readjusted to pH 7.4 before is used. This was a huge breakthrough in the development of the protocol). The eluted protein was collected in a series of 1mL fractions (Figure II.2A). Fractions were analyzed by SDS-PAGE and peak fractions were combined right away with NF-κB binding partner as His-tagged IκBζ(404-718) does not keep well by itself and must be complexed to p50 before the end of the day.

1.3 Expression and Purification of Recombinant GST-tagged IκBζ

Since the expression and purification of GST-tagged IκBζ is so similar to that of His-tagged IκBζ, only the differences will be discussed below. First, because GST-tagged IκBζ has a different tag than that of His-tagged IκBζ, it has to be purified via affinity chromatography with glutathione sepharose 4 fast flow (GE Biosciences) resin. The amount of packed resin used in the column was about 5mL. Second, the elution buffer components for this protein were 10mM glutathione, 25mM Tris-HCl pH 7.4, 500mM NaCl, 10mM β-ME and 0.5mM EDTA. The addition of glutathione to the buffer decreases the pH. Therefore, it was readjusted with the addition of NaOH.

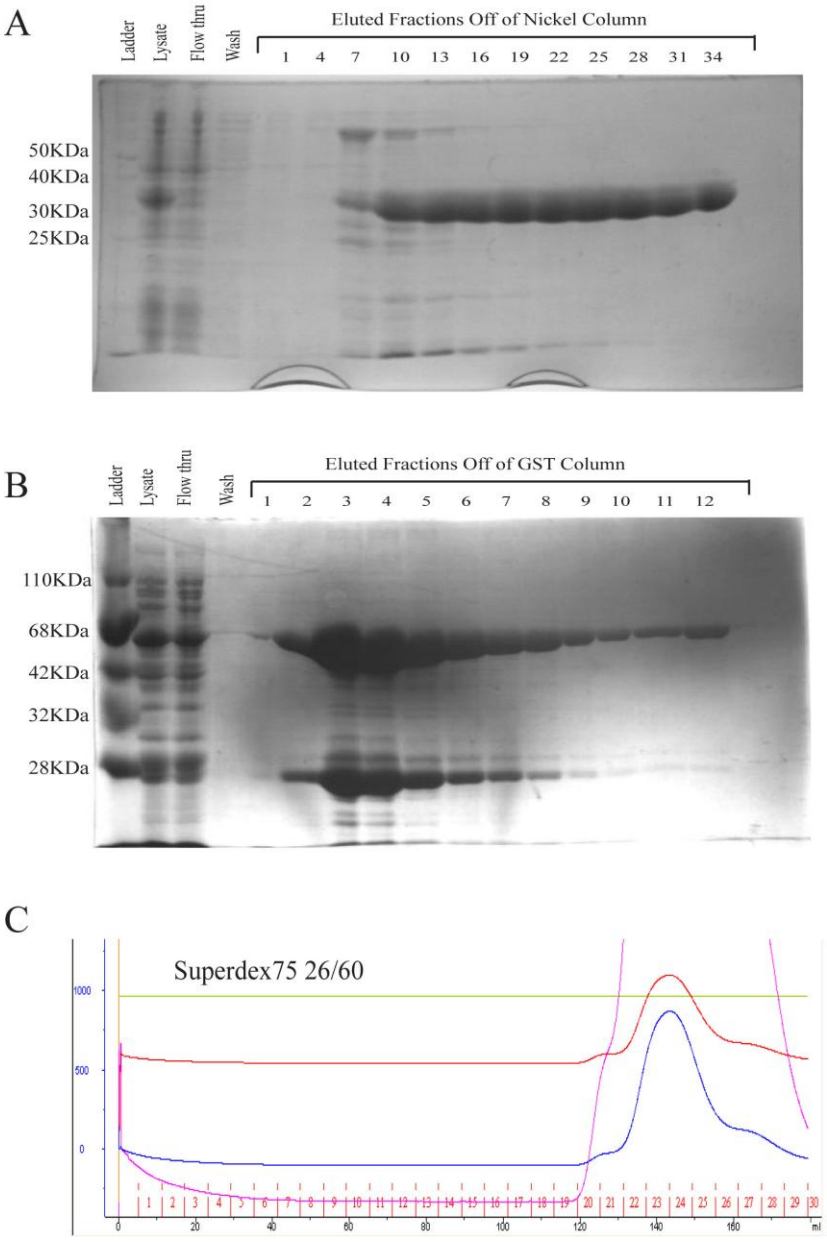

Figure II.2 A. SDS PAGE analysis of His tagged IκBζ(404-718) samples as its being eluted off of the nickel affinity column. B. Fractions of GST tagged IκBζ(404-718) as it came off the GST affinity column. The bands with 28KDa correlate to the free GST. C. Size exclusion chromatograph of GST tagged IkBz(404-718) as it came off of Superdex75 26/60 column.

After the sample was eluted off the column the fractions containing the bulk of the protein, which were fractions 2-5 (Figure II.2B), were concentrated down with centriprep-30. Once the volume had gone down to around 2mL it was filtered with a 0.2μm filter and loaded onto the Superdex200 26/60 size exclusion column (GE). The running buffer for the column is composed of 25mM Tris-HCl pH 7.4, 500mM NaCl, and 1mM DTT. The fractions under the peak were pooled and concentrated with Centriprep-30 (Figure II.2C). The concentration of the protein was monitored by absorbance at 280 nM. The protein was stored away in the range of 6mg/mL by flash freezing with liquid nitrogen.

2. Formation of the p50(245-376)/ His-tagged IκBζ(404-718) Complex

2.1 Complex Formation

Because p50(245-376) is a much more soluble protein than IκBζ, it was purified one day ahead and left in the cold room overnight prior to IκBζ purification. All of the following steps were then carried out at 4°C. Before mixing the two proteins together, an exact molar concentration for each was determined by absorbance at 280 nm. His-tagged IκBζ and p50(245-376) were then mixed together at a stoichiometric ratio of 1 to 4, respectively. The reason for excess p50 is to push for the complex formation so that excess p50 can ensure every IκBζ was bound to a p50 preventing it from crashing out.

The solution with both proteins was placed in a dialysis bag and dialyzed with 1liter dialysis buffer containing 25mM Tris-HCl pH 7.4, 500mM NaCl, 10mM β-ME and 0.5mM EDTA. The 1 liter dialysis buffer was exchanged three times to remove most of imidazole from the solution. This was important because imidazole interferes with thrombin digestion in the next step. The dialyzed solution was concentrated down to 30 mL with CentriPrep-10 (Millipore).

2.2 Removal of the His-tag by Thrombin Digestion

To the 30 mL solution I added enough thrombin to give it a final concentration of a unit of thrombin per 100 μg of IκBζ. This mixture was left to digest overnight with gentle stirring in 4°C. Next day the digestion was stopped by adding of PMSF to give it a final concentration of 0.5mM. The digested product was concentrated further with Centriprep 10 before being put through the Superdex200 26/60 size exclusion column (Figure II.3A). The running buffer for the column contains 25mM Tris-HCl pH 7.4, 50mM NaCl and 1mM DTT. The fractions under the peak are run on SDS PAGE gel (Figure II.3B). The ones contain the correct stoichiometric ratio of both are consolidated to be concentrated again. The success of the digestion was verified by the shifted weight of the IκBζ protein compared that to the uncut protein (Figure II.3C). The complex was concentrated to a concentration of 13mg/ml before been aliquoted and flash frozen and stored in -80°C.

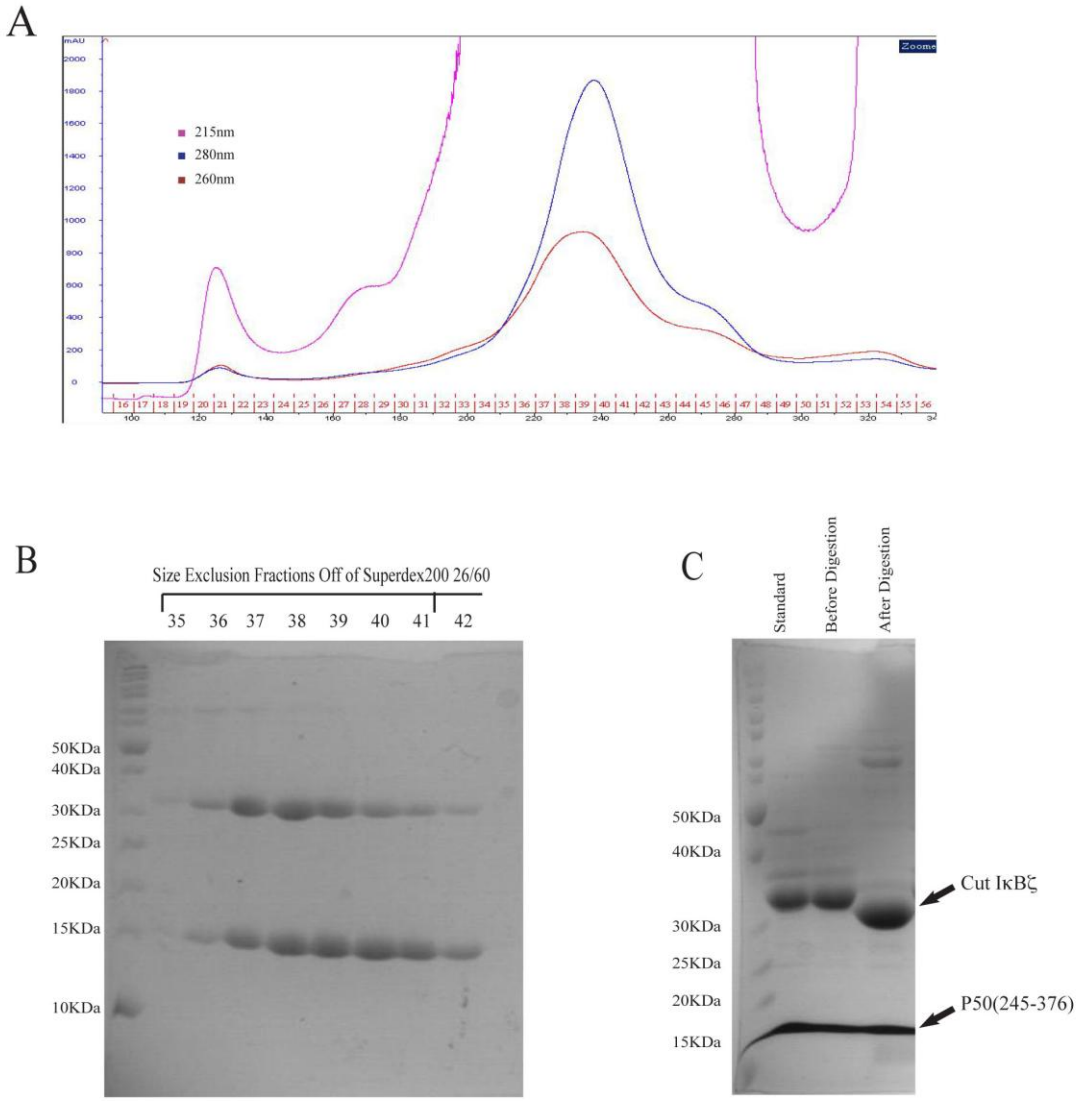

Figure II.3 A. Size exclusion chromatograph of P50(245-376)/IκBζ(404-718) complex as it was been purified by Superdex200 26/60 column. B. Fractions under the peak were analyzed by SDS PAGE followed by Coomassie Blue Staining. The gel shows the two proteins do travel as a single stable complex. C. To remove the His tag from IκBζ the complex were exposed to thrombin digestion prior to purification by gel filtration. The cut products were ran on 12% SDS gel alongside of the uncut protein. The shift of the IκBζ band confirmed the removal of the His tag.

3. Purification of DNA Oligos

3.1 Untagged DNA Oligos

The custom designed oligos were purchased from Integrated DNA Technology in single strand lyophilized form. Before it could be purified the ~1µg samples were first dissolved in 800µL of low salt solution made up of 10mM NaOH and 100mM NaCl. This solution was then spun down at 16,000rpm for 5 minutes. This got rid of any non-soluble debris that may have been in the sample. The soluble portion of the solution was sucked up in a syringe and loaded onto a source 15Q anion exchange column (Amersham) equilibrated with 90% low salt and 10% high salt solution. The high salt solution is the same as the low salt solution except with 1M of NaCl instead of 0.1M. Upon loading the column was washed with 2 column volumes (CV) of 10% high salt solution. This washed away any non-specific bound particles. The DNA was eluted off with a gradient method. The composition of the elution buffer was ramped up from 10% to 90% high salt solution over the course of 10 column volumes (Figure II.4). The peak fractions were then collected and neutralized from its high pH with 12.5µL 0.5M MES pH6.5 per mL of. The lowering of pH protects DNA from hydrolyzing effect of the hydroxide ions in high pH environment. A sample of the DNA was taken at this point and its 260nm absorbance measured. An accurate concentration of the sample was deduced from that using its extinction coefficient. This was important for the accurate pairing of the single strand oligos to its complimentary strand in a 1:1 ratio. Once the two strands were mixed together they

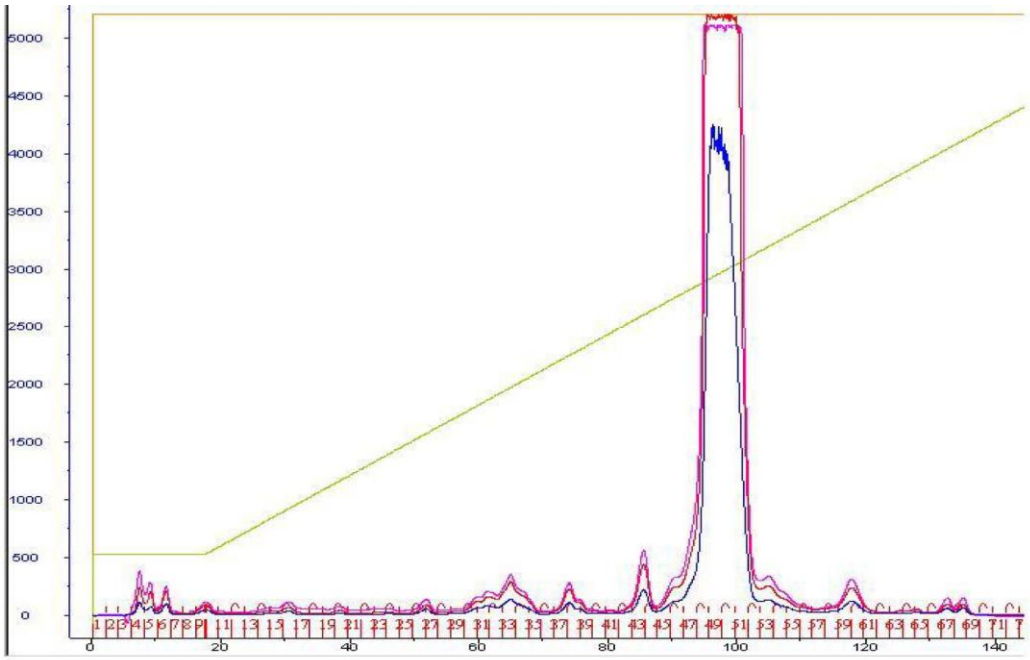

Figure II.4 Chromatograph of the IL-6 17mer sense strand as its been eluted off of the Source15Q anion exchange column. The NaCL gradient, indicated by the green line, was ranged from 0.1M to 1M over the course of 20 column volumes.

were heated to 96°C and allowed to cool down slowly over a course of 20 minutes. This allowed proper annealing of the strands. The annealed DNA was than diluted 4 times with utra-purified water to lower its salt content. This solution was than loaded onto a gravity flex column packed with 2 mL of Q sepharose resin (Amersham). The column was equilibrated with water. The column was washed with 10 column volumes of water before eluted with 1M NaCl water solution. All the DNA came out within the first four 1 mL fractions of the eluted fractions. This was detected by spectrophotometer. The fractions were concentrated with centricon-3 (Millipore). During the last few spin cycles of the concentrating step, pure water was added to the sample to exchange out the high salt buffer. The spinning of the samples were stopped when the concentration reached 2 mM. The purified and concentrated samples were stored long-term at -20°C.

3.2 Biotin Linked DNA Oligos

Since biotin linked DNA oligos were not used for crystallization, its purity was not that crucial of an issue. The lyophilized single strand DNA samples were suspended in water to give a final concentration of 100μM. To ensure full occupancy of the biotinolated strand excess amount of the non-biotinylated stranded were added with a ratio of 2 to 1. The mixture was then heated to 98°C and allowed to cool down slowly to room temperature. The samples were concentrated down with centri-Con3. Since all the DNA probes were needed for kinetic and gel shift studies their relative

concentrations with each needed to be identical. That's why they were normalized to the concentration of 0.2mM with water according to their absorbance at 260nm.

4. p50/ IκBζ Structural Determination

4.1 Crystallization

IκBζ(404-718):p50(245-376) complex crystals were grown by the hanging drop vapor diffusion method. 1 μL of protein complex (13mg/mL) was mixed with 1 μL of reservoir solution containing 20mM acetic acid pH 5.2, 80mM acetic acid pH 5.8, 5.5% polyethylene glycol (PEG) 3350, 10 mM DTT, and 0.5% of 1,2,3 heptanetriol. To help with the nucleation process, the hanging drops were made to exhibit irregular shapes. This was done by dragging of the pipette tip against the cover slip as the protein is being mixed. The sealed crystal tray was then left in 30°C to equilibrate. Rod-shaped crystals were grown out of this condition in about two to three days. Most of the crystals are needle-shaped and very thin. But occasionally a larger rod-like crystal could be seen among the bunch (Figure II.5A). Those were collected for x-ray diffraction experiments.

4.2 Handling and Cryo-Protection of the Crystals

To freeze the crystals for x-ray diffraction data collection, the biggest of the rod-shaped crystals was transferred into a cryo solution containing 20mM acetic acid

pH 5.2, 80mM acetic acid pH 5.8, 16% PEG3350, 10mM DTT, 0.5% 1,2,3 heptanetriol and 22% 2-methyl-2,4-pentanediol (MPD). Essentially, it is just the reservoir liquid with the PEG3350 concentration increased to 16% and 22% MPD added. The crystals behaved well in the cryo solution, no cracking or rounding of the edges of any sort was observed in the process. After soaking for 30 seconds, the crystals were flash frozen in liquid nitrogen.

4.3 Collection of the X-ray Diffraction

Diffraction data were collected remotely on Beamline 8.2.2 at the Advanced Light Source in Lawrence Berkeley National Laboratory. The beamline generates a hard X-ray in the range of 6-15 keV. During the time of collection the beam intensity was attenuated to produce an X-ray with an output power of 1.240keV which correlates to a wave length of 0.99nm. The diffraction pattern, which showed diffracted to 2.0Å, was collected on a 3x3 CCD array (ADSC Q315) detector (Figure II.5C). A total of 512,272 reflections were collected with 330 rejections. The I/sigma ratio for the outer shell was determined to be 2.097. All data processing was done with HKL2000 (Otwinowski and Minor, Academic Press, 1997). The crystal was

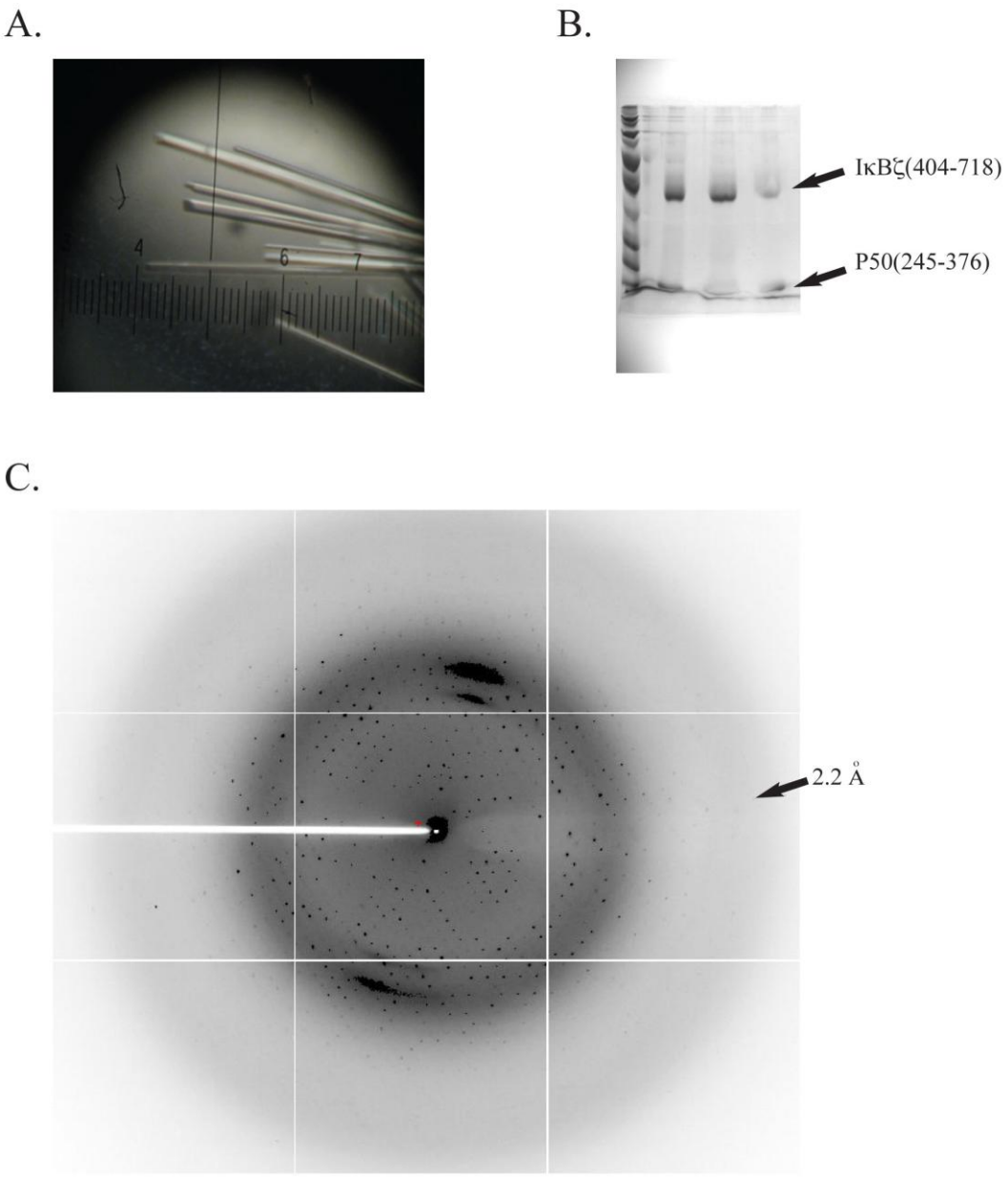

Figure II.5 A. IκBζ(404-718)/P50(245-376) crystals that grew out over the course of three days. Single rods were broken off from the spindle were used for data collection. B. To ensure the crystals contain both proteins they were analyzed with SDS PAGE gel and developed with silver stain. For unclear reason P50(245-376) does not respond well to silver stain but its presence can be confirmed by the negative imprint. C. A sample of the diffraction images generated by the crystal. The CCD detector picked up signal all the way to 2.0A.

determined to be made up of monoclinic unit cells with the space group of $P2_1$. The dimensions of the unit cell are a=51.57Å, b=59.12Å, c=109.57Å and α=90°, β=98.79°, γ=90°. The Matthew's coefficient and solvent content calculations (Matthews, 1968) that there is only one complex per asymmetric unit.

4.4 Structural Determination

The molecular replacement (MR) method was used to obtain a first estimate of phases for model building and refinement. The model used for the IκBζ was the Bcl-3 ankyrin repeat domain structure solved by the Müller group (Michel et al., 2001). For the p50 dimerization region I used the dimerization domain from the NF-κB p50 homoderim:IL-6 κB DNA complex structure. The two pieces were inputted into the Phaser (McCoy et al., 2007) software as two independent ensembles. The resolution range used for the search was limited from 10Å to 4Å. Sequence identity for p50 DD was set at 99% and 40% for between Bcl-3 and IκBζ. The number of complexes in the asymmetric unit was determined to be one by the Matthew's Coefficient Program (Matthews, 1968) from CCP4. The two components of the asymmetric unit were defined as a protein with the MW of 30.6 kDa, referring to the p50 dimerization domain, and another protein with the MW of 33.7 kDa, referring to IκBζ. With these settings Phaser generated a solution that gave an R-free value of 43.72% on Refmac (Murshudov et al., 1997).

4.5 Model Building and Refinement

Most of model building and refinement were done with Coot (Emsley and Cowtan, 2004) and Refmac5 (Murshudov et al., 1997). Minute changes were first done in Coot and verified by restrained refinement in Refmac5. Changes were kept if they lowered the R-free value after maximum likelihood restrained refinement by Refmac5. To avoid introducing phasing errors in the refinement process initial refinements were done with lower resolution data. Once the all possible improvements were exhausted more data was allowed in for the next round of refinement. This process was repeated until all the data were used. To assess the overall geometry, the model was analyzed in Molprobity (Chen et al., 2010) from the Phenix (Adams et al., 2010) software package. It red flags all the Ramachandran, rotamer, and geometry outliers. These were incorporated into the next round of refinement. Towards the end of the refinement process the best overall model was fed into Autobuild program (Terwilliger et al., 2008) in Phenix (Adams et al., 2010). This program is very good at identifying water molecules and adding them to the model. That brought down the R-free value dramatically. However, since the software cannot differentiate patchy electron density from immobilized water molecules it can make mistakes. Therefore, every water molecule was then examined manually to determine whether it fit the profile of an ordered water (hydrogen bonding partners, distances, geometries, B-factors). If not the molecule was removed from the model. A new electron density map was generated from this model and used for one more round of refinement. In the end, the refinement was stopped at an R-free value of 21.19%.

5. p50/IL-6 Structural Determination

5.1 Crystallization

Crystal of the NF-κB p50(39-363) homodimer in complex with κB DNA from the promoter of human IL-6 gene were grown by the hanging drop vapor diffusion method. 1 μL of protein was mixed with 1 μL of reservoir liquid containing 16% of PEG 1500 and 100mM of Na Acetate pH 4.9 and diffused against 1 mL reservoir solution. The tray was left in room temperature (20°C) and one single hexagonal shaped crystal grew up in about seven days (Figure II.6A).

5.2 Handling and Cryo-Protection of the Crystals

The single p50:IL-6 κB DNA complex crystal was harvested with a nylon loop and placed into a cryo protectant solution with 25% glycerol, 20% PEG 1500, and 100 mM Na acetate pH 4.9. The crystal did not show any adverse effect in the solution. No visible changes were observed in the appearance of the crystal. After 30 seconds or so the crystal was removed from the cryo protectant solution and flash cooled in the liquid nitrogen.

A.

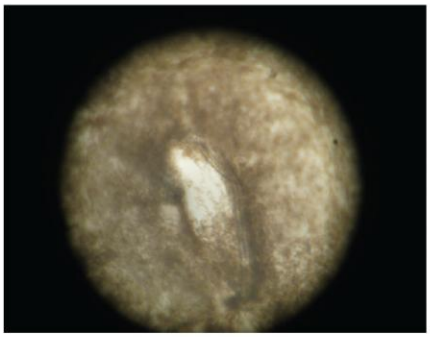

B.

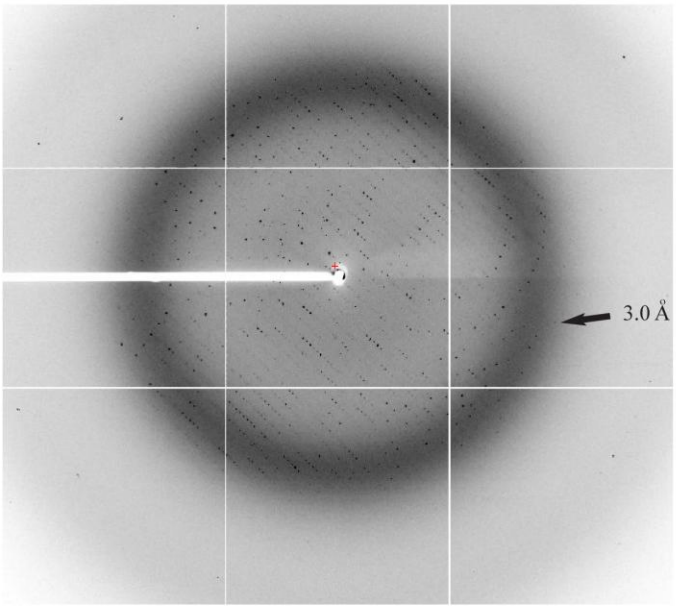

Figure II.6 A. P50(39-363)/IL-6 crystal grew out over the course of seven days. It grew out of the aggregates and gave an appearance of stacked plates. This turned out not to be a single crystal since it ultimately gave us the p50/IL-6 structure. B. A sample of the diffraction images generated by the crystal. The CCD detector picked up signal all the way to 2.8Å with I/s of 2.04 on the outer shell.

5.3 Collection of the X-ray Diffraction

X-ray diffraction data on the p50:IL-6 κB DNA complex crystal were collected at the National Synchrotron Light Source (NSLS) in Brookhaven. We used the wiggler beamline X25 which support a X-ray with energy output of 5-20 keV and beam dimension of 0.25mm H x 0125mm. The wavelength was set at 1 Å during the shooting and the diffraction pattern was collected on ADSC Q315 CCD x-ray detector. A total of 396,510 diffractions were collected. Complete data could be collected to a resolution of 2.8 Å with an I/sigma ratio of 2.04 on the outer shell (Figure II.6B). All data processing was done with HKL2000 (Otwinowski and Minor, Academic Press, 1997). The crystal was determined to be made up hexagonal unit cells with the space group of $P6_5$. The dimensions of the unit cell are a=162.24Å, b=162.23Å, c=60.43Å and α=90°, β=90°, γ=120°. Matthew's coefficient calculation (Matthews, 1968) predicted one molecule per asymmetric unit.

5.4 Structural Determination

The phase information for the p50:IL-6 κB DNA complex crystal structure was solved by using the molecular replacement method. The structure used for the replacement was the p50 homo-dimer bound to κB DNA solved by the Ghosh group (Ghosh et al., 1995). Since both crystals were prepared from the same construct of p50, amino acids 39-363, no residues were removed from the original model. In anticipation of possible conformational changes between the two structures, the search

model was separated into four parts: The dimerization domains, two N-terminal domains, and the DNA. They were fed into the Phaser (McCoy et al., 2007) program as separate ensembles and assigned a MW of 26,668 Dalton for the dimerization domains, 23,165 Dalton for each of the N-terminal domains and 660 Dalton for the DNA portion. A rotation search followed by translation search in Phaser resulted in one clear solution.

5.5 Model Building and Refinement

Most of model building and refinement were done with software program Coot (Emsley and Cowtan, 2004) and Refmac5 (Murshudov et al., 1997). Minute changes to the structure were done in Coot and verified with Refmac5. Any change that lowered the *R*-free values were kept. To limit the amount of phasing error introduced in each round of refinement only low resolution data were used in the initial refinements. Once all the possible improvements were exhausted then more data were added to the next round of refinement. This process was repeated until all the data was used. To improve the geometry, the model was analyzed by Molprobity (Chen et al., 2010). It flags all the Ramachandran, rotamer, and geometry outliers. These were incorporated into the next round of refinement. The refinement was finally stopped when the *R*-free value reached 26.67%.

6. p50/NGAL Structural Determination

6.1 Crystallization

The p50(39-363):NGAL κB DNA complex crystals grew from 2 µL hanging drop that contained 6.5 mg/mL of p50 with 2× amount of DNA was suspended in 50mM acetic acid pH5.4, 0.01mM $MgSO_4$ and 2% PEG 3350. This solution equilibrated against a 1ml reservoir contained 100mM acetic acid pH 5.4, 0.02mM MgSO4 and 4% PEG3350. The p50:NGAL κB DNA complex produced rod-like shaped crystals that grew overnight at room temperature (Figure II.7A). The initial characterization of these crystals indicates that they belong to the monoclinic space group C2 with unit cell dimension of a=68.07Å, b=103.34Å, and c=128.5Å.

6.2 Handling and Cryo-Protection of the Crystals

Crystals of all sizes grew within two days of setting up the tray. Samples from each size category were taken and frozen with different cryo-protectant. In the end it was a small crystal frozen in 50% paratone and 50% 2-Methyl-2,4-pentanediol (MPD) that yield the best diffraction data.

6.3 Collection of the X-ray Diffraction

Complete x-ray diffraction data were collected at 2.8 Å resolution. Data were collected remotely from the Berkeley National Laboratory Advanced Light Source Beamline 8.2.1 (Figure II.7B). The diffraction data was collected by the on site 3×3 CCD array (ADSC Q315R) detector. All processing of the data were done with HKL2000 (Otwinowski and Minor, 1997) software package. The crystal was determined to be made up of orthorhombic unit cells with the space group of $P2_12_12_1$. The dimension of the unit cell is a=67.00Å, b=102.64Å, c=127.70Å, and α=90°, β=90°, γ=90°. Matthew's coefficient (Matthews, 1968) determination indicated that there is one complex per asymmetric unit.

6.4 Structural Determination

To obtain the phase information for the structure I used molecular replacement method through the program Phaser (McCoy et al., 2007) from CCP4i (Winn et al., 2011). The resolution range used for the determination was from 80-3.3Å. The p50 homodimer:IL-6 κB DNA complex structure was used for the search model. To allow for any movement between the domains the p50:IL-6 model was broken up into four sections: the two dimerization domains as one body, the two N-terminus domains as two separate bodies, and the DNA structure. This was done simply by editing the

A.

B.

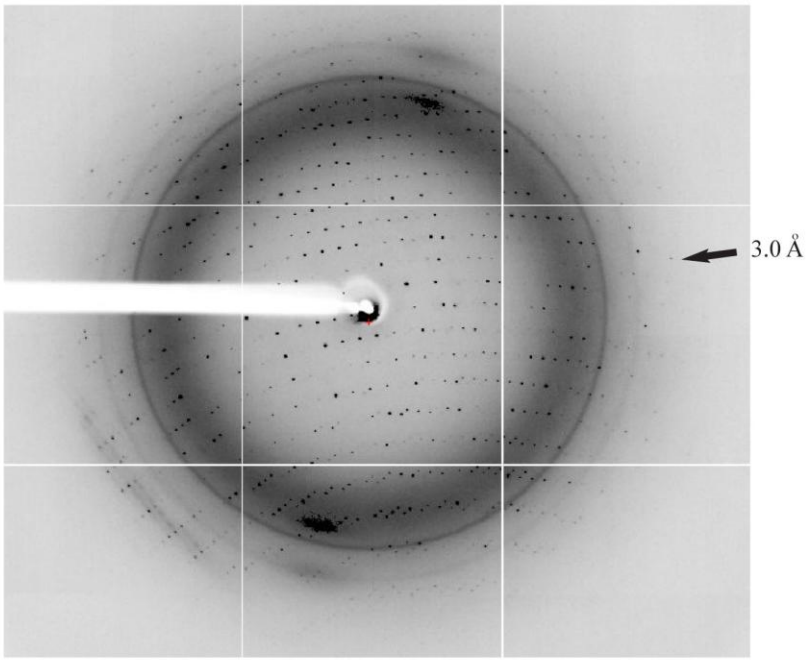

Figure II.7 A. P50(39-363)/NGAL crystal grew out over night in clear solution. The crystals were large and with some containing cracks in them. Large crystals were broken apart to give the single crystals. The broken pieces with various sizes were collected for data collection. B. A sample of the diffraction images generated by the crystals. The CCD detector picked up signals all the way to 2.8Å with I/s of 3.5 on the outer shell.

atomic coordinates from the coordinate files. Since the DNA in the IL-6 structure is longer than that of NGAL DNA, it was trimmed from the ends to contain only 10 bp. The bases were then changed to that of NGAL sequence in Coot (Emsley and Cowtan, 2004) and saved as a new .pdb file. These four structures were then loaded onto Phaser as four separate ensembles. Sequence identity for each was set at 99%. Components inside of the asymmetric unit were defined as a 26,668 Dalton unit referring the dimerization domains, two 23,165 Dalton units for the N-terminal domains and a 660 Dalton nucleic acid unit. A clear solution was found.

6.5 Model Building and Refinement

Most of model building and refinement were done with software programs Coot (Emsley and Cowtan, 2004) and Refmac5 (Murshudov et al., 1997). Minute changes were first done in Coot and verified by Refmac5. Changes were kept if had lowered the *R*-free value generated by Refmac5. To limited the amount of phasing error introduced in each round of refinement only low resolution data were used in initial refinement. Once the all the possible improvements were exhausted more data were added to the next round of refinement. This process was repeated in four stages until all the data was used.

An interesting thing we discovered during the model building process is that there are naked DNA stacked at both ends of the bound DNA. One of these naked DNA is actually part of the asymmetric unit. I went back into the molecular

replacement program and added another DNA to the ensemble list. The solution generated by the program placed the lone DNA. Using the show symmetric unit function in Coot I manually cut and pasted the floating DNA into its correct position in the asymmetric unit. The discovery of this packing order would explain why excess DNA was required for the crystallization process.

To assess the geometry of the model we used program Molprobity (Chen et al., 2010). It flags all the Ramachandran, rotamer, geometry outliers, and collisions. These were incorporated into the next rounds of refinement. The refinement was finally stopped when the *R*-free value reached 28.12%.

7. Limited Proteolysis of GST-IκBζs

To assess the effect that removing the capping helix has on the rest of the IκBζ structure two different constructs of IκBζ were made, one with the capping helix, one without. Their structure stability was assayed by limited proteolysis by chymotrypsin. The recombinant proteins were expressed in *E coli.* BL21(DE3) cells and purified by affinity and size exclusion chromatography. The protein concentrations were normalized to 1.6mg/mL based on their 280 nm absorbance. Two reactions were carried out, one with 0.05 unit/μL of chymotrypsin and the other with 0.2 unit/μL. The digestion was carried out in 37°C and with buffer contained 25mM Tris-HCl pH 7.5, 50mM NaCl and 1mM DTT. Samples were taken out at time points 0 min, 30 min, 1 hr and 2 hrs. The reaction was stopped by addition of 4× SDS loading dye and

boiling at 98°C for 5 min. The digested products were analyzed by running on a 12.5% SDS PAGE gel and staining with Coomassie dye.

8. Protein Stability Study by Circular Dichroism

Note: All protein stability studies by circular dichroism (CD) were generously done by Dr. David Heidary at University of Kentucky.

8.1 Thermal Denaturization

Briefly, for the thermal denaturation experiment the proteins were assayed at 0.18 mg/mL in buffer (50 mM K_2HPO_4, 10 mM NaCl pH 7.6). The temperature ranged from 20 to 80°C with 222 nm absorbance data collected every 2°C while full spectra from 190 to 250 nm were collected every 10°C. All temperature data measured at 222 nm and plotted against elipticity.

8.2 Urea Denaturization

For the urea denaturation experiment the proteins were assayed at 0.18 mg/mL in buffer (50 mM K_2HPO_4, 10 mM NaCl pH 7.6 and various urea amounts). The concentrations of urea ranged from 0.5 to 8 M with the doubling of its amount every increment. A full absorbance spectra, from 190 to 250 nm, were collected for every

IκBζ(404-718) sample. For IκBζ(437-718), only 0 and 7.5M urea samples had their full spectra collected. All urea data measured at 222 nm and plotted against elipticity.

9. Mutations by QuickChange Site Directed Mutagenesis

9.1 p50 KEE to p50 AAA

Residues 354-356 of p50(245-376) were mutated to alanine to assess their importance in binding to IκBζ. Site-directed mutagenesis by PCR was used to do this. The Stratagene QuickChange protocol was adopted for this experiment.

The primer design:

Sense: 5'-CTACTACCCTGAAATCAAAGACAAAGAGGAAGTGCAAAGGAAACGCCAG-3'

Anti: 3'-GATGATGGGACTTTAGTTTCTGTTTCTCCTTCACGTTTCCTTTGCGGTC-5'

Reaction mixture

- 1μL template pet11a p50(245-376)
- 1.25μL of 0.1μg/μL of sense and antisense primers
- 5μL of 2mM dNTPs
- 5μL 10× pfu running buffer
- 1μL pfu polymerase
- 35μL of water

==========

50μL Total

Thermal cycles

- 95°C 2min
- 95°C 30sec
- 55°C 1min 18×
- 68°C 7min
- 68°C 5min

9.2 p50 RKR to p50 AAA

Residues 357-359 of p50(245-376) were mutated to alanine to assess their importance in binding to IκBζ. Site-directed mutagenesis by PCR was used to do this. The Stratagene QuickChange protocol was adopted for this experiment.

The primer design:

Sense: 5'-GACAAAGAGGAAGTGCAAGCGGCAGCCCAGAAGCTTATGCCGAAC-3'

Anti: 3'-CTGTTTCTCCTTCACGTTCGCCGTCGGGTCTTCGAATACGGCTTG-3'

Reaction mixture

- 1μL template pET11a p50(245-376)

- 1.25μL of 0.1μg/μL of sense and antisense primers
- 5μL of 2mM dNTPs
- 5μL 10× pfu running buffer
- 1μL pfu polymerase
- 2.5μL of dimethyl sulfoxide (DMSO)
- 35μL of water

==========

50μL Total

Thermal cycles

- 95°C 2min
- **95°C 30sec**
- **55°C 1min 18×**
- **68°C 7min**
- 68°C 5min
- 0°C Finished

10. GST-IκBζ Pull-down Assay

All recombinant GST-IκBζ and NF-κB proteins were expressed in *E coli.* BL21 (DE3) cells. GST-tagged proteins were first purified with Glutathione Sepharose 4 Fast Flow Affinity column (GE Biosciences) and NF-κB with SP

Sepharose Fast Flow column (GE). All were passed through size exclusion as the final cleanup step. The final protein concentrations were determined by their absorbance of 280 nm. During the pull-down the two proteins were first mixed together at various molar concentrations in a binding buffer containing 25mM Tris-HCl pH 7.4, 50mM NaCl and 1mM DTT. The typical concentrations ranged from 0.1μM to 4μM with a total volume of 250μL. The proteins were allowed to bind in room temperature with gentle rotation for 30min. After incubation the mixture was transferred to another tube with 20μL of pre-equilibrated Glutathione-sepharose resin. The mixture was incubated for 10 minutes with gentle rotation at room temperature. To collect the resin all samples were spun down at 7,000 × g for 1min. The supernatant was carefully removed with a pipettor without disturbing the resin. This is done by leaving ~100μL of solution behind. It is crucial that all samples retain same amount of resin throughout the whole process. For each wash, 1mL of binding buffer was added to each sample and placed back on the tumbler for 5min. After the wash the samples were spun down at 7,000 × g for 1min. The supernatant was drawn out carefully with a pipettor. This is considered one wash and was repeated three times. At the end of the washes a smaller pipettor was used to remove all of the supernatant. To extract what is bound to the resin, 20μL of 2× SDS loading buffer were added to each sample. They were placed on 98°C heating block for 5min. The samples were analyzed on 12.5% SDS PAGE gels.

11. Surface Plasmon Resonance

Note: All Surface Plasmon Resonance (SPR) experiments were performed with the generous assistance of Mingde Zhu, a senior scientist at Bio-Rad who happens also to be the researcher's father. Mr. Zhu carried out the experiments free of charge and provided us his expertise every step of the way. My lab and I are deeply indebted to him.

11.1 IκBζ and p50 Interactions

Sensorgrams were recorded on a Bio-Rad Proteon XPR36 instrument using His-tag capture chip (Bio-Rad). The multichannel chip design allows for monitoring of six sets of interactions simultaneously (Figure II.8A). In order to activate the chip 100μM of nickel sulfate was loaded onto the chip. Four of the six channels were labeled with His-tagged IκBζ proteins, two for each construct of protein. Since it was uncertain how much immobilized IκBζ would give us the best result, two different concentrations were used for each protein. In the end, 0.005mg/mL proved to be the best. The two empty channels were used as control, "labeling" them with the running buffer (10mM phosphate pH 7.4, 150mM NaCl, 0.05% Tween-20 and 0.05% of BSA). Following a brief wash, five different concentrations of p50, in the range of 50nM to 3.12nM, were flowed over the chip simultaneously at the rate of 100μL/min. This was done for 150sec during which the on rate of the binding were monitored. This was followed by 350sec period of washing when disassociation of p50 was monitored.

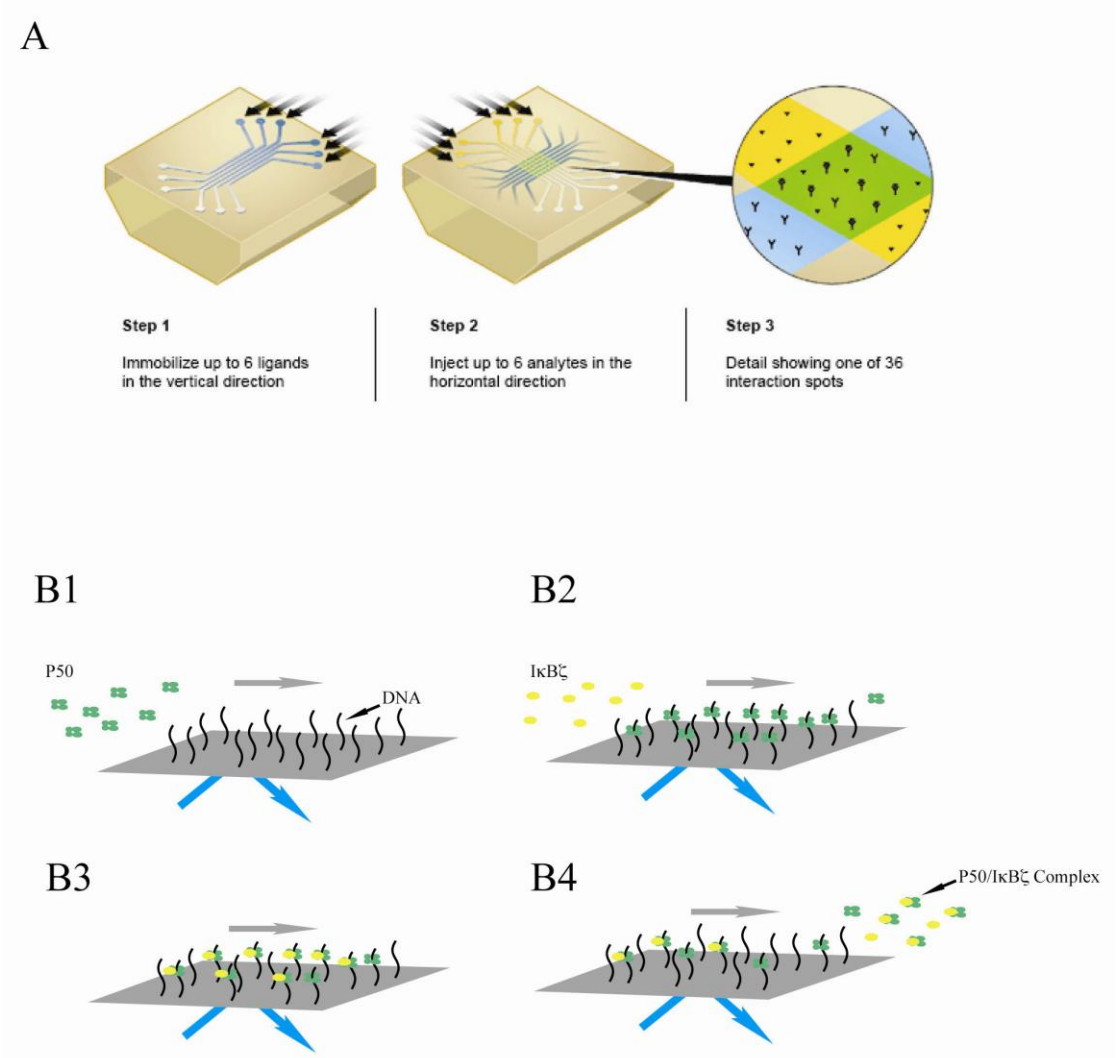

Figure II.8 A. Illustration showing the loading of ligands and the detection of the analytes in the multi-channel system. SPR is great at measuring the binding affinity of a single ligand against a single specie of substrate, such as the case in P50 and DNA. However, in the case of a multi-ligand and substrates system the detection can only be qualitative. This is because the instrument cannot differentiate the different disassociations from one another. This concept is demonstrated in Figure B1-B4. As P50 and IκBζ disassociate from the DNA (B4), the instrument can only detect lost of mass but not which type of protein.

The disassociation constant (K_D) was calculated by dividing the off rate (k_{off}) from the on rate (k_{on}). Sensorgrams were analyzed by ProteOn Manager Version 2.0 software (Bio-Rad) to determine the rates of association and dissociation. We used homogenous single-state binding mode for presupposed search model as it gave the best fit. All experiments were performed at 25 °C

11.2 IκBζ and DNA Bound NFκB Interactions

The technique used to measure the interaction between IκBζ and DNA bound NF-κB is very similar to that described above. Briefly, all interactions were done in a running buffer containing 10mM phosphate pH 7.4, 150mM NaCl, 0.05% Tween-20 and 0.05% of BSA and at flow rate of 100μL/min. To immobilize DNA to the chip surface we used Streptavidin NCL chips with biotinylated DNA. To give flexibility and sufficient space to bind one of the DNA strand contain an18 poly-adenosine linker with a biotin at the 5' end. This strand is coupled to a 17 bases complementary strand.

IL-6 Probe: `Biotin-5'AAAAAAAAAAAAAAAAAATGTGGGATTTTCCCATG -3'`

`3'-ACACCCTAAAAGGGTAC-5'`

The DNA ligand was loaded onto the chip at a concentration of 10nM. After a 3min wash NF-κB at a concentration of 50nM were loaded onto the DNA. The binding was allowed to reach its saturation point, which took about 3min. After

washing for 3min different concentrations of IκBζ were flowed over the complex. This lasted for 3min before following with a wash. No K_D was determined for this type of three component experiment because there are two disassociations happening simultaneously, one between DNA and NF-κB and one of NF-κB and IκBζ (Figure II.8B). What this experiment did tell us was whether IκBζ dislodges NF-κB from DNA. This was determined by comparison of the sensorgrams from two channels, one with IκBζ added and without. If the presence of IκBζ had increased the rate of NF-κB disassociation then that would indicate IκBζ dislodged that particular NF-κB from that particular DNA sequence. If NF-κB disassociation rate was unaffected it would mean the opposite.

12. Eletrophoretic Mobility Shift Assay

DNA probes were prepared in the laboratory by denaturing SDS-PAGE purification of single-stranded DNA oligonucleotides (IDT). One strand was next labeled with ^{32}P in a reaction catalyzed by T4 polynucleotide kinase (New England BioLabs) according to the manufacturer's instructions. The labeling reaction was cleaned up by passage through a microspin G25 column (GE Healthcare) and the labeled oligonucleotide was annealed to its complement. Electrophoresis was run as continuous native polyacrylamide gels in 1× TGE buffer (24.8 mM Tris-HCl base, 190mM glycine, and 1 mM ethylenediaminetetraacetic acid, pH 8.0). Appropriately diluted samples of NF-κB and IκB proteins were mixed in binding buffer to a final

composition of 10 mM Tris–HCl (pH 7.5), 50 mM NaCl, 10% (v/v) glycerol, 1% (v/v) NP-40, 1 mM EDTA (pH 8.0), 0.1 mg/mL poly(dI-dC), 0.2 mg/mL BSA, and 1 mM DTT. After incubation for 30 min, radiolabeled κB DNA probe (0.001–2μCi) was added. The order of mixing proteins and DNA did not affect the outcome of this equilibrium experiment. After pre-running the gel for approximately 1 h at 200 V and rinsing each of the loading wells with 1× TGE, samples were run at 200 V for approximately 90 min. The gel was then dried and exposed overnight to a phosphorimage plate (GE Healthcare). The gel was scanned by a Storm 860 phosphorimage plate reader and band intensity was quantified by ImageQuant TL software version 2005 (GE Healthcare).

IL-6 κB DNA Probe:

5'-AGA TTT ATC AAA TGT **GGGATTTTCCC** ATG AGT CTC AAT ATT-3'
3'-TCT AAA TAG TTT ACA **CCCTGAAAGGG** TAC TCA GAG TTA TAA-5'

Chapter III

Results

1. DNA P50 Homo-dimer Complex Structure

1.1 IL-6 p50 Homo-dimer Structure

1.1.1 The Overall Structure of p50 Homo-dimer

Note: Because the p50 homo-dimer structure contains two p50 subunits, to distinguish the two, the subunit contacting the three consecutive guanines on the sense strand is designated A, and the other subunit B.

The x-ray crystal structure of NF-κB p50(39-363) homodimer bound to the IL-6 17-basepair promoter κB site was solved by molecular replacement and refined against diffraction data that was complete to a resolution of 2.8 Å. All the refinement statistics associate with the structure are listed in Table III.1. The overall structure is very similar to that of the published structures of p50 homodimer bound to κB site (Ghosh et al., 1995) and p50 homodimer on MHC class enhancer site (Müller C., Nature, 1995). The protein is separated into two well-ordered domains with a flexible linker in the middle. Both domains contain β-barrels similar to that found in immunoglobulin (Ig) fold (Bork, J.Mol.Biol, 1994). To better distinguish the two domains, the one near the amino-terminus will be referred to as N-terminal domain (NTD), and other one as the dimerization domain (DD) because of its role in mediating dimerization between the two p50 subunits (Figure III.1A).

Table III.1 Data collection and refinement statistics

	p50/IL-6
Data collection	
X-ray source	NSLS#25
Wavelength (Å)	1.0000
Space group	P65
Unit cell	
a	162.17 Å
b	162.17 Å
c	60.38 Å
α	90.00°
β	90.00°
γ	120.00°
Molecules/asymm. unit	1
Resolution range (Å)[1]	50.00 – 2.80 (2.85 – 2.80)
R_{sym} (%)	7.9 (59.4)
Observations	112,366
Unique reflections	22,645 (1,144)
Completeness (%)	100.00 (100.00)
Redundancy	5.0 (5.0)
<*I*/□>	17.93 (2.04)
Refinement	
R_{cryst} (%)	20.63
R_{free} (%)[2]	26.79
Protein atoms	5599
R.m.s.d.	
Bond lengths (Å)	0.013
Bond angles (°)	1.630
Mean *B* factors(Å^2)	58.23
Ramachandran plot[3]	
Favored	90.00%
Allowed	9.84%
Disallowed	0.16%
PDB accession code	

Data in parentheses are for highest resolution shell [2]Calculated against a cross-validation set of 5.0% of data selected at random prior to refinement.[3]Calculated from MOLPROBITY

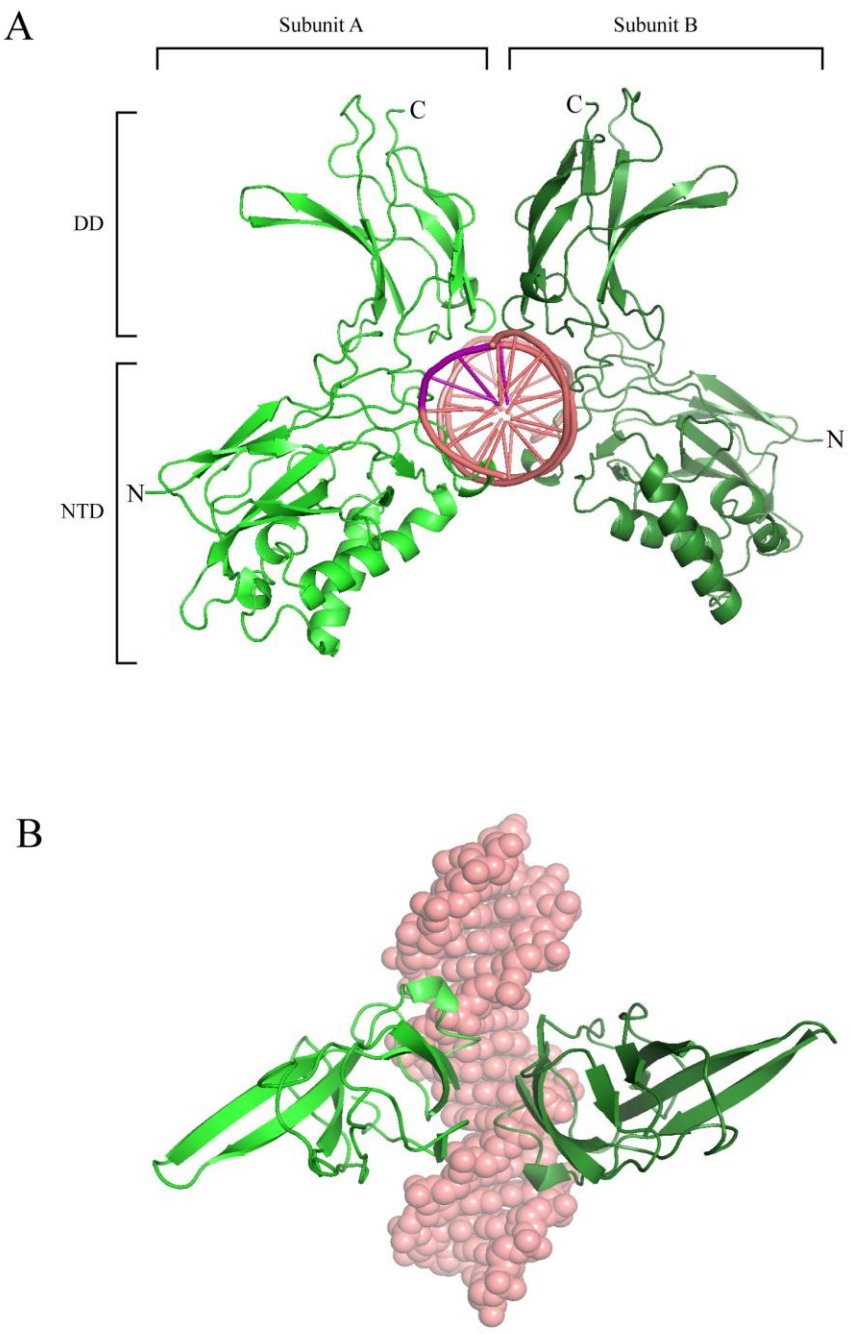

Figure III.1 A. Overall structure of P50(39-363) homo-dimer bound to IL-6 DNA. The two subunits of p50 are designated as A and B, with A being the subunit (in light green) making base contacts with the three consecutive guanines (in purple) on the sense strand. B. Image showing the rotation symmetry exists between the dimerization domains (DD).

The NTD structure can be classified as an I-type Ig barrel made up of three anti-parallel β-strand sheets and four alpha-helices. Two of the larger sheets make up the walls of the barrel and the smaller sheet hovering over the opening of the barrel like a lid. The helices interact with each other to form a bundle like structure that sits next to the barrel. The group looks as though it can be separated into two independent domains but the interaction between the two are so strong they move as a whole.

The structure of DD is that of a C-type Ig barrel with three β-strand sheets forming the walls. When dimerized, the two DDs related to each other by a 180° rotational symmetry down the vertical axis of the interface (Figure III.1B).

The DD and the NTD are connected by a flexible linker about ten residues long. The linker allows the two NTDs to spread, rotate and slide back and forth relative to the DDs, very much like that of legs on a person. This flexibility allows the p50 homo-dimer to dock on DNA like a person riding on top of a horse. In this comparison, the horse is the DNA, the torso of the rider being the two DDs and the two legs of the rider are the two NTDs (Figure III.2A). However, the two NTDs of p50 are not exactly orthogonal to the DNA. Rather, they are slightly slanted one from another with one NTD further upstream of the DNA and other further back (Figure III.3B). In the horse and rider analogy, it's like having one leg of the rider closer to the front of horse and the other further toward the back of the animal. The torso of the rider does not seem to be affect by this scooting of the legs. It still sits relatively square on the horse.

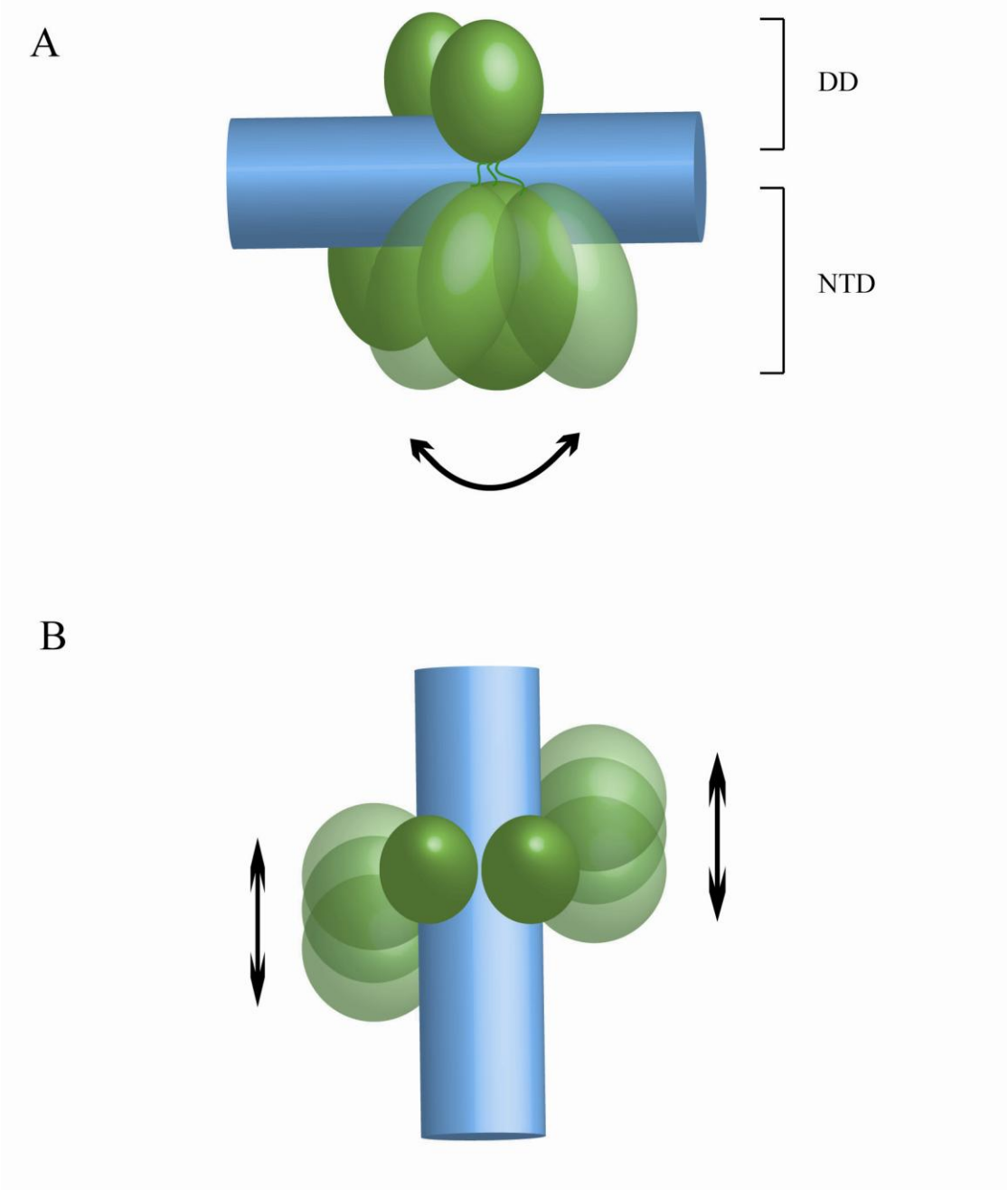

Figure III.2 A. Side view illustration of P50 demonstrating the movement of NTD relative to the DD. B. Top view illustration of NTD movement relative to each other.

1.1.2 The Dimer Interface

To help in describing the structure, I will adopt the naming convention for p50 used by the Sigler group (Gouri, Nature 1995). By that convention, all the β-strands in the dimerization domain are alphabetized in accordance to their equivalent strand found in the canonical Ig light chain (figure here). The strand closest to N-terminus is named a, and the strand furthest away is named g. No strand named d is because that equivalent strand found in IgV but is not found in p50. The dimerization process between two p50 subunits is facilitated entirely by the dimerization domain located in its C-terminal portion of the RHR. No other inter-subunit contacts are detected anywhere else in the protein. The two dimerization domains orient themselves in such a way that the two β-barrels come alongside of each other side by side. The two domains relate to each through a twofold rotational axis. The contact interface is composed of strands a, b, and e as well as a small flexible loop located at the tips of strand a and a' (Figure III.3). The interface buries 1,354 $Å^2$ of solvent accessible area. The interaction between the two domains is so tight and rigid that the two domains move as single unit. Comparison of all the dimerization domains from four solved p50 homodimer structures shows they are virtually identical (Figure I.4B). The average root mean square deviation (RMSD) value obtained from all the alpha carbons was determined to be 0.92Å. What that means is that if you were to randomly pick a residue out of the IL-6 dimerization domain, its alpha-carbon position would only deviate on average of 0.92Å from its counterpart in another p50 homodimer structure. This value goes down even more, to

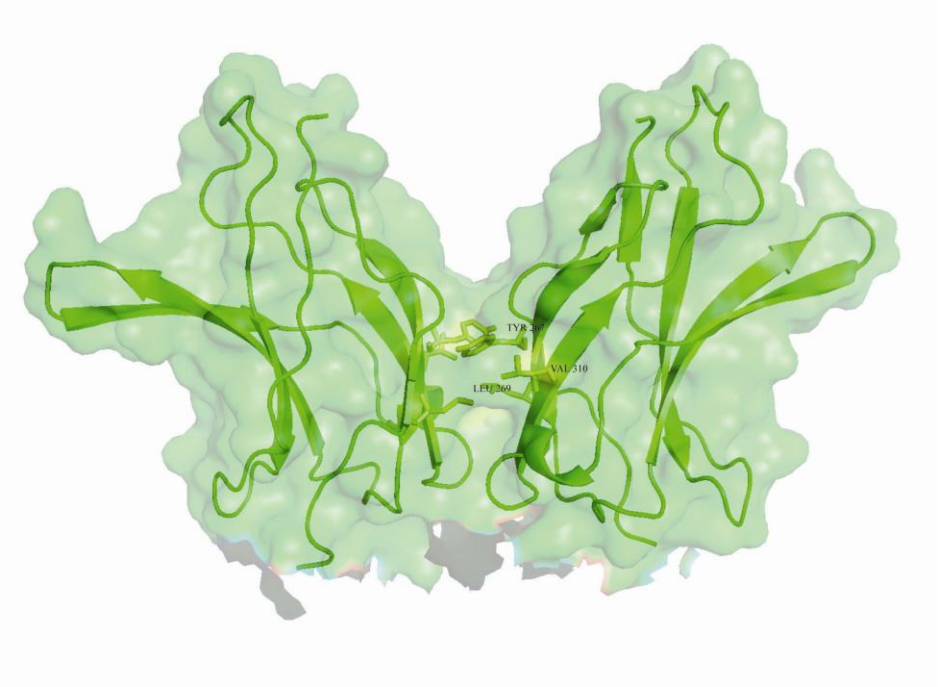

Figure III.3 X-ray structure of the dimerization domains taken from the IL-6/p50 structure. The surface contour of the region is shown in the green silhouette. The three residues (TYR 267, LEU 269 and VAL310) make up the binding "hot spot" are shown in stick figure with labeling.

0.73Å if we were to remove the flexible loops between strands e and f, c and c'. The dimerization domains as a whole vary very little from one p50 structure to another. What facilitates this rigid and tight binding are the eighteen amino acid side chains, nine from each subunit, in the interface. Of those nine side chains, three are engaged in hydrogen bonds, two in ionic bonds, and three in hydrophobic interactions.One of the hydrogen bonds is between Asp254 and its counterpart from the other subunit. This is quite unusual, but not unprecendented, since negative charges typically repel each other. However, buried at the interface within a relatively non-polar environment the pK_a of the aspartic acid side chains appears to change considerably. This is because it is more energetically favorable to hold on to that hydrogen, which balances out the two negative charges from the two aspartic acid side chains, than to have a charge in nonpolar environment. The second hydrogen bond is orchestrated by the hydroxyl group on Tyr267 with the amine group on the Met253 backbone. The last hydrogen bond is between His304 and the carbonyl group of Cys270.

The two ionic bonds include interactions between Arg252 and Glu265 and Asp302, and their reciprocal counterpart on the other side. For the two non-polar interactions one of them is the Leu269 side chain residing in a hydrophobic pocket made up of Val310, Ala308, and the side chain of Tyr267. The other non-polar interaction is carried out by the side chain of Phe307 with the hydrophobic portion of Arg305 side chain. Of all these interactions, Try267 has been shown to be the most important (Gouri, JMB, 1999). Point mutation on the position to an alanine reduced the dimer interface stability by 2.0 kcal/mol. Leu 269 and Val310 also significantly

destabilized the p50 interface. Together these three residues constitute the "hot-spot" of protein-protein interaction within p50 dimerization.

1.1.3 NF-κB p50 Homo-dimer and IL-6 DNA Interactions

In order to describe the IL-6 κB DNA structure with some clarity the bases are numbered S1 to S17 for the sense strand and AS1 to AS17 for the anti-sense strand. The two subunits of p50 are designated as A or B, A being the subunit making the base specific contacts on the three consecutive guanines on the sense strand. As previously described, the NF- κB p50 homodimer docks on the IL-6 DNA like rider saddled on a horse, the two N-terminus domains being the legs, and the dimerization domains being the torso of the rider. In this conformation, p50 contacts DNA with its dimerization domains, N-terminal domains, as well as the flexible linker that connects the two folded domains. For the dimerization domains, a loop between strand d and e touches the phosphate backbone of DNA with its Arg305 and Gln306 (Figure III.4). The contacts are made on phosphate of guanine S6 and phosphate of adenine S7, respectively. Another loop between strand b and c reaches down with its Gln274 and Lys275 to touch the phosphate group on guanine S6 and adenine S7, respectively. Because the two subunits in the dimerization domain are completely symmetrical, the same contacts are replicated by the other subunit on the anti-sense DNA strand. All the contacts made by the dimerization domains are on the phosphate backbone of DNA and none are with the bases. The contacts are made in such way to situate the

dimerization domains on top of major groove of the DNA like a train on a track (Figure III.5A). Because DNA backbone are the same for all the bases, the dimerization domains do not seem to play a role in selectivity of the binding site but rather positioning the p50 over the major groove. This may be needed for the correct positioning of the N-terminal domains, which do contact the bases.

For the flexible linker region between the two domains Lys241 reaches out to hydrogen bond with carbonyl group on the A11 position. The identical residue on the other subunit forms the same bond with a thymine on position AS11 on the antisense strand. The position is conserved as a lysine on Dorsal (a homolog of NF-κB in the fruit fly *Drosophila melanogaster*), p52, and RelB. On p65 and c-Rel, this residue is conserved as an arginine. Because of the common charge, length, and the flexibility of these side chains, is unlikely it can discriminate one base from another. Thus it is more likely that this contact point serve to anchors the N-terminal domain in an orientation suited for binding.

Within the N-terminal domain (NTD), DNA contacts can be classified into two types: phosphate backbone contacts or base specific contacts. The phosphate backbone contacts are orchestrated by the amino group of Lys144 and the hydroxyl group of Try57 on the same phosphate group of adenine S10 or AS10, depending which subunit you are referring to. The sense strand is being contacted by residues from subunit A and vice versa. The base specific contacts are mediatd by Arg54, Arg56, Glu60 ,and His64 of subunit A to the guanine S6, guanine S5, cytosine AS12,

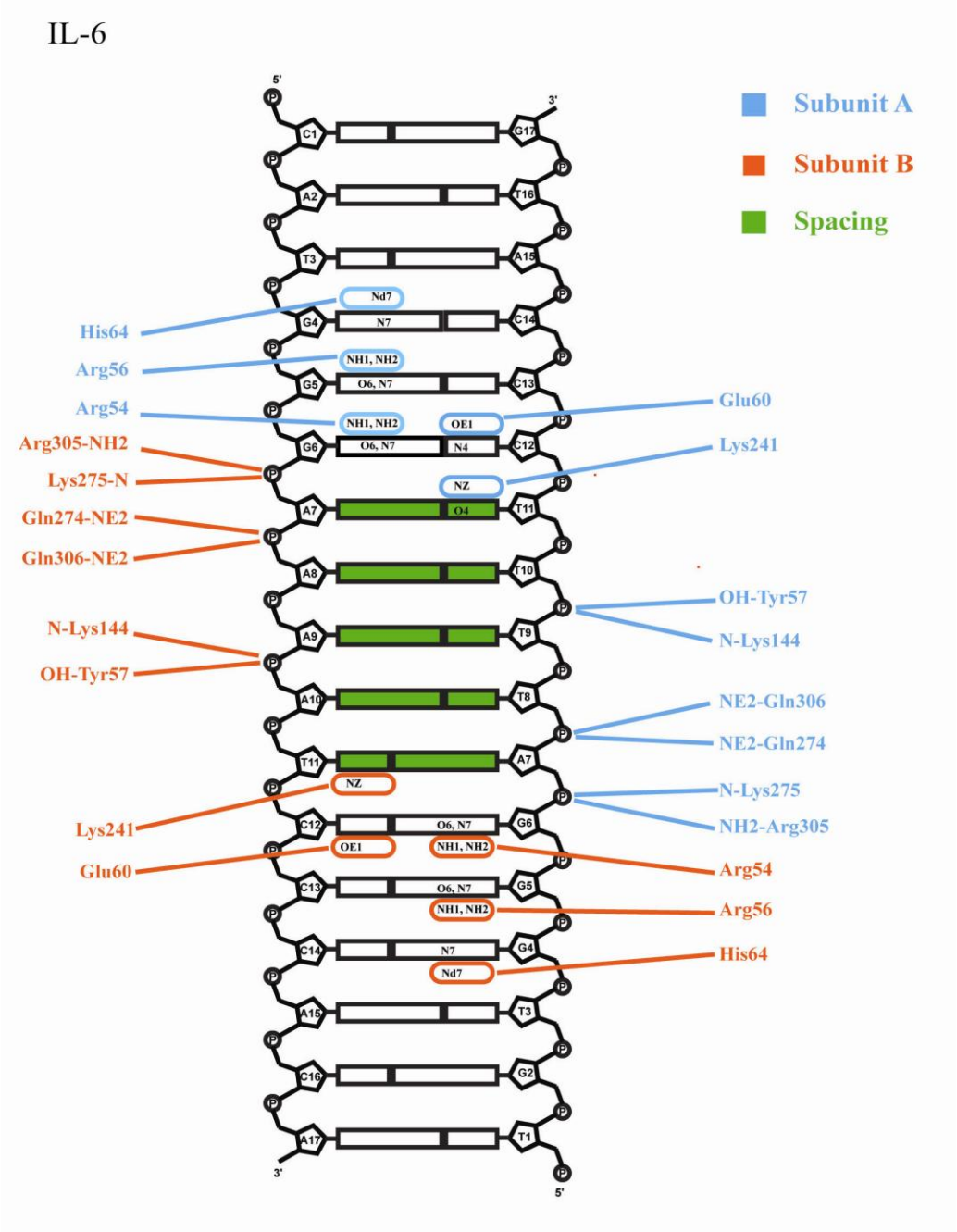

Figure III.4 Illustration of all the DNA contacts made by p50 homo-dimer on the IL-6 promoter. Base specific contacts are shown in the center of the helices while the phosphate backbone contacts on the outside. The particular atoms making the contacts are labeled according to their designation in the crystal structure. The number base pairs between the arginine on position 54 are colored in green.

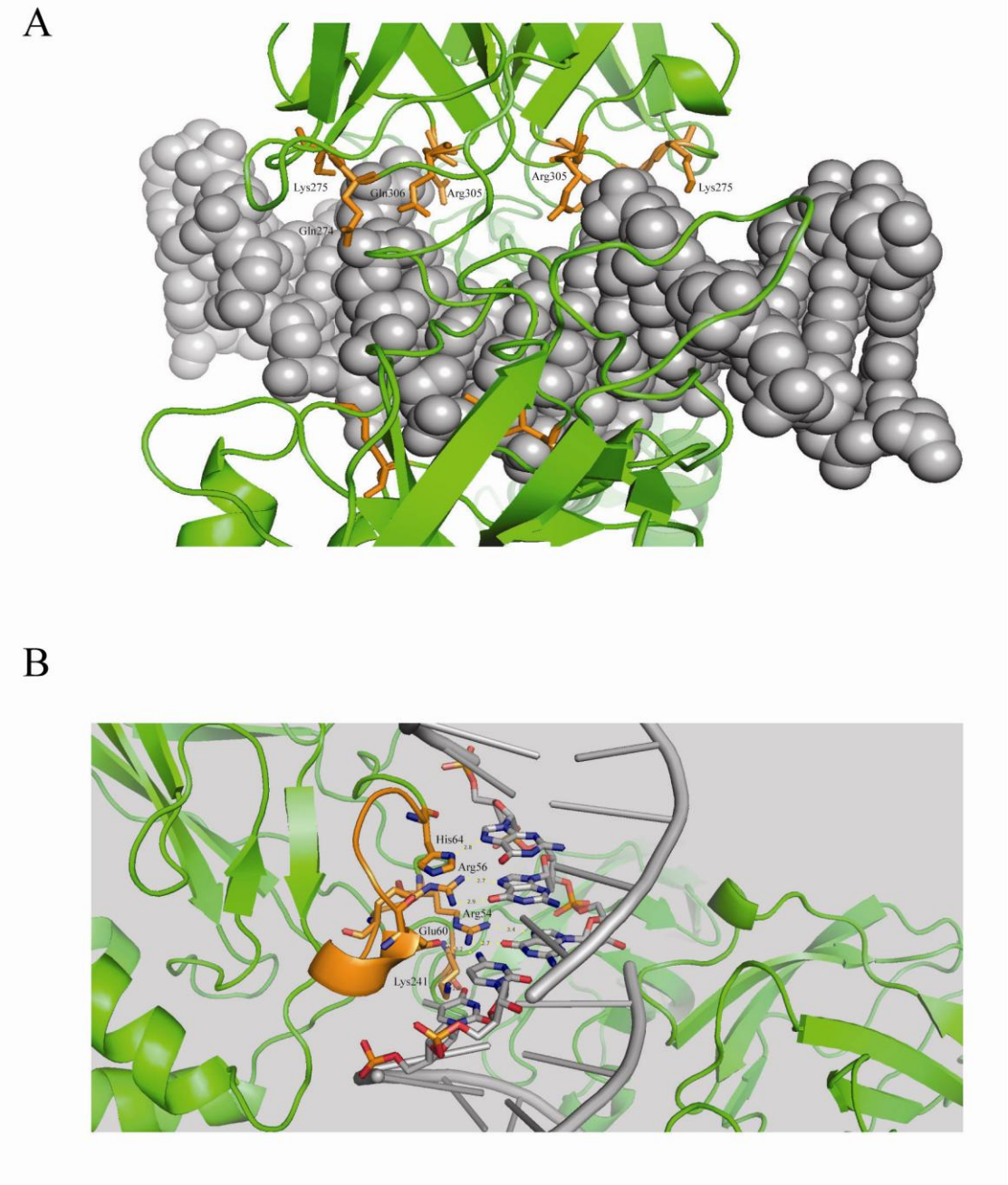

Figure III.5 A. Illustration showing most of the phosphate backbone contacts in the IL-6 structure, specifically the ones from the dimerization domains. They seem to situate the p50 over the major groove of the DNA like a train on its track. B. Base specific contacts made by the recognition loop.

and guanine S4, respectively. The same contacts are replicated by the subunit B on the anti-sense strand. All of these residues are part of a loop connecting β-strands A and β-strand B of the β-barrel structure in the NTD (Figure III.5B). This loop nestles in the major groove of the DNA where it covers the distance of roughly four base pairs.

1.1.4 IL-6 DNA Structure

To assess the effect that p50 binding has on the IL-6 promoter DNA, an idealized DNA structure was generated using 3D-DART software web portal (van Dijk and Bonvin, 2009). The DNA model generated exhibits the typical dimension of B-form DNA with 10.5 base pair (bp) per turn and 35.9° rotation per bp. To determine the difference between this canonical DNA and the IL-6 κB DNA from the NF- κB complex crystal structure, their structures were superimposed using the least square fit function in Coot. Upon overlaying the two structures, subtle differences emerge. First of all is a widening of the major groove (Figure III.6). The width of the major groove increased to 22.4Å from the 15.8Å on the ideal B-form DNA double helix. The regions that experience the widening correlate to the sites where base contacts are made by p50. This widening of the groove is most likely due to the insertion of a loop by p50 which recognizes the three consecutive guanines typical of NF-κB binding sites. Because p50 homo-dimer is perfectly symmetric, the same expansion of major groove is also observed by the other subunit in the region

correlating to the three consecutive guanines on the anti-sense strand. This twin widening of the major groove causes a second distortion to the DNA structure: a consequent narrowing of the minor groove as it is squeezed by the two major grooves. The squeezed region on the promoter is between thymine S8 and cytosine S12 of the sense strand and their complimentary bases on the antisense strand. The width of the minor groove is changed from 13.3Å on the ideal DNA to approximately 9.5Å. The observed widening and narrowing of the DNA grooves caused by NF-κB p50 homodimer binding changes how the bases interact with their complimentary strand partner (Table III.2). First off, stretching, which measures the hydrogen bond distance between the bases, is observed. The first three thymine bases in the middle of the promoter are most affected in this parameter. Their hydrogen bond distances shorten by average of 0.31Å. Second is staggering, which measures the distance of one base relative to its complimentary base in the y-axis. For that parameter bases number 7, 8, and 13 on the sense strand and their complimentary bases are most affected (Table III.3). The third parameter that showed changes is buckling which measures the bending of the base pairs relative to each other. The greatest effects are seen in bases 2, 7, 10, 11, 13, 16, 17 and their complimentary bases.

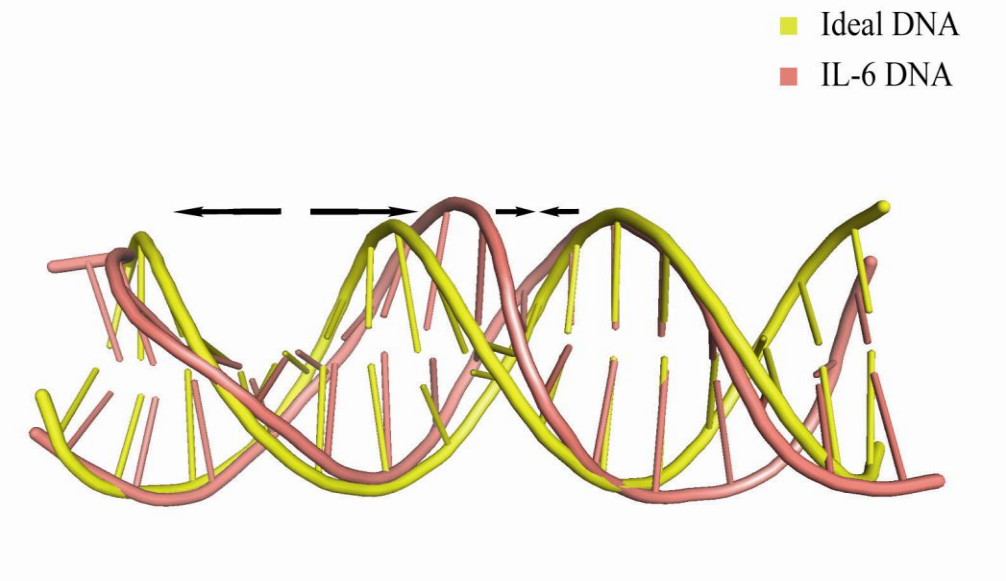

Figure III.6 Superposed images of the IL-6 DNA on top of ideal DNA. The ideal DNA model was generated using the 3DDART modeling software. The binding of p50 caused the pinching of the minor groove while widening the major groove.

Table III.2 IL-6 DNA opening

Differences		
	Minor	Major
1 TG/CA	---	---
2 GT/AC	---	---
3 TG/CA	0.2	2.5
4 GG/CC	0.7	5.1
5 GG/CC	1.6	6.6
6 GA/TC	3	4.9
7 AT/AT	4.1	2.6
8 TT/AA	3.7	0.7
9 TT/AA	3.6	1.1
10 TT/AA	3.8	2.7
11 TC/GA	2.7	5
12 CC/GG	1.7	6.6
13 CC/GG	1.1	5.4
14 CA/TG	0.4	2.6
15 AT/AT	---	---
16 TG/CA	---	---

Note: The opening of the minor and major grooves in the IL-6 DNA is compared to that of the ideal DNA. The amount of distortion is recorded in unit of Å with largest change shaded in dark green.

Table III.3 DNA base variances

		Differences					
Pair ID	**Pair**	**Shear**	**Stretch**	**Stagger**	**Buckle**	**Propeller**	**Opening**
1	T-A	1.2	0.02	0.05	3.14	2.46	18.24
2	G-C	0.34	0.02	0.19	10.27	1.29	9.62
3	T-A	0.18	0.14	0.14	2.22	3.44	1.66
4	G-C	0.41	0.01	0.25	4.85	5.77	2.36
5	G-C	0.27	0.07	0.17	1.14	13.81	4.1
6	G-C	0.19	0.16	0.19	3.54	11.59	0.33
7	A-T	0.54	0.09	0.44	12.88	11.63	4.87
8	T-A	0.68	0.28	0.51	5.99	2.04	1.6
9	T-A	0.19	0.32	0.1	1.24	3.99	4.41
10	T-A	0.32	0.34	0.04	9.05	0.77	0.45
11	T-A	0.48	0.15	0.08	7.4	6.42	1.35
12	C-G	0.13	0.05	0.19	1.8	7.17	0.93
13	C-G	0.14	0.21	0.59	11.68	9.65	3.55
14	C-G	0.45	0.15	0.09	5.45	3.39	1.06
15	A-T	0.1	0.11	0.01	1.94	7.5	2.23
16	T-A	0.29	0.16	0.27	14.86	5.54	4.8
17	G-C	0.37	0.38	0.09	15.52	1.21	3.85

Note: Base pairing geometry of p50 bound IL-6 DNA was assessed with the W3DNA program compared to that of ideal DNA. The deviations are ranked by color with the larger change shaded in darker green. Shear, stretch and stagger are in unit of Å while buckle, propeller and opening are in unit of degrees.

1.2 NF- κB p50 Homodimer:NGAL κB DNA Complex Crystal Structure

1.2.1 The Overall Structure of p50

The x-ray crystal structure of the NF-κB p50(39-363) homodimer bound to a 10 base pair κB DNA from the promoter site of NGAL was solved to a resolution of 2.8 Å. All the refinement statistics associated with the structure are listed in Table III.4.

The overall of structure of p50 while bound to the NGAL promoter is very similar to that of p50 on IL-6. Because of their close resemblance, I will not describe them in the level of detail as I have already done for IL-6. Briefly, p50 maintains the conventional immunoglobulin fold in both of its domains. All the β-barrels and α-helices are assembled together in the same way found in other p50 structure. No inter-domain conformational changes were found. The two DDs are locked in a tight formation in the same 180° rotational symmetry. The DDs are situated right above the middle region of the 10bp NGAL binding site. At the end of flexible linkers, the two NTDs saddled over the DNA with one extending forward on the promoter, and the other projected back.

Table III.4 Data collection and refinement statistics

	p50/NGAL
Data collection	
X-ray source	ALS 8.2.1
Wavelength (Å)	0.99999
Space group	$P2_12_12_1$
Unit cell	
a	68.07 Å
b	103.34 Å
c	128.50 Å
α	90.00°
β	90.00°
γ	90.00°
Molecules/asymm. unit	1
Resolution range (Å)[1]	50.0 – 2.80 (2.85 – 2.80)
R_{sym} (%)	8.3 (76.40)
Observations	138,228
Unique reflections	23,123 (1,129)
Completeness (%)	100.00 (99.90)
Redundancy	6.0 (6.1)
<*I*/□>	18.96 (2.33)
Refinement	
R_{cryst} (%)	24.32
R_{free} (%)[2]	27.77
Protein atoms	5718
R.m.s.d.	
Bond lengths (Å)	0.013
Bond angles (°)	1.637
Mean *B* factors(Å^2)	91.69
Ramachandran plot[3]	
Favored	91.13%
Allowed	8.39%
Disallowed	0.48%
PDB accession code	

[1]Data in parentheses are for highest resolution shell [2]Calculated against a cross-validation set of 5.0% of data selected at random prior to refinement.[3]Calculated from MOLPROBITY

1.2.2 The Dimer Interface

The dimer interface of p50 on NGAL κB DNA is exactly the same as that of p50 on the IL-6 κB DNA. The interaction between the two DDs are so rigid that no inter-domain shift was detected. This interaction is carried out by the same nine residues, namely Arg252, Asp254, Glu265, Tyr267, Leu269, Ser270, Asp302, His304, and Phe307 from each subunit. The most important of these residues, Tyr267, is still tucked in the middle of the pocket formed by the other subunit's Leu 269, Arg 252 and Met 253.

1.2.3 P50 and NGAL DNA Interactions

To describe the DNA structure with some clarity the bases are numbered S1 to S10 for the sense strand and AS1 to AS10 for the anti-sense strand. The P50 subunits are designated A or B, with A being the subunits making the base specific contacts on the three consecutive guanines on the sense strand. How p50 binds to NGAL DNA is very similar to the IL-6 structure in some respects. But in other aspects it is significantly different. Similarities include that all of the residues that contact the DNA are more or less the same. The contacts can be generalized into three categories based on the contact residue's location in p50. The three categories are dimerization domain contacts, flexible linker contacts, and the NTD contacts. Dimerization domain contacts are carried out by Gln274, Lys275, Arg305, and Gln306 from each subunit

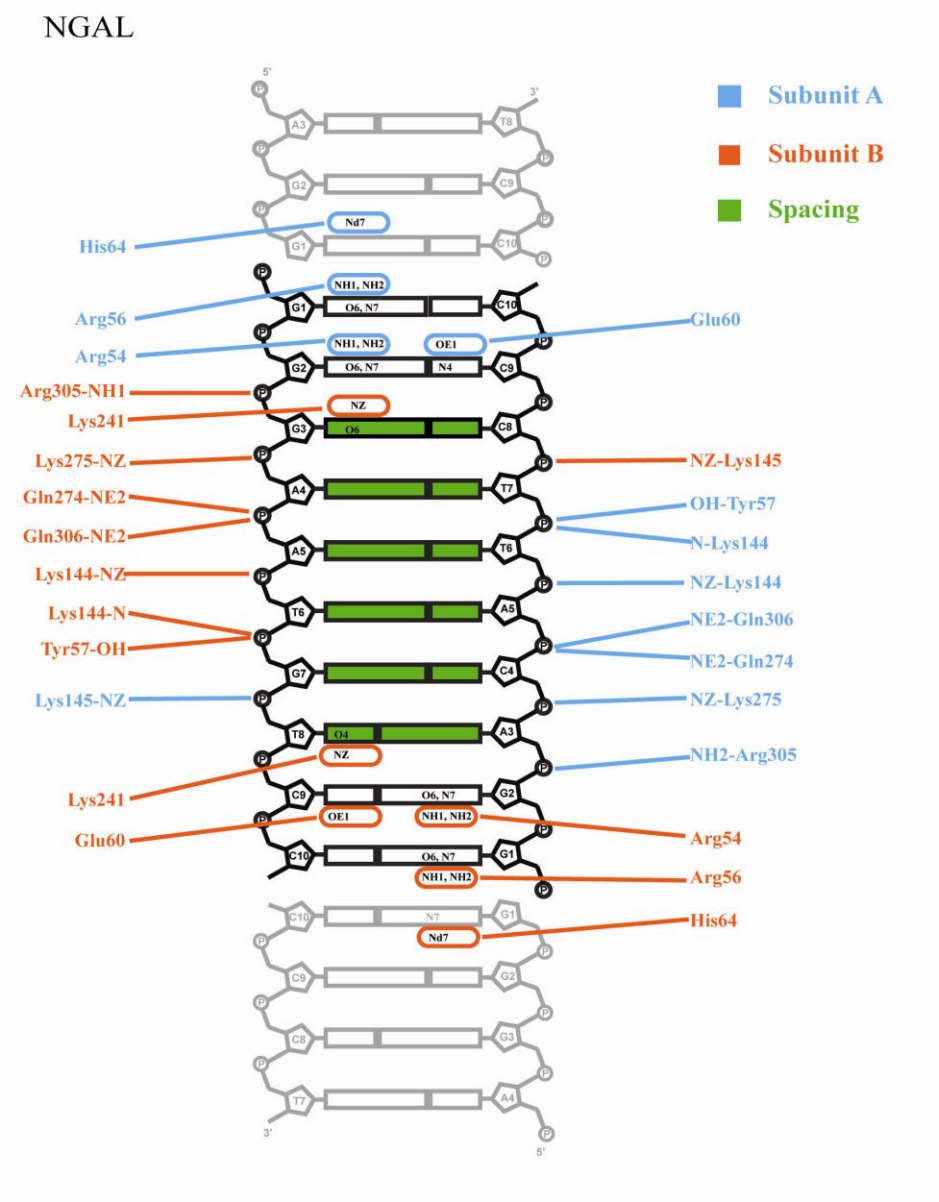

Figure III.7 Illustration of all the DNA contacts made by p50 homo-dimer on the NGAL promoter. Base specific contacts are shown in the center of the helices while the phosphate backbone contacts on the outside. The particular atoms making the contacts are labeled according to their designation in the crystal structure. The spacings between the two subunits are shown in green according to the number of bases between the two arginines on position 54.

Gln274 and Gln306 of subunit A contact the phosphate backbone of adenine on the AS5 position of the DNA. Lys 275 of subunits A contacts phosphate backbone of adenine on the AS4 position. Arg305 contacts the backbone phosphate of cytosine an the AS4 position. The same residues on the other subunit contact their reciprocal position on the sense strand of the DNA. These positions are S5, S4 and S3. Judging by these positions alone, the two subunits of p50 are binding to the 10 bp DNA in such a way as to make the phosphates between 5 and 6 positions of both strand the center. All the backbone contacts on the first bases can be seen on the last five bases by the other subunit.

In the flexible region the only contact is made by Lys241 from both p50 subunits. The amino side chain of the residue reaches out far enough to hydrogen bond with the carbonyl portion of the guanine base. The reciprocal Lys241 has its side chain in the vicinity to hydrogen bond with base of thymine. Even though this second p50 subunit Lys241 makes direct contacts to a nitrogenous base they are less likely to be base specific but rather promiscuous to what it binds to. This is because the lysine residue in the structure has plenty of slack to move around. It would not have matter what base pair would have been there, it would have adjusted to hydrogen bond with it. For example, Lys241 have been shown to bind to thymine AS11 in this structure; to guanine S3 in the NGAL structure; to guanine S3 and thymine AS7 in the κB structure (Ghosh et al., 1995); and the phosphate back bone of the MHC structure (Müller et al., 1995). What all this structural evidence suggests is that Lys241 contact to DNA serves to stabilize the protein-DNA complex rather than to discriminate for

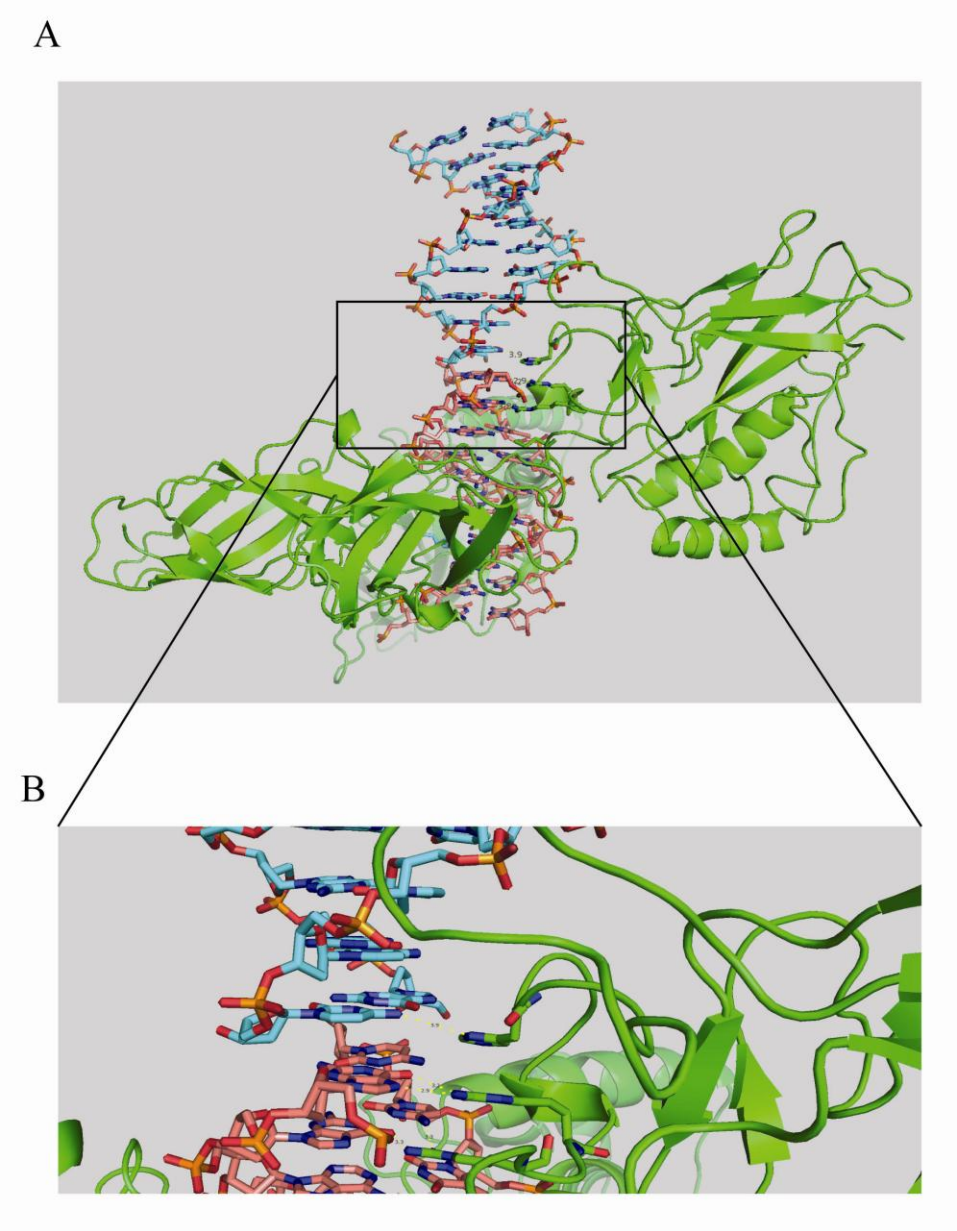

Figure III.8 A. Structure of the asymmetric unit in the NGAL crystal. The p50 bound DNA is colored in salmon and the lone DNA in cyan. B. Zoomed in image of the bracketed area in figure A. His64 can be seen hydrogen bonded to the cytosine of the lone DNA. The His64 on the other subunit does the same on the other lone DNA on the end.

binding to a specific DNA sequence. For the two NTDs there are six residues contacting the DNA, four are on the bases and two are on the phosphate backbone. All base contacts are mediated by residues located in an unstructured loop extending from between β-strands A and B. This long loop is made up of roughly 33 amino acids with a portion tucked inside of the major groove of the DNA. Four out of five base contacting residues are within this region thus fittingly this loop since then has being named the "recognition loop" by Müller's group who is among the first to solve the p50 structure. In subunit A, Arg54 and Arg56 hydrogen bond with S1 and S2 guanine of the sense strand. Glu60 hydrogen binds with the AS9 cytosine of the antisense strand. Interestingly, His64 is hydrogen bonded to the S1 guanine of the neighboring DNA (Figure III.8A). This was made possible since the crystal packing had forced an unbound DNA to be stacked right on top of the bound DNA (Figure III.8B). This head to tail stacking have made a pseudo 20bp DNA with 5 extra base pairs at either end of the bound 10-mer NGAL DNA. The two phosphate backbone contacts are down two residues away from the recognition loop. Lys144 and Lys145 hydrogen bond with phosphate group of thymine AS6 and thymine AS8, respectively. On subunit B all of the contacting residues made the same contacts on their reciprocal bases or phosphate according to the position. The identity of those bases did not seem to play a role in dictating p50 conformation.

1.2.4 NGAL DNA Structure

Note: To describe the DNA structure with some clarity the bases are numbered S1 to S10 for the sense strand and AS1 to AS10 for the anti-sense strand.

To analysis the NGAL DNA I took its sequence and used an open source web based web server called 3DDART (Van Dijk and Bonvin, 2009) to generate an ideal NGAL DNA model. The model has the typical dimensions associate with form-B of DNA, 10.5 bp per turn and 35.9° rotation er bp. This model was than over lapped on top of the actual crystal DNA structure with least square fit function in COOT. What interestingly glaring out from the comparison is only one of the strands has its structure distorted, the sense strand (Figure III.9). Its phosphate backbone and the geometry of the bases align very closely to the ideal DNA. The antisense strand on the other hand its phosphate backbone from the region of AS5 to AS9 have been shift in way to narrowing the minor groove by an average of 3.3Å (Table III.4). Of the narrowing of the minor groove unavoidably led to the widening of the major groove by the same amount.

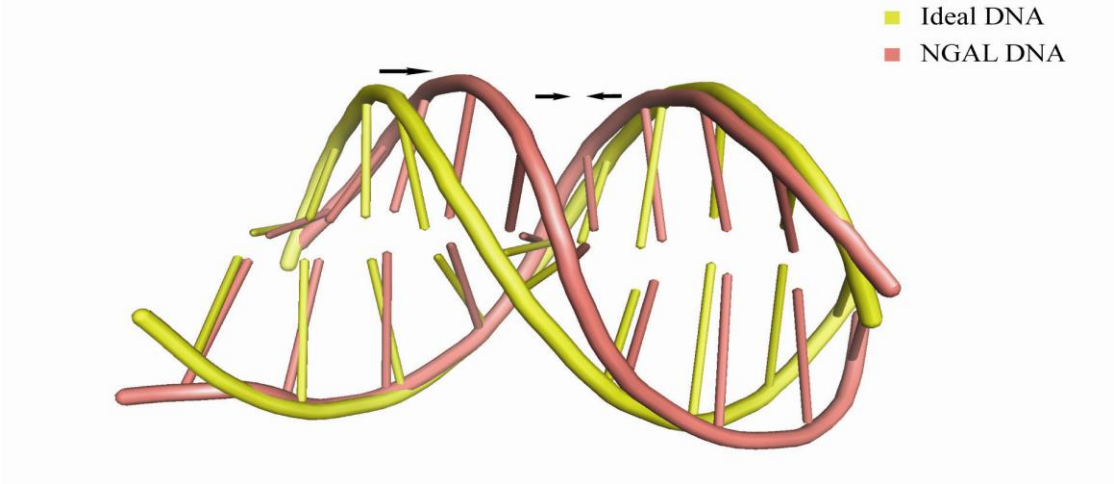

Figure III.9 Superposed images of the NGAL DNA on top of ideal DNA. The ideal DNA model was generated using the 3DDART-modeling program. The binding of p50 dramatically pinch the opening of the minor groove while widening the major groove.

Table III.5 DNA opening

Differences			
		Minor	Major
1	GG/CC	---	---
2	GG/CC	---	---
3	GA/TC	2.7	3.3
4	AA/TT	3.6	2.2
5	AT/AT	3.9	0.1
6	TG/CA	4.2	2.6
7	GT/AC	3.1	4.5
8	TC/GA	---	---
9	CC/GA	---	---

Note: The opening of the minor and major grooves in the NGAL DNA is compared to that of the ideal DNA. The amount of distortion is recorded in unit of angstroms with the largest changes shaded in darker shades of green.

Table III.6 DNA base variance

Differences							
Pair ID	Pair	Shear	Stretch	Stagger	Buckle	Propeller	Opening
1	T-A	0.19	0.08	0.17	5.67	17.07	6.1
2	G-C	0.09	0.23	0.35	11.67	12.74	0.6
3	T-A	0.45	0.13	0.1	7.6	10.03	4.23
4	G-C	0.05	0.33	0.04	10.86	11.82	3.76
5	G-C	0.12	0.15	0.78	9.38	4.55	1.55
6	G-C	0.61	0.08	0.49	8.87	0.1	1.17
7	A-T	0.58	0.14	0.11	12.3	18.43	3.94
8	T-A	0.38	0.11	0.33	10.84	15.37	1.21
9	T-A	0.12	0.18	0.01	0.86	11.6	0.68
10	T-A	0.27	0.46	0.6	10.95	7.75	0.87

Note: The geometry of the bases in the NGAL structure was assessed with the W3DNA program. The deviations from that of the ideal DNA are ranked by severity indicated by darker shades of green. Shear, stretch and stagger are recorded in unit of Å while buckle, propeller and opening are in unit of degrees.

1.3 Compare and Contract of the p50 Structures

Comparison of the two newly solved p50 homodimer:κB DNA complex structures alongside the two previously solved structures suggests that the four complexes can be classified into two two groups. One group has their NTDs spread one bp further than the other group. The structures with wider spread are the NGAL and the κB structures (Ghosh et al., 1995). The structures with smaller spread are the IL-6 and the MHC (Müller et al., 1995) structures (Figure III.10). The spread of the NTDs were measured by the DNA contact point made by the two Arg54s, one from each subunit. Arg54 was chosen as the marker because it is part of the four residues (Arg54, Arg56, Glu60 and His64) of the recognition loop that recognizes the three consecutive guanines in the beginning of every p50 binding site. It is closest to the center, which marks the beginning of the gap. The p50:DNA complexes that disply the wider spread have six bp in this region while the narrower spread has five. This difference in spacing seems to be a result of p50 shifting its position along the promoter. In some situations p50 sets its center on the phosphate between the third and fourth bp of the gap. With three bp on either side of this midline it forms the six bp spread. But when it sets its center on the third bp, it has two bp on either side of the midline. This forms the five bp spread. All of the DNA contacts on either sides of the midline are identical and can relate to its counterpart by a 180° rotation symmetry. However, what remains unclear is the cause this difference in DNA binding conformation. There is nothing particularly unique about the IL-6 and MHC promoters that stand out from NGAL and κB promoters. All promoters except for

NGAL obey the canonical NF-κB sequence of GGGRNWYYCC, where R=A or G; N=any bases; W=A or T; and Y=C or T(Ghosh et al., 2012). NGAL has a guanine on the seventh position rather than the C or T.

This does not seem to have any obvious effect since there are not any base specific contacts to this base to begin with. Another thing we looked at was the number of bp between the consecutive guanines and cytosines. Perhaps, we thought, this could play a major role in the spacing of the NTDs since that is where all the base specific contacts are. It makes sense that if they are spread further then that would lead to the spreading of the NTDs or vice versa. However, there does not seem to be any correlation there. Both IL-6 and NGAL promoters have six bp between the GGG and CC yet one has 6bp spacing between p50 subunits and the other is 5bp. The κB DNA promoter has four bp between the GGG and CC while MHC promoter has only three. Actually, since MHC promoter is made up of GGGG and CCCC with AAT in the middle, this should be able to accommodate either p50 conformation. The fact that it settles on the 5bp spacing shows that, when given the choice, the 5bp spread is the conformation preferred by the p50 homodimer. This theory is further supported by the binding affinity data where 5bp spread promoters, MHC and IL-6, has on average 2.5 times higher affinity toward p50 than 6bp spacing promoters, κB and NGAL (Table III.6). Also, if we were to expand this comparison past p50 to include all the NF-κB structures, there are ten structures that adopt the 5bp spacing conformation with only three adopting the 6bp spacing conformation. Nevertheless, it is still a puzzle why p50 did not adopt the favored conformation in the case of NGAL and κB promoter

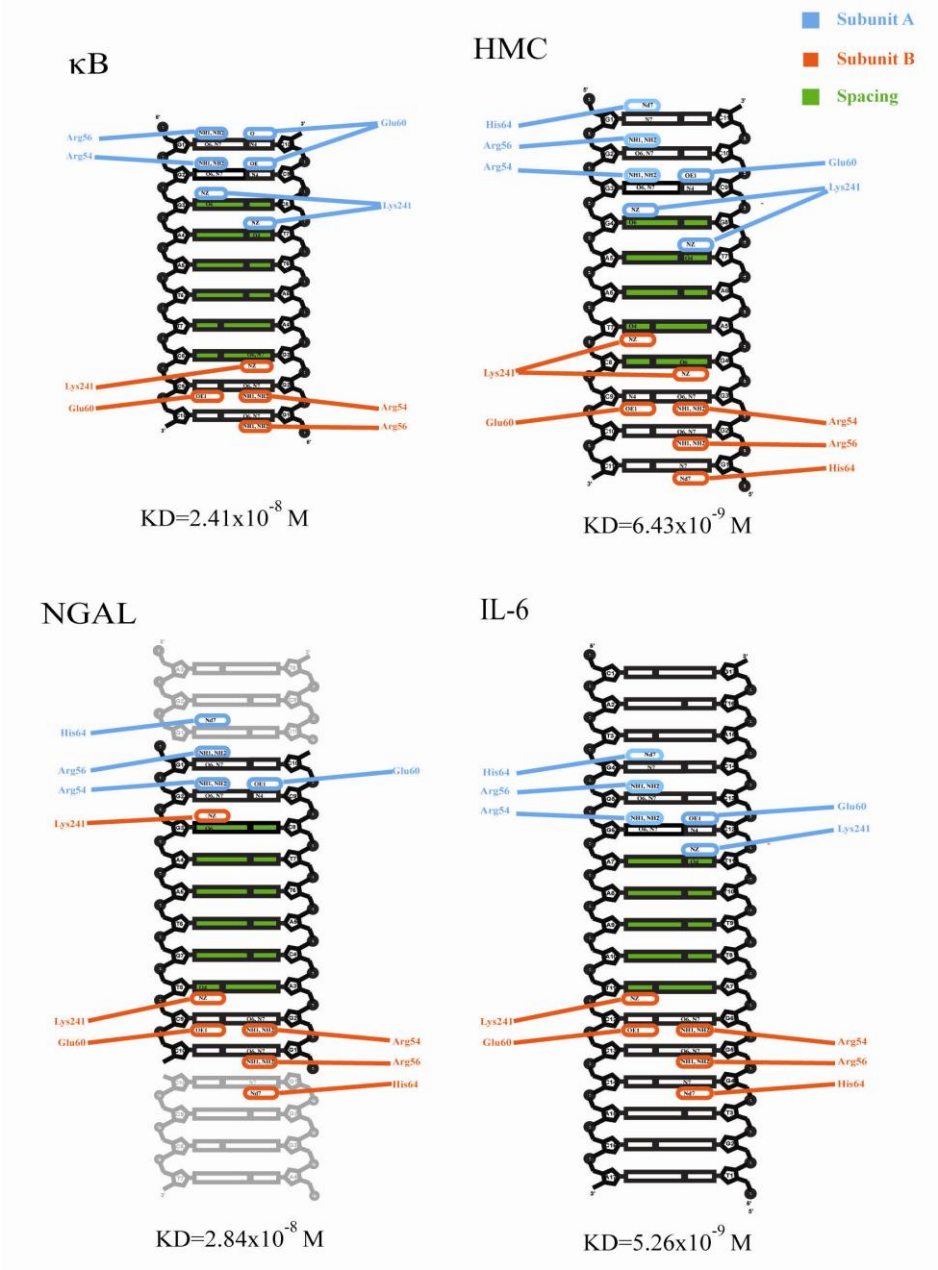

Figure III.10 DNA base specific contacts made by p50 on different promoters are shown above. The bp spacings between the p50 subunits are made clear by the green shading of the bases. The two promoters on the left have six bp spacing while the two promoters on the right have five bp spacings. Binding affinity between the p50 and DNA measured by SPR in forms of KD are listed below each DNA promoter.

when there are guanines or cytosines in position to accommodate the shift. It is possible that this difference is caused by thermodynamic favorability, which has many contributing factors that are not easily apparent in the structure.

Whatever different conformations p50 may adopt on the promoter, the DNA structures beneath it appear relatively the same. Superposition of all four DNA from the p50 homodimer:DNA complex structures shows that they are nearly identical (Figure III.11). They all have the same narrowing of the minor groove and widening of the major groove to the same degree.

2. IκBζ:p50 Dimerization Domain Structure

2.1 The Overall IκBζ Structure

The x-ray crystal structure of p50(245-376) homodimer bound to the IκBζ(404-718) was solved to a resolution of 2.0 Å. This contains the entire dimerization domain and NLS polypeptide regions of two NF-κB p50 subunits as well as the entire C-terminal ankyrin repeat domain of IκBζ. All the refinement statistics associate with the structure are listed in Table III.7.

The overall structure of IκBζ shares many similarities to the previously solved IκB structures, such as Bcl-3, IκBα, and IκBβ. Its main body is made of seven ankyrin repeats (AR) stacked on top of each other to form an elongated globular shape (Figure III.12). The dimension of the structure measures approximately 24.7Å x 22.2Å x 76.2Å.

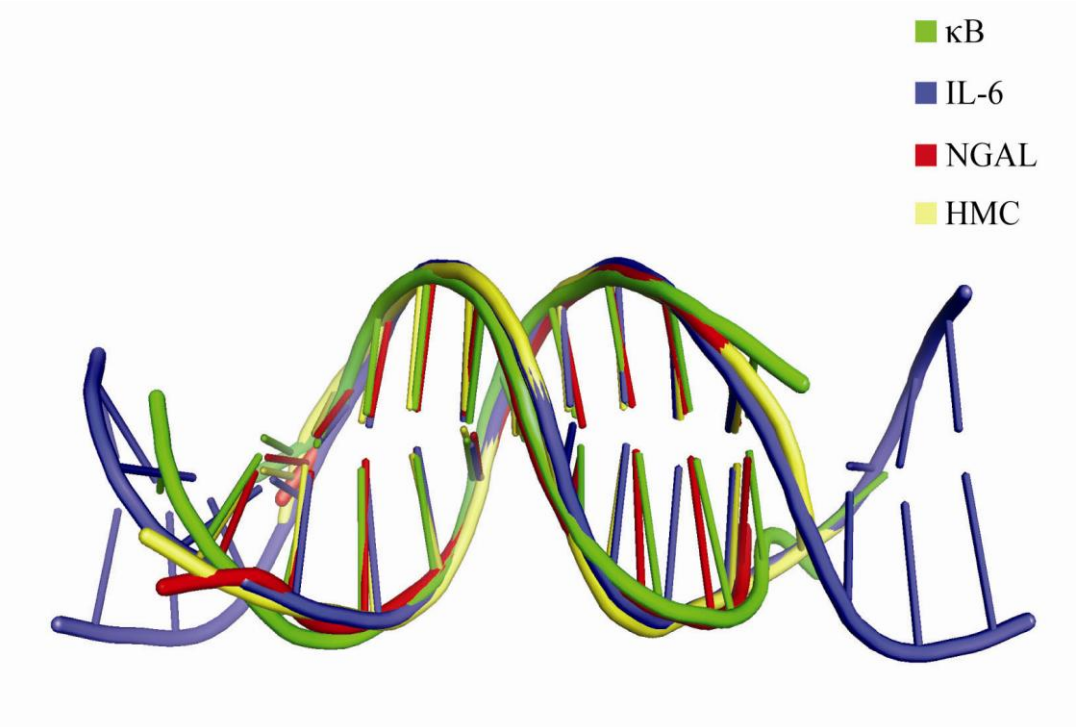

Figure III.11 Overlapping of DNA structures from four p50/DNA structures using the Least Square Mean function in the COOT model-building program. The alignment was made according the consensus sequences at center of every promoter site.

A slight left-handed twist accompanied with a gentle curve can be seen spread across the whole structure. This twist and curvature is evenly distributed so there are no kinks or sudden bends in any one particular area. What caused this is mostly likely due to the wedge shape of each individual AR as they are being stacked.

Individually, each AR is composed of a single beta hairpin loop followed by two alpha helices with a short flexible linker between them two (Figure III.13). The beta hairpin loops are made up of roughly six residues with a third of them fold back on itself to form two anti-parallel strands. The strands are kept together by the hydrogen bonds typically seen in beta sheets. After the beta hairpin loop the residues make a sharp 64 degree turn and began the first helix. This helix, which will be referred to as α1 from now on, is made of approximately nine residues. It is fairly short, usually with only two complete turns. It ends with a short S shaped linker that points out at a 90 degree angle. This linker then starts the second helix ending the other way. This second helix, which will be referred to as α2 from now on, is composed of approximately thirteen amino acids. It is slightly longer than α1 with three complete turns in its helical structure. It runs anti-parallel to α1 with a slight downward tilt toward starting point of the next AR underneath. The two helices are kept together by the hydrophobic interactions between the non-polar residues on both sides of the interface. Taken together overall structure of an AR takes on the shape of a boomerang with the beta hairpin being the one blade and the two helices make up other blade.

Table III.7. Data collection and refinement statistics

	p50:IκBζ
Data collection	
X-ray source	ALS 8.2.2
Wavelength (Å)	1.0000
Space group	$P2_1$
Unit cell	
a	51.42 Å
b	58.93 Å
c	108.81 Å
α	90.00°
β	99.15°
γ	90.00°
Molecules/asymm. unit	1
Resolution range (Å)[1]	50.0 – 2.00 (2.03 – 2.00)
R_{sym} (%)	5.5 (46.8)
Observations	157,487
Unique reflections	43,393 (2,080)
Completeness (%)	99.0 (96.4)
Redundancy	3.6 (3.4)
<*I*/□>	20.4 (2.09)
Refinement	
R_{cryst} (%)	19.4
R_{free} (%)[2]	21.6
Protein atoms	4,104
Solvent atoms	244
R.m.s.d.	
Bond lengths (Å)	0.007
Bond angles (°)	1.154
Mean *B* factors(Å^2)	44.493
Ramachandran plot[3]	
Favored	95.12%
Allowed	4.88%
Disallowed	0%
PDB accession code	

[1]Data in parentheses are for highest resolution shell [2]Calculated against a cross-validation at of 5.0% of data selected at random prior to refinement.[3]Calculated from MOLPROBITY

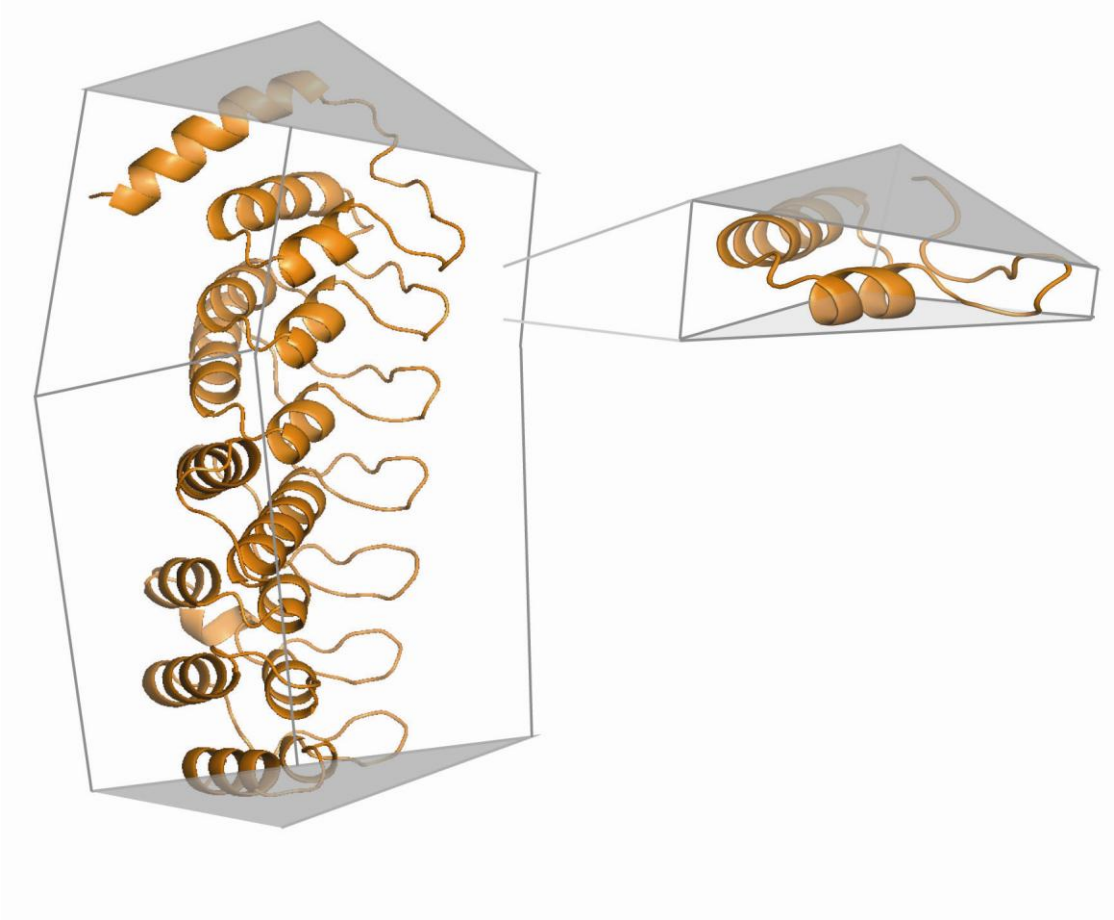

Figure III.12 The ankyrin repeats region of IκBζ(404-718) taken from the complex structure. The globular shaped protein is made up of seven ARs each consist of two helices and a hairpin loop. Each wedge shaped AR gives the overall structure a slight bent along with a left handed twist.

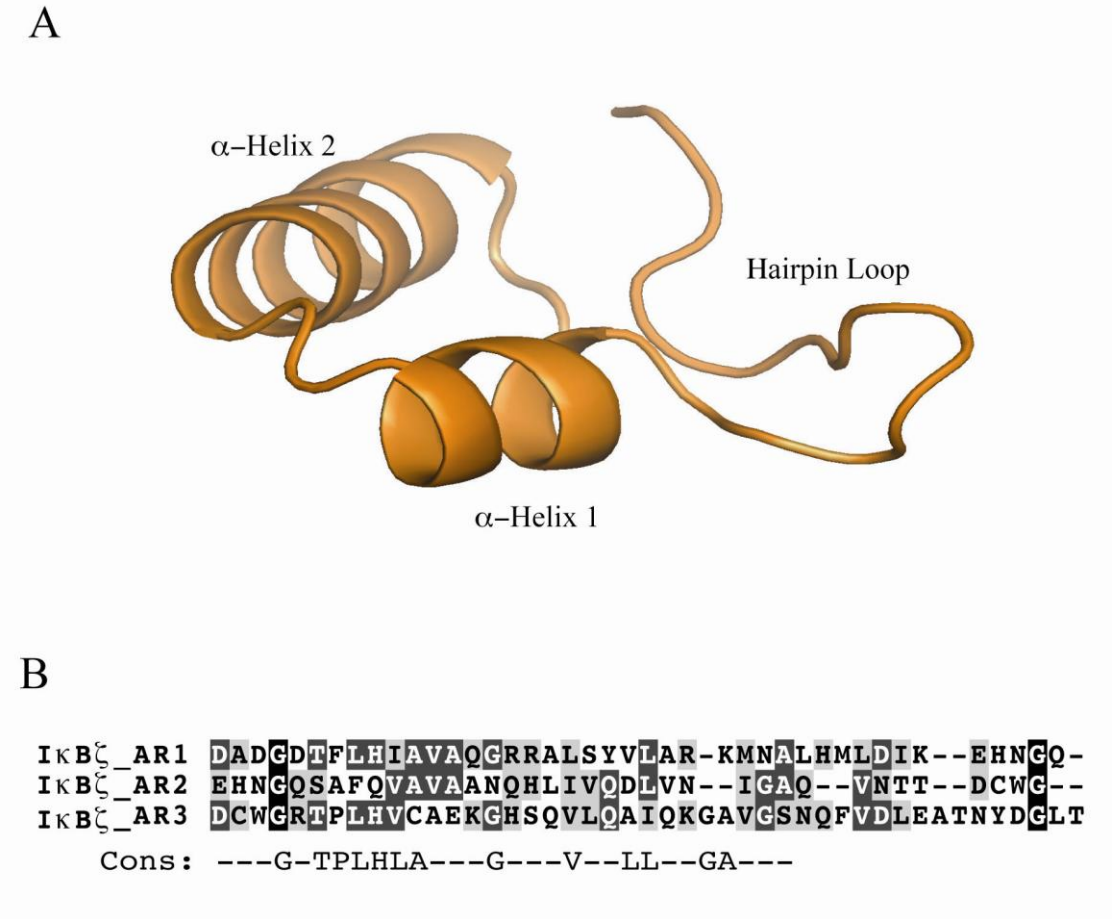

Figure III.13 A. A single subunit of ankyrin repeat (AR) is made of one hairpin loop and two α–helices. The helices were numbered base on their nearness to the N-terminus. B. An sequence alignment of AR1, AR2, and AR3 show the conservation of the key residues relative the AR consensus sequence. Researches have shown the closer the sequences alignment to the consensus the more stable the AR structure.

Because the two helices take up more room to stack than the hairpin loop the ARs cannot be stacked on top one another in a straight up and down fashion. It is this uneven stacking phenomenon that gives the slight twisting and curvature in the overall structure of IκBζ. Because the beta hair-pin loops kind of look like fingers the structure have also been likened to a "cupped hand" coined by Steven Harrison's lab who solved the BCL-3 structure. The seven beta hairpin loops being the fingers and the stacked helices being the palm (Figure III.14A).

2.2 The Capping Helix

Beside the overall contour of IκBζ, this structure does have three unique characteristics that are not seen in any of the IκB structures. The first one is a capping helix that drapes over the AR1 (Figure III.14B). It is a relatively long alpha helix with four and a half turns N-terminal of AR1. The helix lays on top of α2 of AR1 to form an angle of 122 degree; the point of intersection being the midsection of the capping helix and the N-terminus of α2. The orientation of the helix is dictated by the position of 4 polar and 7 non-polar residues from both helices. Interestingly, overlapping of this structure with IκBβ structure shows this capping helix occupies the same area as nuclear localization sequence (NLS) from p65 does on IκBβ (Gouri JBC 2003) (Figure III.15). What this implies is, without the helix being moved, IκBζ is inherently incapable of binding to p65 due to this collision.

Furthermore, the region of collision on p65, residues 305-321, has shown to be critical for the binding of p65 to IκBβ. The truncation of these residues led to the reduction of binding affinity by 10,000× (Bergqvist, jmb, 2006). This observation is in agreement with findings that showed IκBζ preferentially binds to p50 but not to p65 (Danny Trinh, J Mol. Biol 2008) (Yamazaki jbc. 2001). One obvious way to test this theory would be to remove the helix and see if that would change the specificity of IκBζ binding. However, removing the capping helix could lead the aggregation of the protein due to the hydrophobic patch underneath. One positive indicator that may not happen is that all other crystal structures that were solved did not have that helix in their structure and they too have a greasy patch underneath but did not run into any problems. Moreover, the concentration of the protein doesn't need to be that high for pull down assays. Interestingly, this does raises up a question: Could this capping helix be present in other IκB proteins as well? There is evidence to support this claim. First of all, all of the IκB proteins, either based on X-ray structure or sequence alignment, have a hydrophobic region on top of AR1 α2 helix (Figure III.16). Of the four hydrophobic residues in that region that make contact with IκBζ, two of them (L459 and L463) are conserved for non-polar residues while one (A458) is found on IκBα and IκBε. It is reasonable to speculate this region either needs to be protected by something, like a helix, or else it is primed to bind to something else, possibly another transcription factor. Furthermore, sequence alignment of the all the IκB proteins shows in the region of the capping helix many position are conserved for residues within the same group. This pattern is indicative of helix structure. For instance,

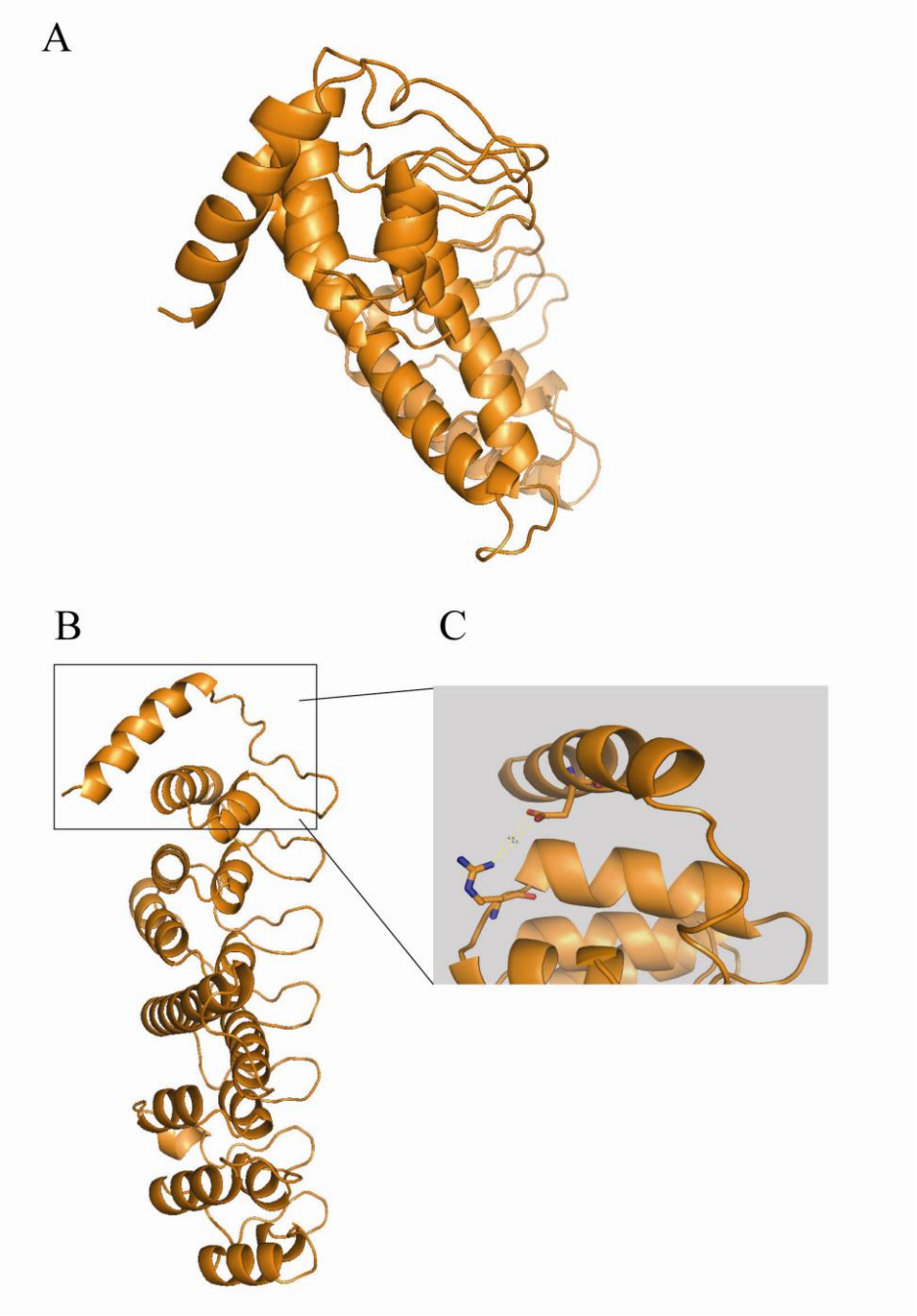

Figure III.14 A. Image of IkBz from the orientation that best show the “cupping hand” shape. The hairpin loops make up the “fingers” and the a-helices make “palm” of the hand. B. Image showing the position and orientation of the capping helix. C. Magnified image of the bracketed region with the Glu425 and Arg456 engaged in an ionic bond.

positions F418, V422, L429 and I432 are conserved for hydrophobic residues and Q421, E423, E425, S427, K428 are conserved for hydrophilic residues. The distribution of these conserved positions strongly suggests the presence of a helix since that would place all the hydrophobic residues on one side and hydrophilic residues on another. However, this matter cannot be fully settled until more crystal structures come out. But, in light of this IκBζ structure, future crystallographers may want to include this region in their IκB constructs.

2.3 Structure of AR4

The second structural characteristic that is unique to the IκBζ ARD structure is its AR4. The two α-helices within the domain are much longer than the rest, about twice as long as the helices in other ARs (Figure III.17A). The position and orientation these helices are no different than the rest. They are just longer. Because the two helices are not perfectly parallel to each other, their tips intersect each other with α2 on top of α1. The ends at the intersection are connected by a short linker of seven amino acids. The two helices pack against each other by the hydrophobic interaction between the non-polar residues on either sides of the interface. This extension of AR4 does not make contact with any part of dimerization domain of p50 (Figure III.17B). Clear electron density of this region shows the structure is rigid and well ordered without need of support from anything else.

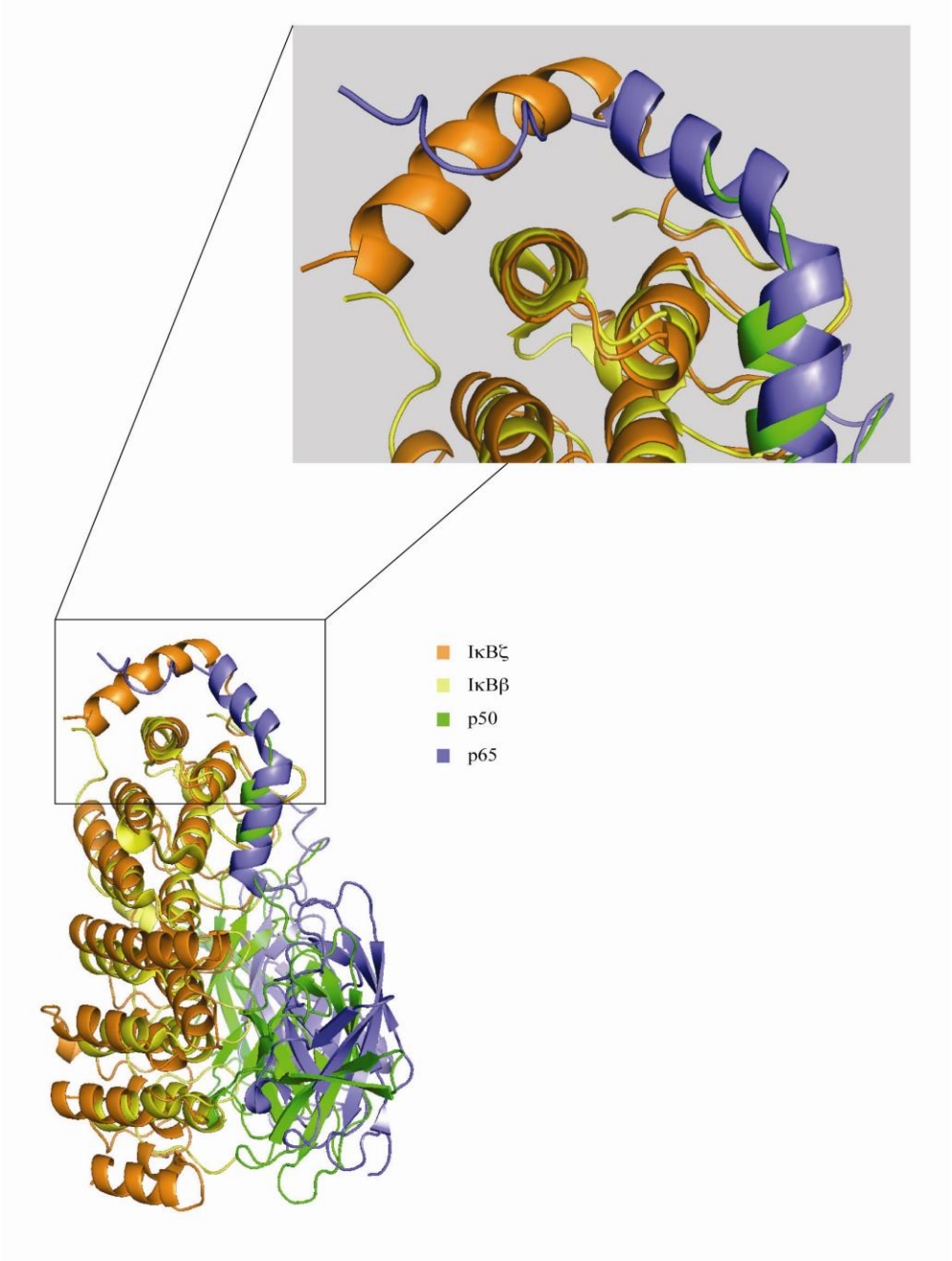

Figure III.15 Superposed image of IκBζ/p50 structure on top of IκBβ/p65 complex structure. The comparison is designed to show the differences between the NLS from p50 and that of p65. The enlarged image shows if p65 were to bind to IκBζ its NLS would collide with the capping helix above AR1.

2.4 AR7 of IκBζ

The third area of the IκBζ structure that stands out is its AR7. The only other IκB protein that is known to have an AR7 is Bcl-3. It extends far enough to contact the DNA. Superposing of the IκBζ structure on top of p50 homodimer structure bound to the IL-6 promoter shows its beta hairpin loop on AR7 collides with the phosphate backbone of the DNA (Figure III.18A). However, this finding seems to be by one AR in contrast to what we have reported in a previous paper (Trinh, JMB. 2001) and in my own findings, which I will detail in a later section. Both in our early and recent studies we detected stable ternary complex of IκBζ, p50 and IL-6 DNA. I believe this disparity can be resolved by two possible solutions. First, is the AR7 possesses some inherent flexibility which allows to shift in the case of DNA encounter. This shift could either allow it move "upward" as to give room to the DNA or to slight into the major groove. The second possibility is that the whole AR structure shifts up by one position upon DNA binding. Since all of the contact points along the hairpin loops are few and hydrophobically driven, it is plausible this shift is energetically favorable with the addition of DNA. This theory supported by the slacking of the peptide between its DD of p50 and its NLS region (Figure III.18B). Furthermore, we have data to show IκBζ, p50 binding recognition is most done through its NLS and not the DD. Even the DD of p65 were able to accommodate it.

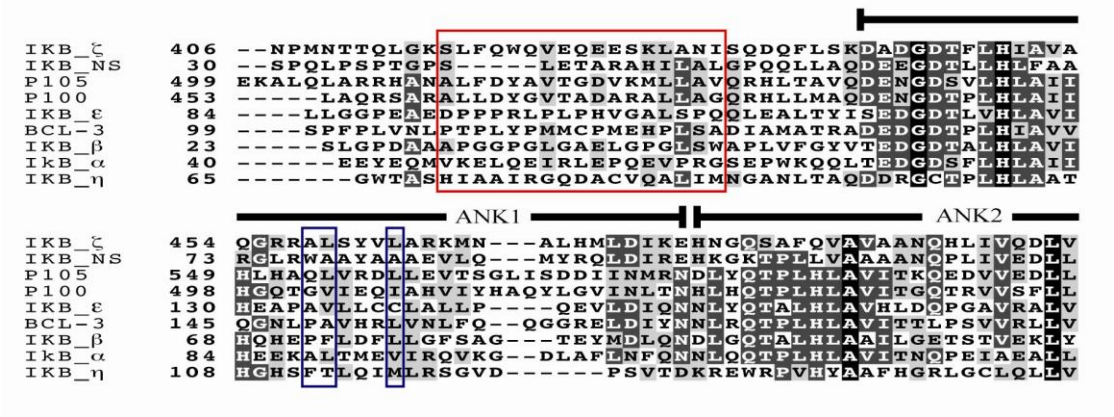

Figure III.16 Sequence alignment of the AR1 region for all the IκB proteins. The region correlate to the capping helix is boxed in red. The conserved amino acids make up the grease patch underneath the capping helix are boxed in blue.

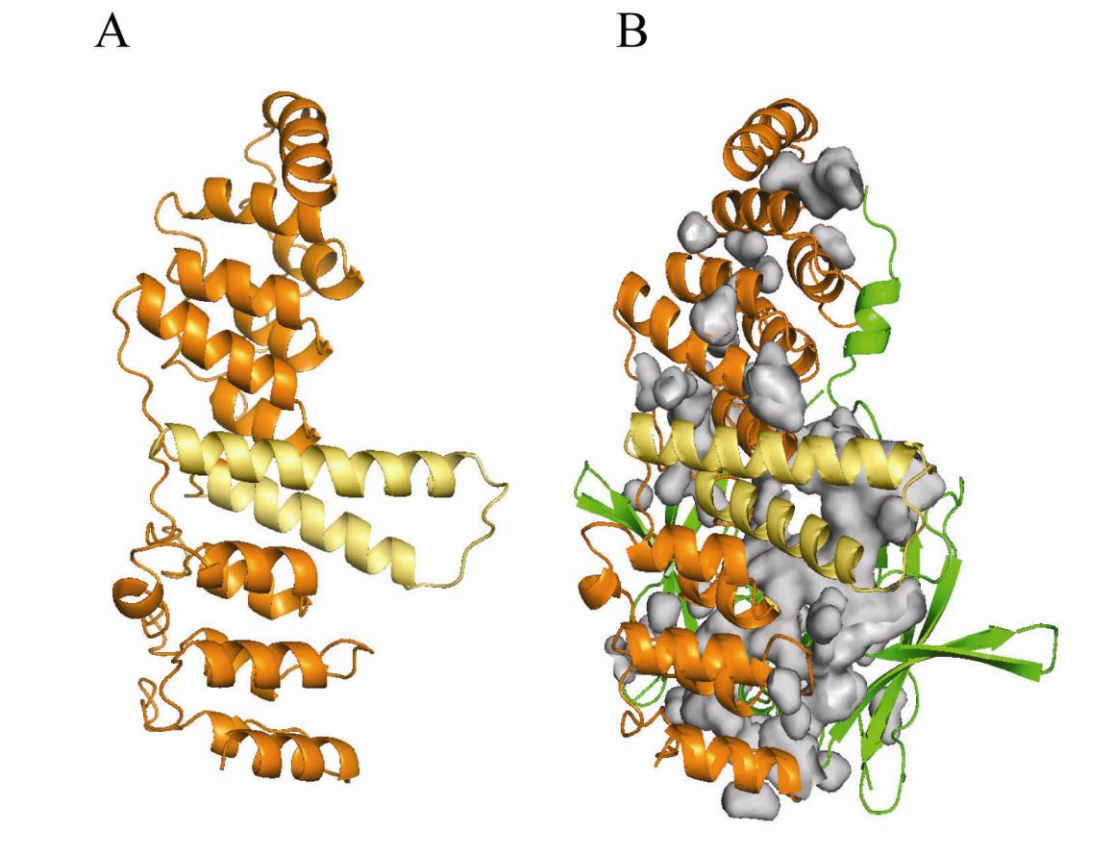

Figure III.17 A. AR4 (yellow) of IκBζ is exceptionally longer than the other ARs. B. The extended helix does not seem to make any specific contacts with p50 as the two are separated by large cavities (shown in grey).

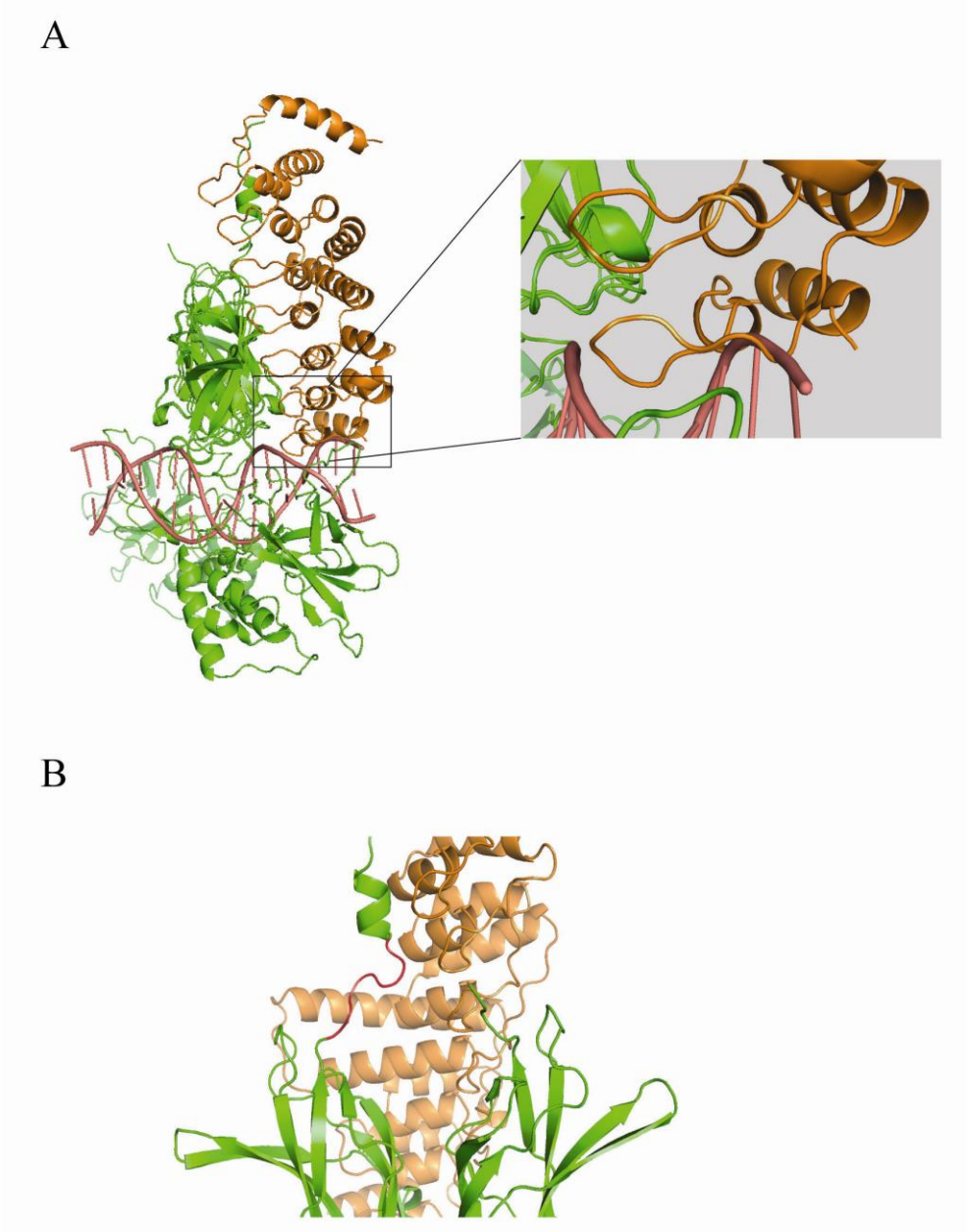

Figure III.18 A. IκBζ/p50DD structure was combined with the IL-6 p50 structure based on the alignment of DD region. This compiled model shows a collision between the AR7 of IκBζ and the DNA. B. To avoid this collision one of the possibility is IκBζ scoot up

2.5 P50 IκBζ Interface

IκBζ binds to the dimerization domains of p50 in a similar fashion as other IκB:NFκB structures. IκBζ orients itself in such a way that the beta hairpin loops from its ARs 4-7 extend into the crevice between the two dimerization subunits. ARs 1-3 make contact with p50 as well. It is away from the dimerization subunits in the NLS region. The combined interface covers 1,742 $Å^2$ of solvent inaccessible area. Binding of IκBζ does not induce conformational change of any kind within the All of the contact points that make up the interface can be separated into three categories: 1) NLS related; 2) Hairpin loop mediated; and 3) Rel positions Met365 and Lys354 on p50 (Figure III.19A). For Met365, its side chain sits in a hydrophobic pocket made up of Phe447, Ile450, Ala451, Leu459, and Leu463 of IκBζ. And for Lys354 its hydrocarbon portion of the side chain lays flat against the aromatic rings of Trp512 on IκBζ. Interestingly all the interactions between these two positions are ionic in nature: Glu355 and Glu356 of p50 are bound to Arg514 and His478 of IκBζ, respectively, Arg359 of p50 to Asp443 of IκBζ, Lys360 of p50 to Asp445 and Glu477 of IκBζ, Lys363 of p50 to Asp441 and Asp 445 of IκBζ (Figure III.19B). The two hydrogen bonds observed are between Arg361 and Lys363 of p50 with the carbonyl group and the amino side chain of Gln454 respectively. In this NLS consensus sequence region, namely between Lys354 and Met365, 58% of the residues are participating in some form of binding interactions.

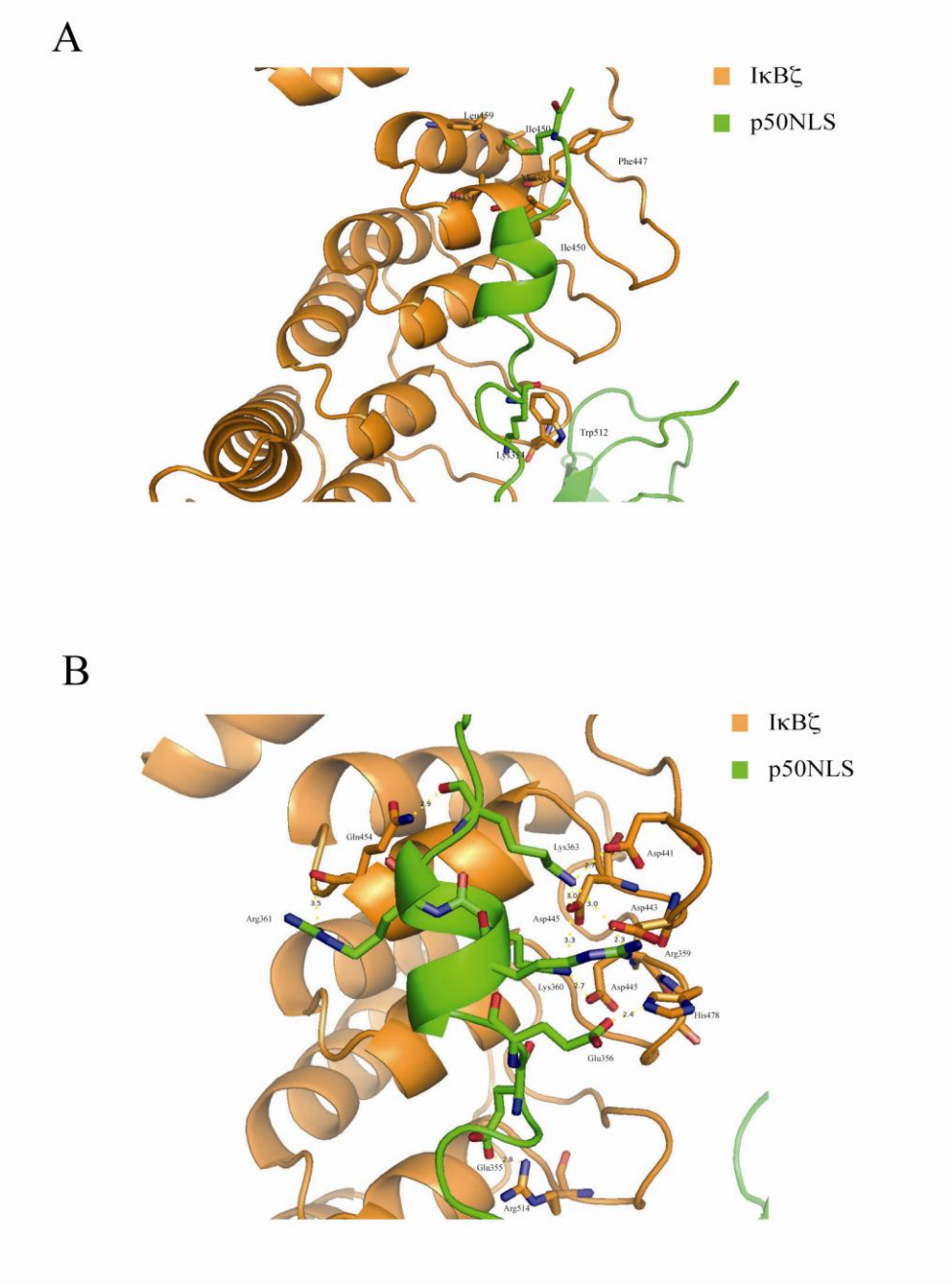

Figure III.19 A. Image showing all the hydrophobic interactions between the NLS region of p50 and IκBζ. B. Image showing all the ionic and hydrogen bond inter-actions between the two proteins. The distances between the interactions are measured and shown as doted lines.

dimerization domain (DD) of p50. We know this since superposition of the DD from this structure with that of DD from the IL-6 structure matched perfectly (Figure I.4B).

The second category of contacts found between IκBζ and p50 are between the hairpin loops of IκBζ and the dimer interface on p50. Only the loops from AR4-7 are making these contacts since the rest of the loops are higher up on the N-terminus of the side of IκBζ (Figure III.20). Describing them in the numerical order of the loops, on the AR4 loop Tyr550 reaches out to lay flat against Tyr348 from the subunit of p50 that does not have the ordered NLS region, which I will refer to subunit C from now on. On the next loop Arg610 and Lys611 of IκBζ lay flat against the surface of would justify their charges. On that same loop a little away from the tip Arg614 is an ionic bond with Glu265 of p50 from subunit B. The next contact is by Tyr647 of IκBζ hydrogen binding to Lys343 of p50 on subunit C. This interaction could also be hydrophobically driven since portion of the lysine side chain runs parallel to the benzene ring of the tyrosine. On the last AR loop glutamic acid in position 687 of IκBζ is ionically bound to the basic side chain of Lys275 on subunit B of p50.

The third category of contact points are not mediated through hair-pin loops but rather by residues from α1 helices and short linker of AR5 and AR6 (Figure III.19). These residues include Glu622 of α1 from AR5, Gln 660 and Arg662 from short linker of AR6 to Ser299, Lys334 and Asp297 of p50 subunit B, respectively.

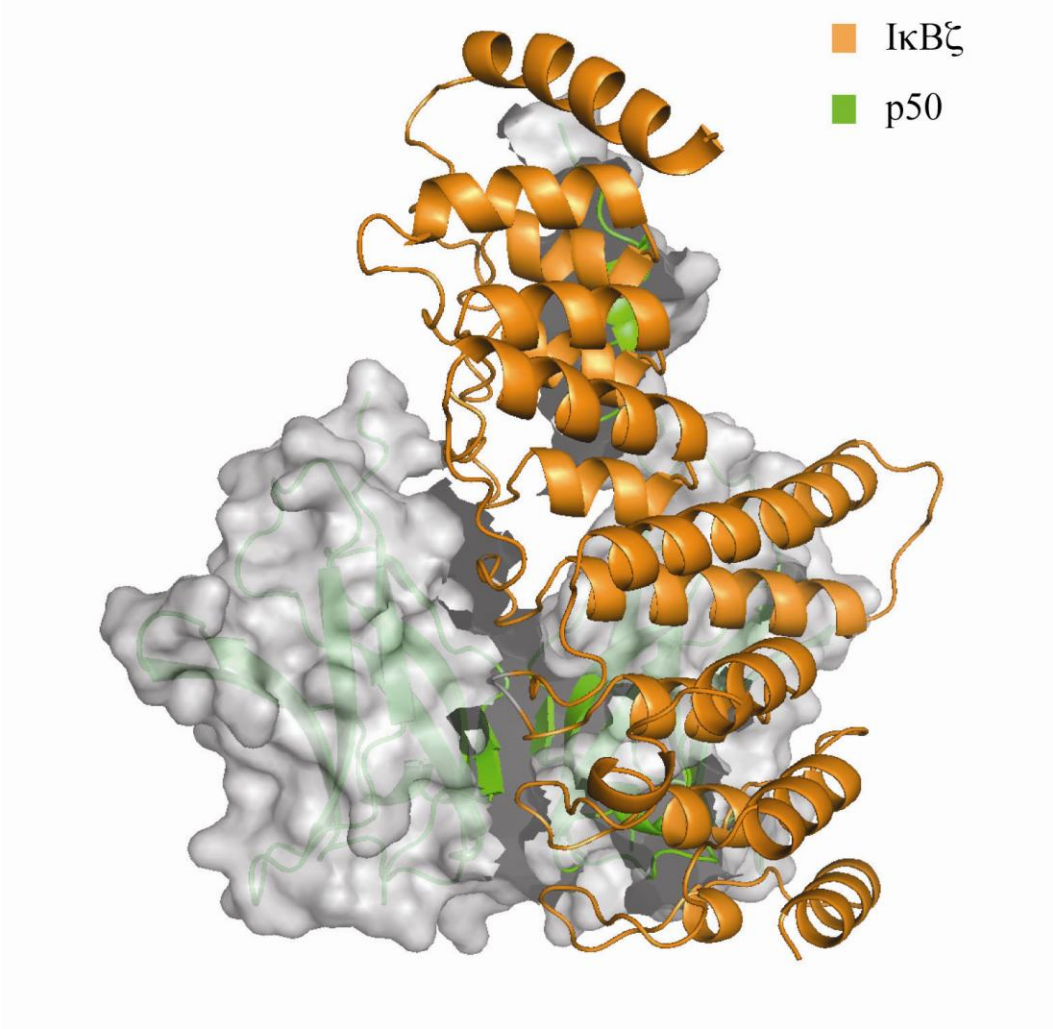

Figure III.20 Image showing IκBζ and p50 contacts along the dimerization interface. The contact regions are shown in discontinued surfaces. These area include NLS region (top), the dimerization interface region (center) and the AR5 and AR6 short linker region (Bottom right).

2.6 Recognition of p50 by IκBζ

IκBζ has consistently been shown to preferentially bind to p50 homodimer but not to homodimers of p65 (Danny Trinh, J Mol. Biol 2008) (Yamazaki jbc. 2001) (Hoffmann et al., 2006). This is intriguing since the two proteins are so similar structurally, especially in the region of the dimerization domain where IκBζ binds. Overlapping of p50 structure on top of p65 structure shows they are virtually identical except for in the region of nuclear localization sequence (NLS). For p50, its NLS region is made up of a short alpha helix flanked by two random coils. It sits within a crevice formed by the bending of the hairpin loops relative to the α1 and α2 helices of AR1 and AR2. Going back the "cupped hand" analogy, the crevice would be the space between the first two fingers and surface of the palm. The portion of p50 NLS that extends outside of the crevice becomes disordered and can no longer be seen in the crystal structure. For p65 its NLS region is much longer and helical. In fact, it's one long alpha-helix with six complete turns. The helix has a bend in the middle, which allows it to hug the contour of AR1 on the IκBβ structure (Malek, JBC, 2003). The two NLSs occupy roughly the same region on their respective IκB proteins. In fact the overlapping of the two structures showed that if p65 were to bind to IκBζ, the helical tip of its NLS region would collide with a capping helix on the AR1 region of IκBζ (Figure III.15). Immediately, this made us wonder if the collision is the reason or part of the reason why p65 cannot bind to IκBζ.

To test this hypothesis we constructed a truncated version of IκBζ with the capping helix removed, IκBζ(437-718). This was then used in a pull-down assay

against p50 and p65. Interestingly, the result showed without the capping helix IκBζ lost its ability to bind to p50 homodimer as well (Figure III.24A&C). This was surprising to us since we didn't expect the mutant to lose its ability to bind to p50. According to the crystal structure no parts of the helix interacted with the p50. Apparently the removal of the helix created a disturbance to the rest of the IκBζ structure as well.

This result doesn't necessarily disprove the collision theory but does make the experiment invalid. Knowing what we know now, a better way to design the experiment would be to leave the IκBζ alone and avoid the collision from the other end, by truncating parts of NLS from p65. However, this design has its own flaw. According to the published results from another lab, the portion of NLS on p65 we would need to cut off is critical to its ability to bind to IκBα (Komives, JMB, 2006). Without it the binding affinity decreased by 10,000-fold. In that case, we would most likely get the same result as the previous experiment where the positive control also fails (the positive control being the binding of p65 to IκBα) rendering the experiment invalid. The next best thing we can do here is truncate as little as possible from the p65 to avoid the collision while retaining its ability to bind to IκBα. From the crystal structure that place seems to be at Met313. Future experiments are needed to see if this construct of p65 can prove our collision theory. The positive result would be if this shorter construct of p65 can bind to IκBα and IκBζ.

Besides the region where the collision would be, we also looked at how the p50 NLS is accommodated by IκBζ and whether there are "hot spots" where the

interaction(s) is or are absolutely needed. However, since there are quite a few interactions along the NLS and we didn't want to start looking for these critical residues before knowing if the whole NLS is even important. That is why we constructed a shortened version of p50(245-350) with the NLS removed and did a pull-down assay with that. The result shows the NLS is definitely needed for p50 to bind to IκBζ. The result for that is explained in detail in the biochemical assay portion of the dissertation.

Next, we began to look for what is distinct about p50 NLS that set itself apart from p65. The region that jumped out is the area right before the NLS consensus sequence. It is made up of three charged residues Lys354, Glu355, and Glu356. Lys354 is hydrophobically bonded to Trp512 of IκBζ, which is a residue unique to it. No other IκB protein has a tryptophan there. Bcl-3, the closest homolog to IκBζ which is also known to bind to p50 but not p65, has a histidine there which is similar to tryptophan (Figure I.10). With its imidazole ring it should be able to accommodate lysine in the same manner. In fact, in another portion of the same structure, His525 can be seen doing just that, binding to Lys523 of IκBζ. The long hydrophobic side chain of lysine lying flat on top of the imidazole ring of the histidine. More interestingly, at this position IκBα and IκBβ, which cannot bind to p50, has an arginine, a basic residue that would repel the lysine residue from p50. At the same position p65 has an arginine by sequence alignment but in the crystal structure nothing can be seen within this vicinity. The helical form of p65 NLS points the arginine in another direction.

The next residue after Lys354 is Glu355. It is bonded to R514 of IκBζ through an ionic interaction. This arginine is also found on IκBNS, which preferentially binds to p50 but not p65 (Hirotani, J.Immunol. 2005). IκBζ and IκBβ, on the other hand, have an asparagine and histidine, respectively. They can theoretically bind to the Lys354 but only as a weaker hydrogen bond. On this position p65 has a histidine by sequence alignment but Asp294 by over lapping of the crystal structure. The next residue in this triad is Glu356. It contacts His478 of IκBζ. This hisidine is conserved in IκBNS and p100. In IκBα and IκBβ this position is an asparagine and aspartic acid, respectively. Glu356 can form hydrogen bonds with asparagine but not with aspartic acid. In the position of Glu356, p65 has an arginine by sequence alignment and the same residue in the crystal structure. Arginine is unsuited to interact with the histidine on IκBζ.

After this point is the NLS region. The consensus sequence for this region is KRKR, or some slight variation of it. The high conservation of the sequence and their reciprocal acidic residues among all IκB proteins make them important for function of the protein but less likely to play a selective role. Furthermore, the long flexible side chains of arginines and lysines are likely to be less selective as the exact location of the acidic residues, as long as they are within the vicinity.

Nevertheless, before we can look into specificity we first need to establish necessity. To test the necessity of these residues we have systematically either truncated them or replace it with alanine. The results of these knockout studies are explained in detail in the section below.

3. Biochemical Assay Results

3.1 The Capping Helix on IκBζ Stabilize the Rest of the Structure

3.1.1 Limited Proteolysis

Limited proteolysis was used to assess the effect of the capping helix on the IκBζ ARD structure. The hypothesis that was tested through this experiment was that the capping helix stabilizes the rest of structure by covering a hydrophobic region on top of ankyrin repeat 1. This hypothesis is further supported by a study that showed helix four of the NLS region in p65 stabilizes IκBα structure in binding (Bergqvist et al., 2006). The capping helix covers about the same region on IκBζ as helix four on IκBα (Figure III.15). The logic behind the assay was if the capping helix stabilizes the structures removing it should make IκBζ more susceptible to proteolytic degradation by the digestive enzyme chymotrypsin.

Two constructs of IκBζ were digested side by side under the same conditions. Interestingly, the construct without the helix, GST- IκBζ(437-718), degraded much more rapidly. Within 30 min the high molecular weight band of 58.46kDa were almost completely broken down to smaller constituents (Figure III.21). The three most distinct bands correlate to FW of 27 kDa, 15 kDa, and 11 kDa. The 27 kDa band is most likely to be the GST tag, which is known to be very stable. The 404-718 constructs, on the other hand, were much more resilient under the same conditions. Its high molecular band can be seen even after 2 hours. Interestingly this difference was less apparent in a parallel experiment where four times as much more chymotrypsin

was used. This further supports the different banding pattern between the two constructs was a result of protein stability, which can be overwhelmed by too much chymotrypsin.

3.1.2 Circular Dichroism

The stabilizing effect of the capping helix was also examined by circular dichroism (CD). The thinking behind this experiment was that since CD is a very good quantitative measure of protein secondary structure, especially monitoring the degree of α-helicity in proteins in solution, it should show a strong signal for IκBζ since it is made up predominantly of α-helices. As we expose these proteins to increasingly strong denaturing conditions, such as heat or urea, this signal should persist longer in protein that is more stable. The stability in the tertiary structure typically leads the stability of secondary structures since they enforce each other. In the case of heat denaturation, the construct with the capping helix demonstrated a melting temperature of 42°C (Figure III.22A). The construct without the helix failed to show a change in the CD signal at any temperatures. This is indicative of a protein that is disordered to begin with. To verify this we took a full CD spectrum of both proteins at 20°C. The differences were obvious. The spectrum from the construct

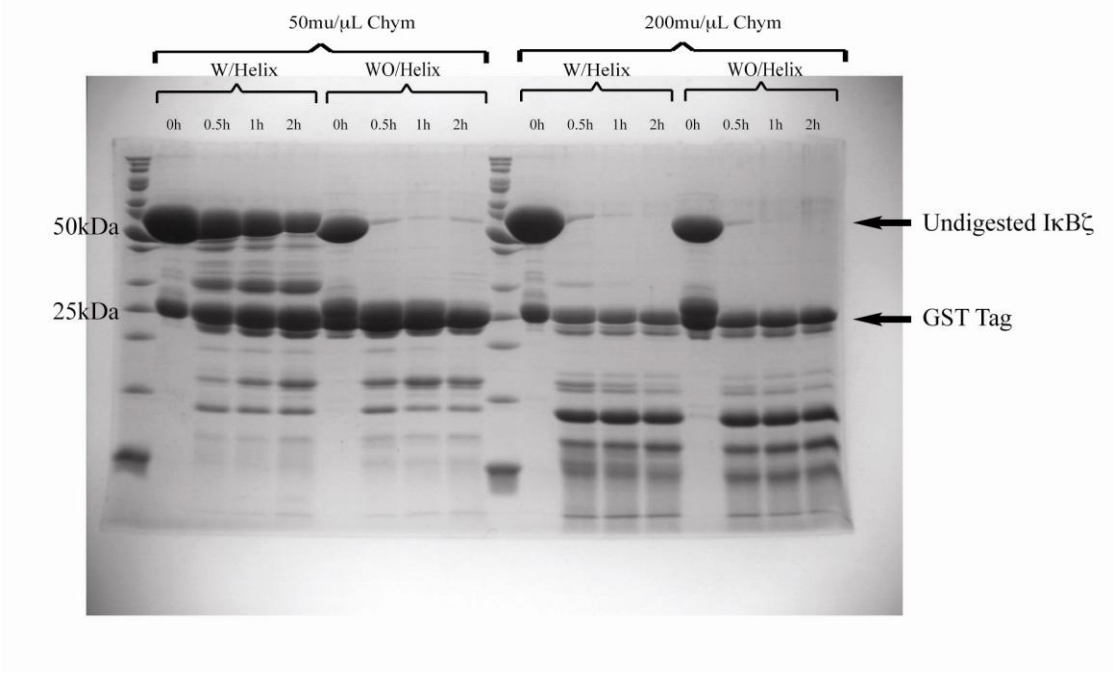

Figure III.21 GST tagged IκBζ with or without the capping helix were exposed to different amounts of chymotrypsin. The left half of gel contains the samples digested with 50mu/mL of chymotrypsin, while on the right 200mu/mL. At the lower concentration, IκBζ with the capping helix withstood the digestion much better than one without it. At the higher concentration of chymotrypsin both proteins behaved the same.

containing the capping helix is indicative of α-helices (Figure III.22B). The spectrum from the construct without the capping helix, even at low temperature, exhibits a spectrum similar to that what is seen for the other construct at the high temperatures (data not shown). This demonstrates without the capping helix IκBζ assumes the same unfolded form as seen at high temperatures.

In order to observe whether the same thing would happen if it were exposed to another form of denaturation, we next tried titration with urea. The concentrations of urea ranged from 0M to 8M. Again we observed that the protein construct with the capping helix showed a decreased 222nm signal upon being denatured, indicative of α-helix rich proteins (Figure III.23A). The other construct showed no change in its 222nm CD signal (Figure III.23B). The 222nm spectra patterns are reminiscent of what was seen in the thermal denaturation experiments.

Putting these two sets of data together the CD experiments indicate that, without the capping helix, IκBζ cannot assemble itself into the α-helix based AR structure. It is unclear what the alternative structure may be but is certainly disordered.

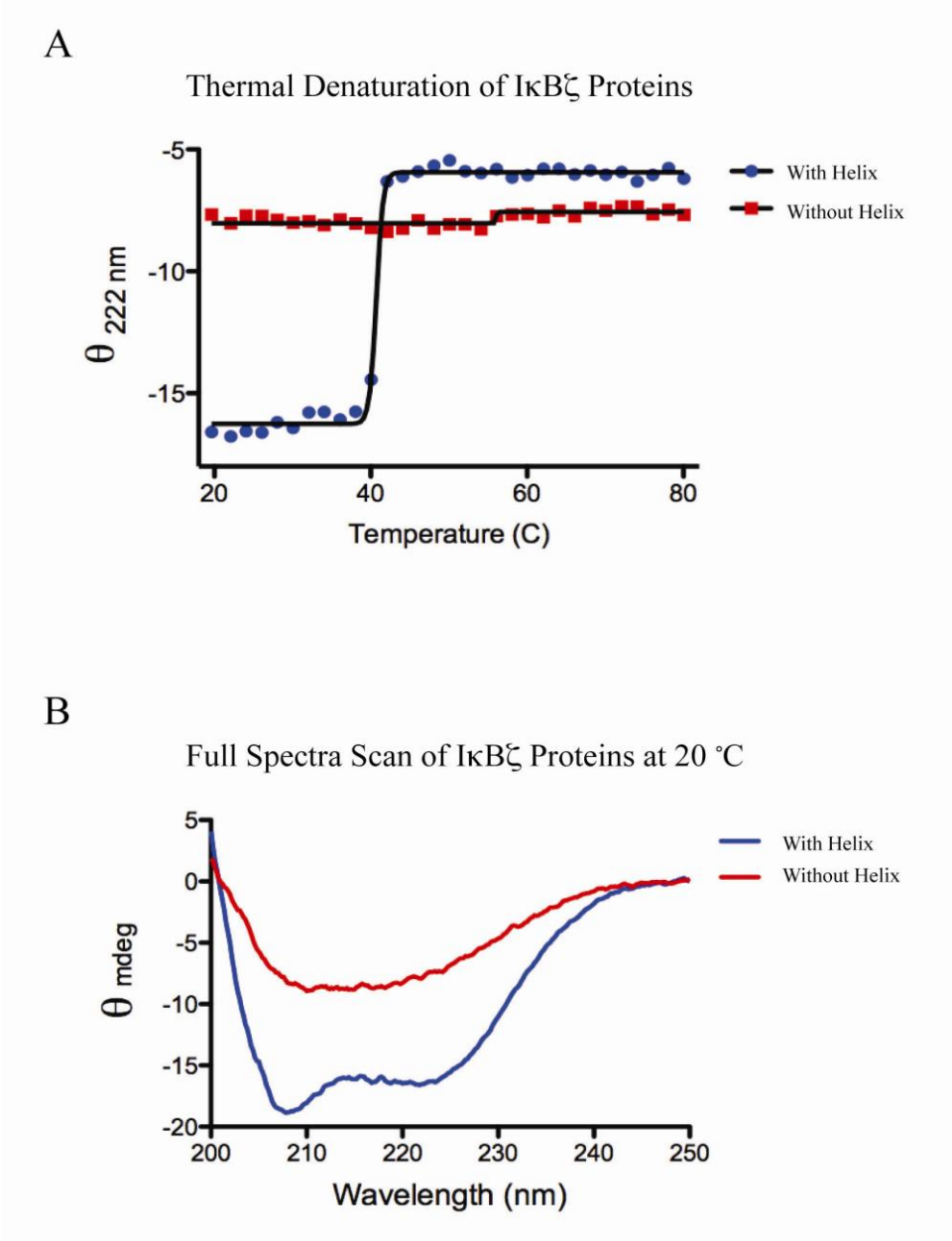

Figure III.22 A. The stability of the different constructs of IkBζ were tested with thermal denaturation and monitored by circular dichroism (CD). The construct with the capping helix gave a melting temperature of 42 C, while the one without it gave a signal correlates to a disordered protein at all temperatures. B. Full spectra scan of the two proteins showed they exhibit a different spectra profile even at room temperature (20°C).

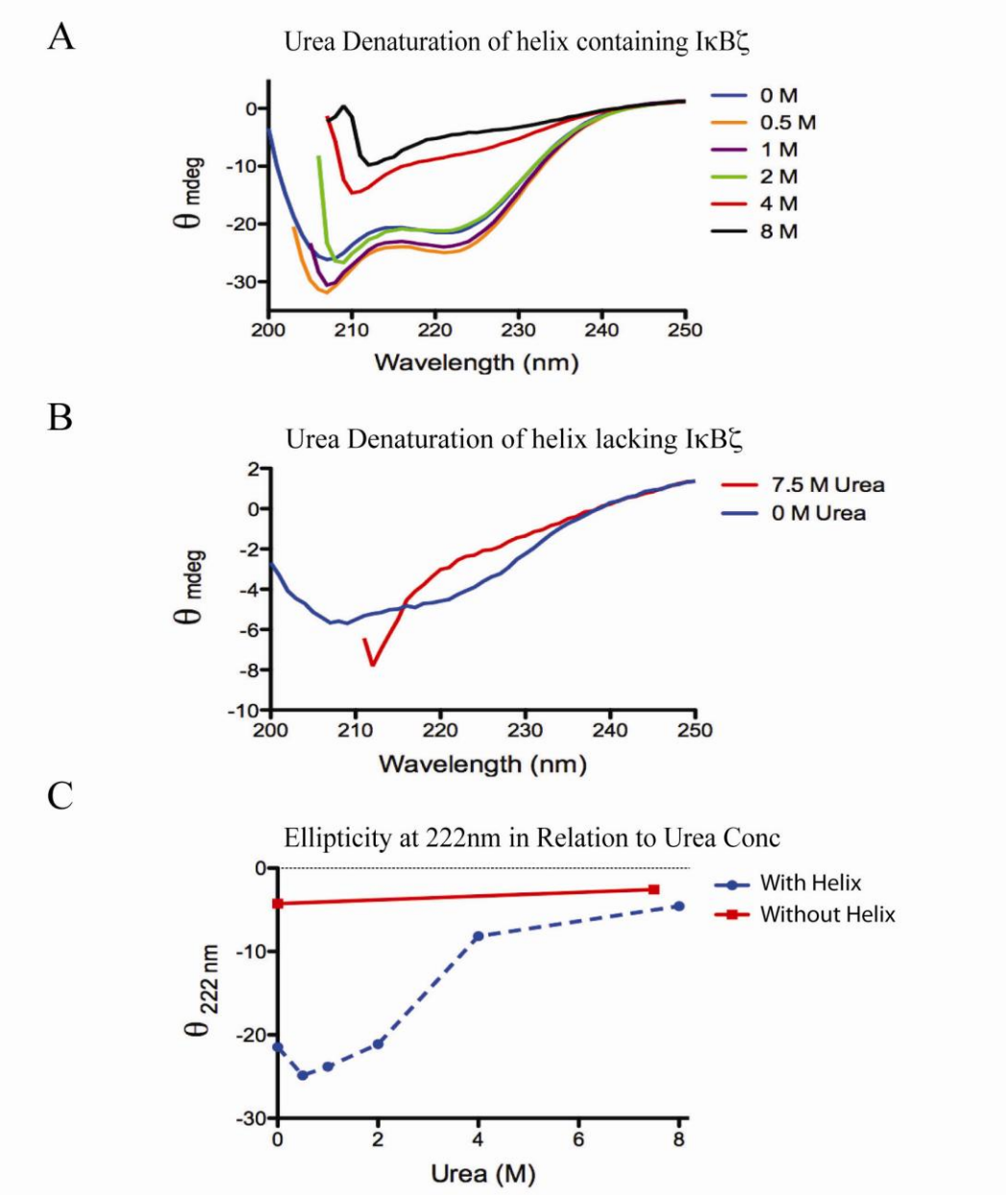

Figure III.23 The stability of the different constructs of IκBζ were also tested with urea denaturation and monitored by circular dichroism (CD). A. Full spectra analysis of the helix containing construct were taken at each urea concentration. B. Two full spectra analyzes of the construct without the capping helix were taken at two extreme concentrations. C. Ellipticity at 222nm for both proteins were mapped out. The result is consistent to what was seen for thermal denaturation.

3.2 The Effect of IκBζ Structural Stability on p50 Binding

3.2.1 GST Pull-down Assay

In light of the fact that the capping helix stabilizes the overall folded structure of IκBζ, we next wished to determine its effect on p50 homodimer binding. A GST-tagged version of IκBζ(437-718) was cloned for the pulldown assay. Its ability to bind to p50 and p65 homodimer was compared to GST-IκBζ(404-718), which contains the capping helix, and GST- IκBα(61-317), which serves as a positive control. The two different constructs of IκBζ and IκBα was incubated with increasing amounts of p50(245-376). After 30min of binding the complex was fished out with glutathione-sepharose resin. Any non-specific bound protein was washed way with repeated buffer changes. The bound proteins were analyzed by SDS PAGE gel and Coomassie staining. As expected, IκBζ with the capping helix bound to p50 than p65 (Figure III.24A) while IκBζ(437-718), without the helix, lost its ability to binding to p50.

3.2.2 Surface Plasmon Resonance

The effect of the capping helix on p50 binding was also assessed by SPR. Because of the surface labeling chemistry of the instrument His-tagged IκBζ was used instead of the GST-tagged version of the protein. The two constructs used were still the same, IκBζ(404-718) with the capping helix and IκBζ(437-718) without. These were immobilized onto the nickel-coated chips by its N-terminal histidine-tag. The interactions were measured in relative units (RU) while p50(245-376) was flowed over

the chip surface. The result showed the construct with the helix was able to interact with various constructs of p50 (Figure III.24B). This was indicated by the immediate increase of the RU following the addition of p50, marked time point zero. Binding, as evidenced by RU on the sensorgram, continued to increase as more p50 was flowed over the chip. Rate of increase in binding begin to slow down a bit towards the end of the 60 second loading phase showing it had approaching saturation point. The loading phase was immediately followed by a dissociation phase, which consists of flowing nothing but buffer over the chip surface. It is during this time that the dissociation constant of the interaction was measured. The dissociation can also be seen in the decreasing of the signal. To ensure the result is not due to non-specific binding we ran a negative control in a neighboring channel on the same chip. In the channel we immobilized His-tagged Ferric Binding Protein A (FbpA), a protein that should should not interact with p50. The result showed just that (Data not shown). All the constructs of p50 gave the same RU response against the buffer. The channel with IκBζ(437-718) gave a signal very similar to that of the negative control lane. Only p50(39-363) gave some signal of interaction but quickly dissociated after loading phase. The interaction seems to be very weak (Figure III.24C).

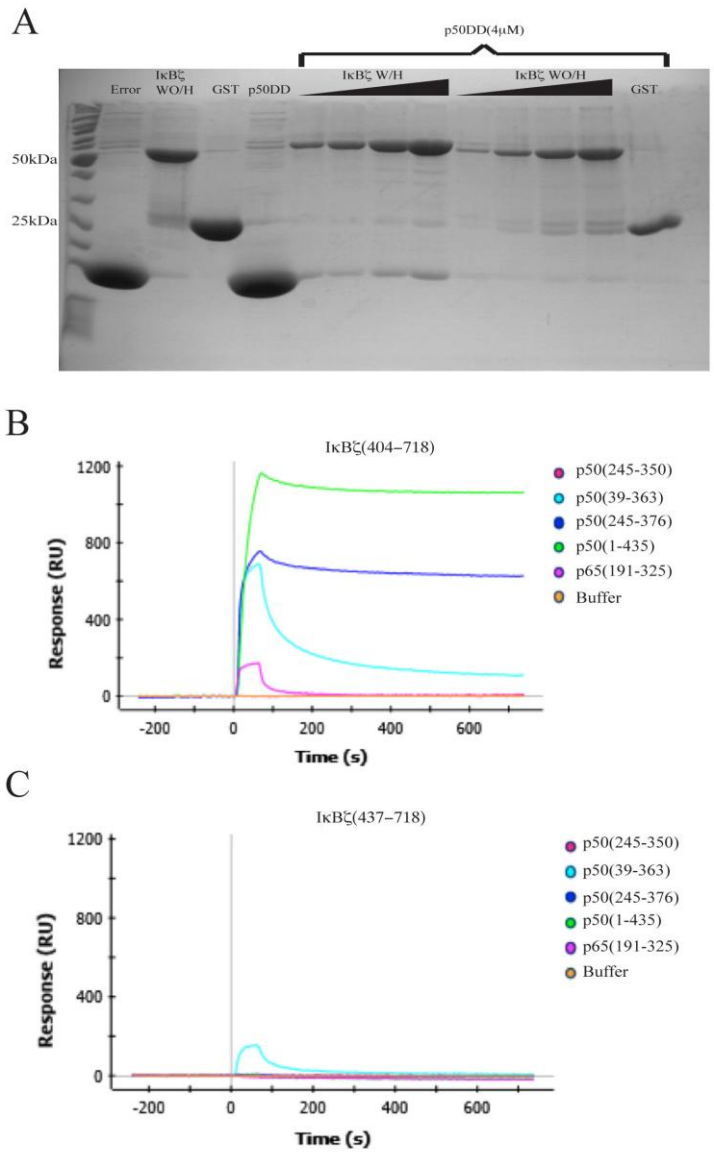

Figure III.24 A. The effect of capping helix has on the binding of p50 was testing with GST pull-down assay. Increasing amounts of IkBζ were incubated with 4mM of p50DD. Following the wash bound P50 were analysed by SDS PAGE. B. This difference in binding was then analysed with SPR. IkBζ with the capping helix interacted with NLS containing p50. C. No or weak interaction were seen for the IkBζ without the capping helix.

3.3 The NLS Region on p50 is Required for IκBζ Binding

3.3.1 GST Pull-down Results

The extensive interactions between the NLS region of p50 and IκBζ led us to speculate its importance for binding specificity. But before the question of specificity can be addressed we need to first establish its necessity. To do that we simply removed to the region 351 to 435 from the p50 structure. The truncation was stopped at residue 350 because it contains all of the NLS region and a flexible linker region which made no contact in the crystal structure. Residue 350 is also where the dimerization domain ends. The ability of the protein to interact with GST- IκBζ(404-718) was compared to that of p50(245-376) which has the NLS intact and was what was used in the crystal. Without the NLS region p50 completely lost its ability to bind to IκBζ (Figure III.25). This was the case even at the highest concentration tested in the experiment, 500nM. While by comparison, IκBζ interactions with p50(245-376) were detected at 125nM.

3.3.2 SPR Results

SPR experiments confirmed the importance of the NLS region on p50 for IκBζ interaction. In that experiment His-tagged IκBζ(404-718) was immobilized onto a nickel-coated chip. Recombinant p50 proteins with or without the NLS were flowed over the chip. The interactions were assessed by the increase of the RU. While

p50(245-376) gave the classical saturation curve associated with binding, p50(245-350) gave a flat line (Figure III.24B).

3.4 NLS Region is Sufficient for IκBζ Binding

3.4.1 GST Pull-down Results

Once the importance of the NLS in the interaction of p50 with IκBζ was established we next wanted to see if it alone was sufficient to transfer the binding specificity of IκBζ from p50 to p65. To do that we made a chimera protein composed of the dimerization domain of p65 and NLS region of p50. The exact residues taken from p65 are 191 to 290, and from p50 are 351 to 376. This chimera's ability to bind to IκBζ was assessed by GST pull-down. 2μM of GST-IκBζ(404-718) was mixed with increasing amounts of chimera ranging from 0.25μM to 2μM. Interaction between IκBζ and the chimera was detected in all the concentrations (Figure III.26A). This was also seen for the wild type p50(245-376) positive control group. Weak interaction was detected for IκBζ and p65, but significantly less than the p50 and the chimera. This weak interaction is known was previously published by our lab (Trinh et al., 2008). However, the difference in binding affinity between p65 and chimera is dramatic and obvious.

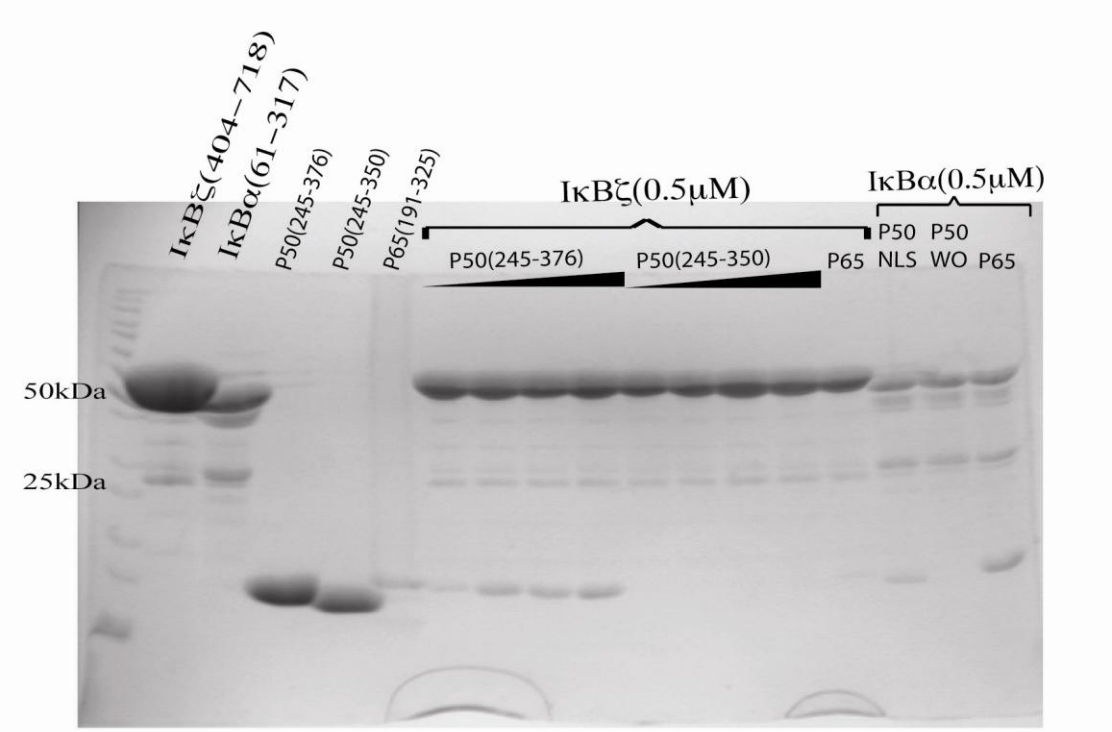

Figure III.25 To assess the role nuclear localization sequence (NLS) region on p50 has on the binding of IκBζ we made a truncated version of p50 with the NLS removed, p50(245-350). Without the NLS region p50(245-350) failed to pull-down IκBζ even at its highest concentration. p50(245-376), on the other hand, interacted with IκBζ even at lowest concentration.

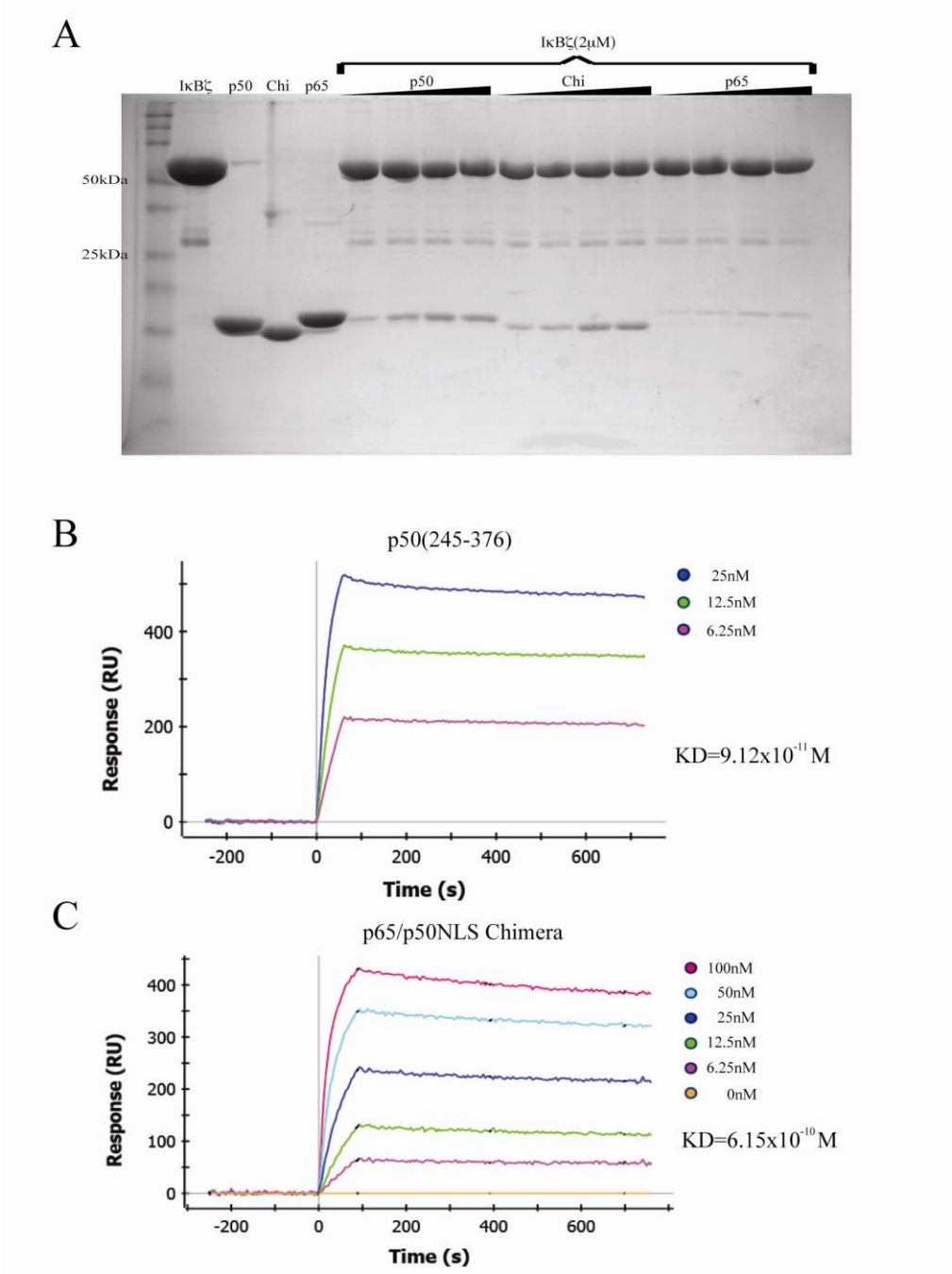

Figure III.26 To test if the binding specificity of p50 can be transferred to p65 by swapping of NLS we made a chimera (Chi) protein of just that. Its ability to bind to IkBζ was tested with GST pull-down assay and SPR. A. The pull-down result showed the chimera bound just as well as the wild-type p50. B. This was confirmed by SPR where it measured comparable KDs for both proteins.

3.4.2 SPR Results

This gain of binding function by IκBζ to p65 by the swapping of NLS region was further analyzed by SPR. For the ligand the His-tagged IκBζ(404-718) was anchored to the nickel-coated chip. The p65DD-p50NLS chimera protein bound to IκBζ with nearly the same affinity as the wild type (Figure III.26C). The chimera protein gave a K_D measurement of 6.15×10^{-10} M, which is very close to the 9.12×10^{-11}M value for K_D measured for the wild type. We also know that this cannot be caused by non-specific binding since p50 has already been shown not to interact with the chip surface itself in a previous SPR experiment (Figure III.24C). Since the proteins gave such close K_D readings, inferences can be drawn that NLS region, compared to that of dimerization domains, contributes majority of the binding forces. The slightly weaker affinity observed in the chimera compared to that of wild type could be due to the less than perfect binding accommodation IκBζ has for the DD of p65.

3.5 NLS has a Binding "Hot Spot"

3.5.1 SPR Results

After determining the importance of the p50 NLS region in mediating interactions with IκBζ, we next wanted to see if every portion of the region contributes equally to the binding affinity of IκBζ. To do that we made different versions of p50 constructs in which different portions of the NLS region was removed. These

constructs include p50(1-435), p50(245-376), p50(39-363) and p50(245-350). Binding affinity for each of them against His-tagged IκBζ(404-718) was measured with SPR. Since these constructs are not the same size their binding affinity cannot be compared directly by the K_D. A more accurate way of measuring that would be by looking at its dissociation kinetic rate constant (k_{off}). This is because in SPR K_D is derived from the association rate constant (k_{on}) and the dissociation rate constant (k_{off}). More precisely $K_D = k_{off}/k_{on}$. The problem with that is not all of the constructs are the same size. This is because we did this experiment with whatever protein we had on hand. The different sizes affect the diffusion rates of the protein thus giving different association rates. Dissociation is less affected by this since it doesn't depend on diffusion. The k_{off} from the experiment (Figure III.27) (Table III.5) showed the last 59 amino acids contributed very little to the binding. This is was not surprising since our crystal structure showed all of the residues past the number of 366 were disordered did not participate in binding. The removal of the next thirteen residues, 364-376, increased the off rate by 10.2 times, significant, but enough to constitute it a "hot spot".

However, the removal of the next 14 amino acids, 351-363, abolished binding altogether. This told us that this region is absolutely required for the binding but we still didn't know if the whole region was required or whether just a few residues within the region were key. Another thing we could not be sure of was whether or not we had discovered a "hot spot" region or did we just finally cut too much of the NLS region off.

To differentiate this we generated a knockout mutant of p50 using site-directed mutagenesis. Residues in question were systematically replaced with alanine while leaving the rest of the NLS intact. Based on our crystal structure we identified seven residues in that region of 351-363 engaged in ionic interactions: Lys354, Glu355, Glu356, Arg359, Lys360, Arg361, and Lys363. Since they are bunched together we decided to replace them in groups of three. Lys 354, Glu355 and Glu356 being one group and Arg359, Lys 360 and Arg361 being the other. The first group is referred to as KEE to AAA, while the other RKR to AAA. KEE to AAA mutations caused minimal amount of disturbance to the ability of p50 to bind to IκBζ. Binding affinity from SPR measured K_D of 2.55×10^{-10}M versus the wild type which was 9.12×10^{-11}M (Table III.5).

The RKR to AAA mutations on the other hand, proved to be much more catastrophic. Without those three basic residues p50 lost all of its IκBζ binding ability (Figure III.28A). It gave the same response as the channel with only buffer loaded.

3.4.3 GST Pull-down Results

To verify what was seen in SPR the interaction between the knockout mutants and p50 was assessed by GST pull-down. The finding correlated to what was seen in SPR. KEE to AAA mutant behaved just like the wild type p50 (Figure III.29). Just as

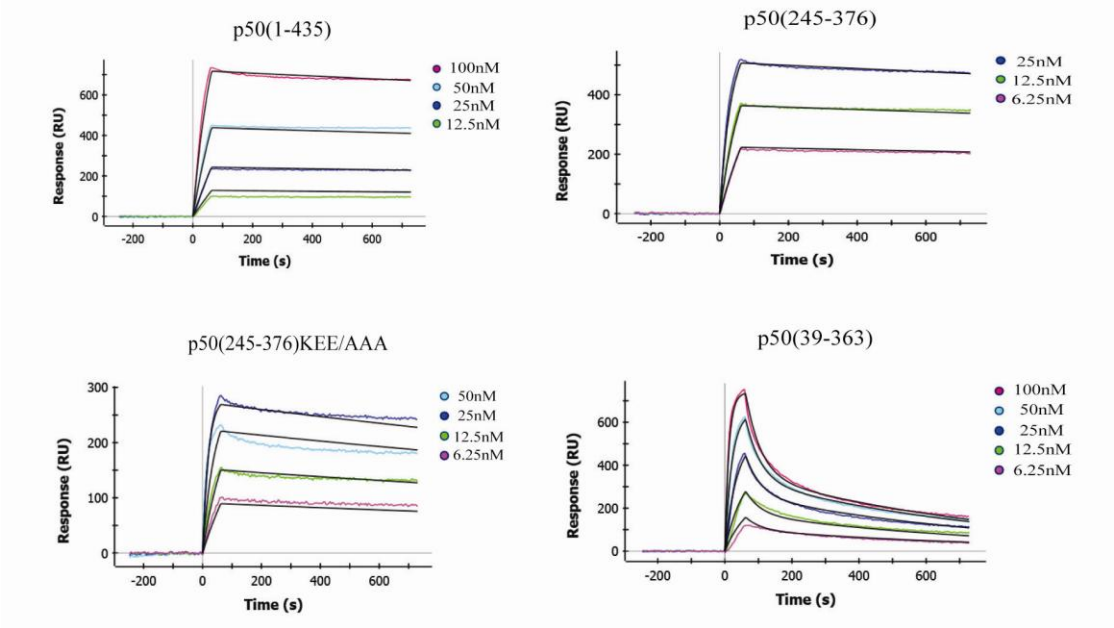

Figure III.27 All the p50 constructs that registered interactions were titrated to have its binding affinity measured. The SPR signals from the different concentrations are shown above.

Table III.8 NLS truncation and mutations

	ka(M)	kd(M)	KD(M)
p50(1-435)	1.43E+05	9.93E-05	6.92E-10
p50(245-376)	1.20E+06	1.10E-04	9.12E-11
p50(245-376)KEE/AAA	9.85E+05	2.51E-04	2.55E-10
p50(245-376)RKR/AAA	n/a	n/a	n/a
p50(39-363)	8.71E+05	1.31E-03	1.51E-09
p50(245-350)	n/a	n/a	n/a

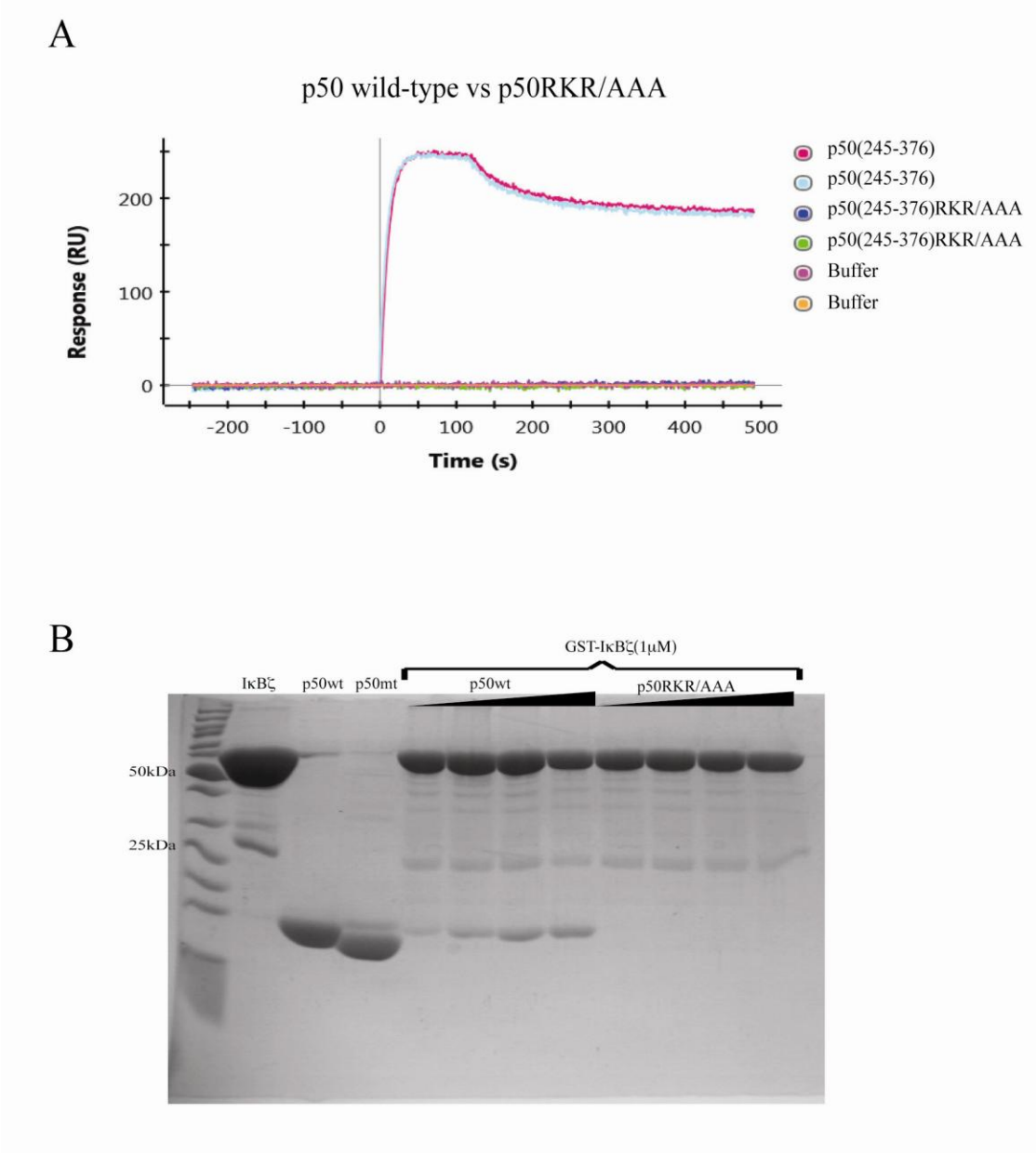

Figure III.28 The three basic residues, Arg359, Lys360 and Arg361, on the NLS region of p50 proved to be crucial for IkBζ binding. A. Without them p50 gave the same SPR signal as the buffer. Note. The experiment was done in doublets because of extra channels. B. GST pull-down assay confirmed the result seen in SPR experiment.

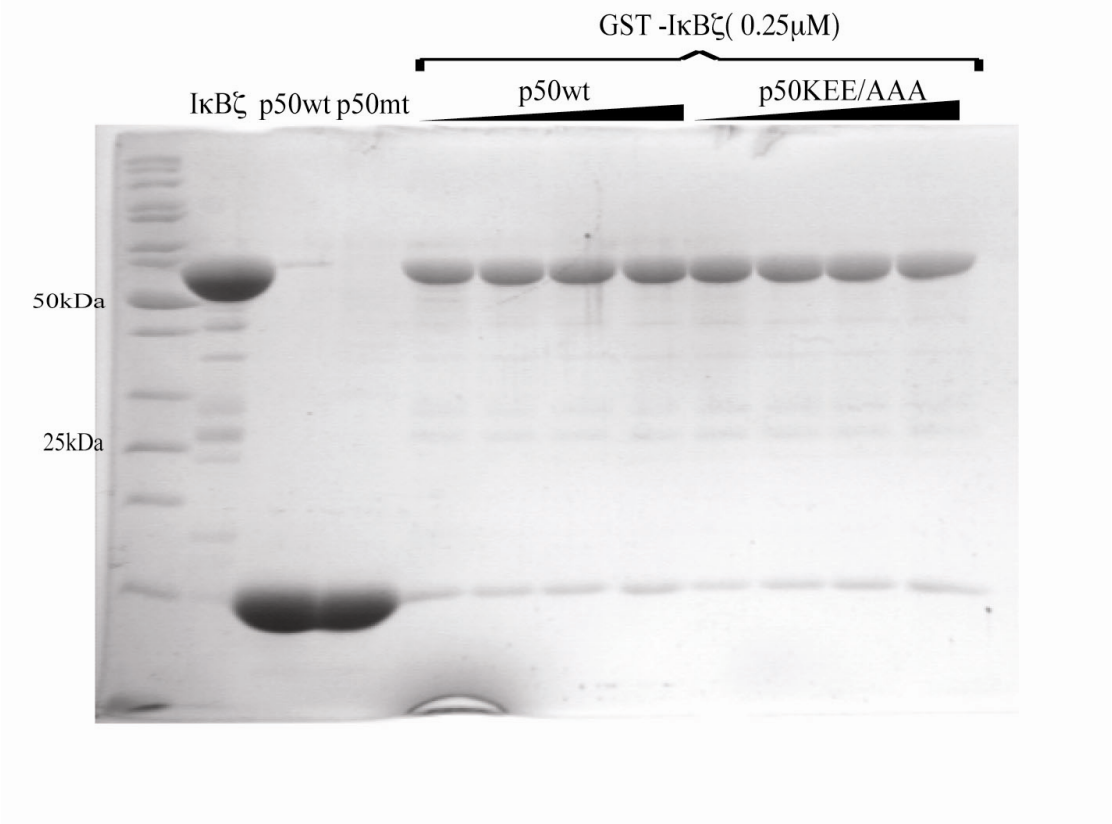

Figure III.29 To verify that the three charged residues immediately after the NLS do not play a critical role in binding we tested their effect on GST pull-down assay. Just as was seen in the SPR result, the p50KEE/AAA mutant behaved indistinguishable from the wild-type.

SPR had predicted, the mutations caused such a minute disturbance to the binding the Coomassie dye stained gel could not pick out the differences. RKR to AAA mutation on the other hand caused complete loss of binding (Figure III.28B).

3.6 Binding Mechanism of IκBζ on DNA Promoters

3.6.1 Detection of p50:IκBζ Ternary Complex on DNA Promoters

3.6.1.1 SPR Results

Because p50 itself does not have transactivation domain it has long been suggested it function as gene suppressor by competitively bind to the promoter, physically blocking other NF-κB proteins from turning on the gene. This theory is best supported by a study that showed that induction of NF-κB activity requires the displacement of p50 by p65 (Zhong et al., 2002b). However, p50 has also been shown to gene activator by its association with one of three of the nuclear IκB proteins, Bcl-3, IκBζ, and IκBNS (Mankan et al., 2009) (Yamamoto and Takeda, 2008), all of which have transactivation capability and one of which is the focus of my study, IκBζ. This raises an interesting question: Does IκBζ activate target genes by forming a ternary complex with DNA bound p50 homodimer or does it do so by removing it from the p50. To explore this question we chose six DNA promoter sites, two of which are the NGAL and IL-6 sites that were included in the complex crystal structures with p50 reported in this dissertation. The other four are major histocompatibility complex (MHC) promoter, κB light chain promoter, IP-10, and PD-

Table III.9 p50 DNA binding affinities

Promoter	Sequence	ka(1/MS)	kd(1/S)	KD(M)
PD-12	CTGTGGGGAATTCCCCATA	5.55E+04	2.54E-04	4.58E-09
IL-6	CATGGGAAAATCCCACA	1.05E+05	5.54E-04	5.26E-09
MHC	CTGTGGGGATTCCCCATGA	4.97E+04	3.20E-04	6.43E-09
κB	CTGTGGGACTTTCCATGA	3.13E+04	7.55E-04	2.41E-08
NGAL	TCCGGGAATGTCCCTCA	1.88E+04	5.33E-04	2.84E-08
IP-10 A/T	CTGTGGGAAATTCCATGA	3.26E+03	9.98E-04	3.06E-07

Note: The binding affinity between p50 homo-dimer and the six DNA promoters are listed above. This was measured with the biotinylated promoters immobilized onto the avidin-coated chip. Different concentrations of p50 were then flown over the promoters.

12 promoters. These four are selected because of their binding affinity for p50 homodimers. We wanted select a spectrum of promoter sites that have high, moderately high, and medium affinities. How these are defined is listed in this table (Table III.6). In order to detect whether IκBζ forms a stable ternary complex with p50 or removes it from promoter sites we immobilized biotinylated DNA on a streptavidin coated chip. The promoters were loaded with 125nM of p50 homodimer to the point of saturation. This was indicated by plateauing of the RU signal. After that the chip was washed with buffer to wash away any non-specifically bound p50. Once the signal leveled out, which took about 3min, various concentrations of IκBζ was flowed over the chip. The relative unit (RU) went up immediately indicating interaction (Figure III.30A). The signal continued to increase during the whole three minutes of the loading phase. This suggests the IκBζ and p50 interaction has a slower on rate than that of p50 for DNA. However, on the subject of ternary complex what is more relevant is the elevation of the RU signal relative to the control channel after loading of IκBζ. The elevation of signal suggests an increase of mass, which can only be explained only by formation of ternary complex. Non-specific binding between IκBζ and the chip was ruled because we measured for interaction of IκBζ with a DNA coated chip. As expected, IκBζ registered zero signals in the absence of p50 (Figure III.31). What further supported the evidence of ternary complex was the concentration dependent increase of RU signal. Higher concentration of IκBζ correlated with greater increase of signal. This makes sense since more IκBζ added should result in a greater amount of ternary complex formation.

3.6.1.2 EMSA Result

To confirm the formation of a stable IκBζ ternary complex on DNA promoter, we employed the time tested method of Electrophoretic Mobility Shift Assay (EMSA). Rather than test all six promoters that behaved very similarly in SPR experiment, we chose only one to prove the point. The promoter we used was a 41bp IL-6. The radio-active probe was incubated with 1μM of either p50 homodimer, p50/p65 hetero-dimer, or p65 homo-dimer and increasing concentrations of GST-tagged IκBζ(404-718). Ternary complex was detected in the p50 lanes with IκBζ concentrations of 0.7μM or higher (Figure III.32). A faint band can also be seen in the p65:p50 lanes with IκBζ concentration of 2.8μM. No ternary complex was detected in lanes with p65 homo-dimers.

3.6.2 IκBζ has no Effect on the Disassociation Rate of P50 from DNA

Further inference can be drawn from the SPR data obtained for the ternary complex experiment. By looking at the slope of the disassociation to we can see if IκBζ alters the

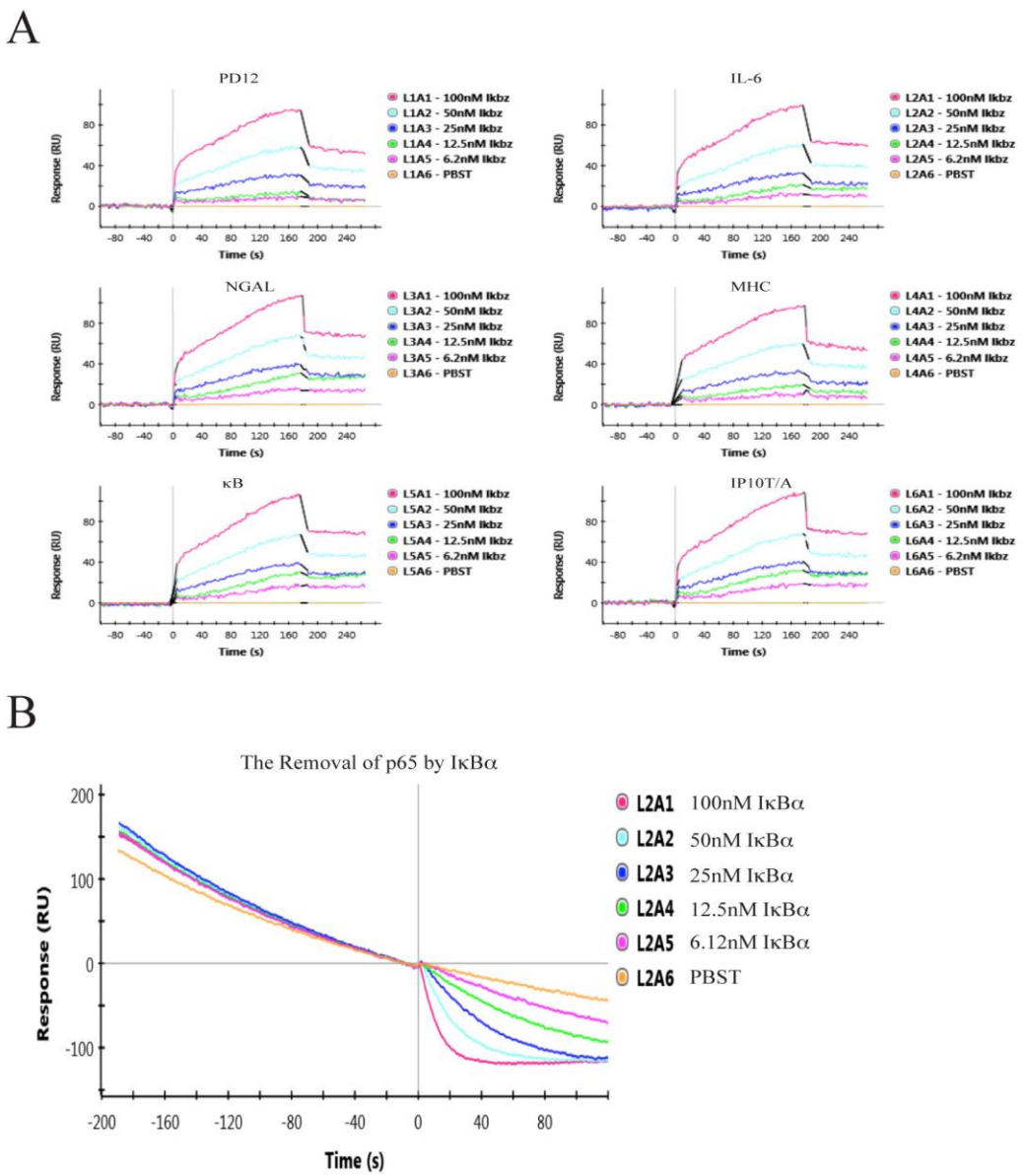

Figure III.30 Using SPR we looked at the effect of IkBζ has on promoter bound p50 homo-dimer. A. IkBζ formed stable ternary complex on all six promoters tested. This is indicated by the elevation and the sustaining of the RU signal after the loading of IkBζ. B. As a negative control, a SPR graph of IkBα removing p65 homo-dimer from IL-6 promoter is shown here. Notice the immediate decreasing of RU signal at time point zero when IkBα was added.

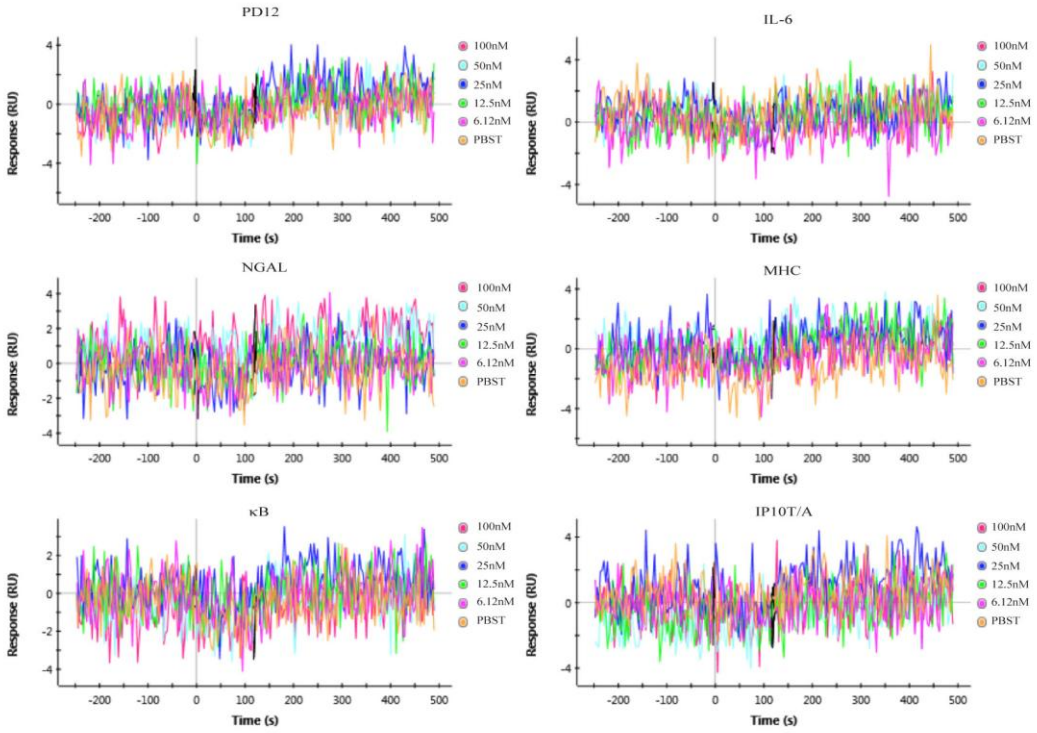

Figure III.31 To ensure the signal we detected for ternary complex was not an artifact of non-specific binding we repeated the experiment without adding p50. Just as expected IkBζ did not show any interaction with the chip surface with DNA promoters on it.

disassociation of p50 from DNA. If IκBζ had accelerated p50's rate of disassociation it would have generated a signal line with a negative slope which given enough time would eventually fall below RU of the base line. What that means is in the presence of IκBζ there now less p50 on these promoters now than if no IκBζ were added. However, if IκBζ decreases P50's rate of the disassociation from DNA it would have generated a line with a positive slope. The positive slope indicate not only the ternary complex is present it also stabilizes p50 more so onto the DNA. The near zero degree slopes of all the lines indicate even though the overall signals have increased but the rates have not changed (Figure III.32). And the fact the same phenomenon was seen for all six promoter sequences show IκBζ behaves the same with P50 regardless of which promoter is bound to supporting the binding of IκBζ does not alter the disassociation rate of P50 from DNA in any way regardless of the promoter sequence.

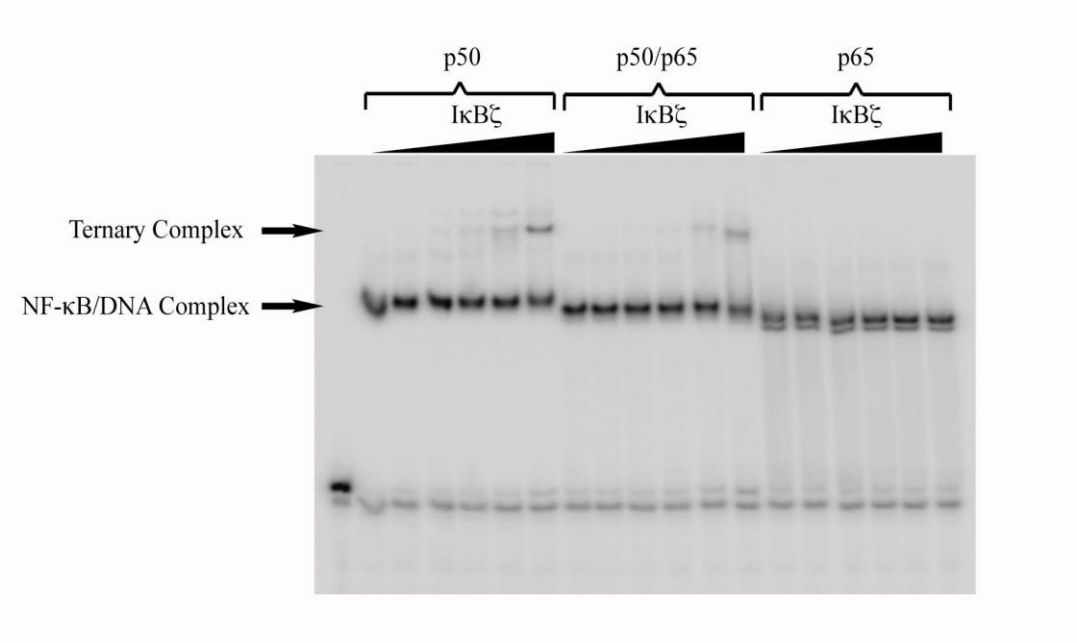

Figure III.32 Ternary complex of IL-6 promoter/p50 homo-dimer/IkBz was also detected by Electrophresis Motility Shift Assay (EMSA). Ternary complex was also detected on the p50/p65 hetero-dimer but to a lesser degree. This makes sense since our crystal structure shows IκBζ interact with p50, which the hetero-dimer only has one. This should reduce their interact by half as seen on the gel. No ternary complex was detected for p65 homo-dimer which is also consistent with our earlier results.

Chapter IV

Discussion

4.1 The p50/DNA Structures

We undertook to crystalize p50/IL-6 and p50/NGAL structures for three reasons: First was to solve the DNA half of the IκBζ/p50/DNA ternary complex structure. Our original attempts to crystalize the complex directly was met with technical difficulties which caused us to seek alternative methods. One of them was to divide the complex in two and crystalize them separately. The p50/DNA structure would be one half of that. The second reason for us to crystalize structure was to see if binding of IκBζ cause any conformational changes in the dimerization of p50. To do that we need to compare an unbound structure of p50 with that of one that is in complex with IκBζ. The p50/DNA structures serve as the unbound structure. The third reason is to see if binding of p50 to IκBζ regulated gene cause conformation changes that are recognizable by IκBζ. This could be the means which p50 recruits IκBζ to its associated genes.

Because the DNA used for the p50/IL-6 structure were much longer than that of p50/NGAL structure it was used to make the composite image of the ternary complex. In the composite image the C-terminus of IκBζ can be seen colliding with phosphate backbone of the DNA. The significance of that will be discussed in greater details in the IκBζ portion of the discussion below.

Overlapping of the DD from two novel structures along with the previously solved p50 structures showed there were no differences. The binding of IκBζ on p50 did not alter its DD structure or its internal conformation in anyway (Figure I.4B).

The uniformity of the inter-domain conformation suggests the DD serves as structure scaffolding on which IκBζ can bind to. It's unlikely it plays any role in the regulatory mechanism in ways of conformational change. Even though we couldn't compare the NTD structures of p50 from the solved structures their internal confirmation are less likely to be altered by IκBζ. IκBζ does not reach far enough to make any contact with this region of p50. The closest gap between the two is 14.9Å.

As for the third question we were wanted to address p50 did not adopt any unique conformation on the IL-6 promoter that would suggest a possible regulatory mechanism. It has the same canonical butterfly shape seen in all of the NF-κB structures. Even all the DNA contacts made by p50 are conserved among the same residues. P50 seems to adopt a similar conformation on all promoters it binds on. This rule out the possibility that p50 somehow relays promoter identity onto other transcription factor, like IκBζ, through conformational changes.

Another thing was saw in the NF-κB structures is the different amount of base pair spacing between the two NTDs. IL-6 structure adopts a 5 base pair (bp) spacing from Arg54 of one subunit to the other. This is the same spacing seen in the MHC/p50 structure from Harrison's group. In that structure the promoter is made up GGGGAATCCCC sequence. The four consecutive GC pairs on both ends of the promoter means it can accommodate both spacing preferences, five or six base pair spaces. The fact it adopted the five suggests it's more thermally stable of the two. Now p50 adopted the same spacing on IL-6 promoter with three consecutive GC pairs separated by five AT base pairs. In that arrangement that sequence can accommodate

the base contacts made by the p50's recognition loop and the more thermal dynamically favored 5bp spacing. These reasons could be why it pushed for the 5bp spacing binding conformation.

NGAL promoter caused p50 to adopt a 6bp spacing conformation. This is the same conformation seen in the κB/p50 structure from the Gouri's group. The κB and NGAL promoters do not share any obvious sequencing pattern that would indicate the cause. One thing the two promoters do have in common is that they are both relatively short, only 10bp long. Intuitively speaking, this should have caused the p50 to move its NTDs in closer but the opposite happened they spread further apart pushing His64 of the recognition loop off of the promoter. In the NGAL structure the His64 is hydrogen bonding with the neighboring DNA stacked right on top of the bound DNA. In the κB structure His64 is just floating in space. Its unclear what caused this but one possibility is crystal packing. Closer examination of the NTDs in the crystal structures showed they all make significant contacts with their neighboring molecules. These contacts could have squeezed or pried the NTDs into the conformation we see. One way to test this theory is to see if this is something also happens in solutions. Froster Resonance Energy Transfer (FRET) technique can be use in this situation. Labeling two ends of DNA probe with fluorophore and one on each of the NTD would tell us if they get close or not.

To see if these two different spacing pattern has any effect on binding affinity we measured their KDs with SPR. The measurements showed they are very close, all within the nM binding affinity range (Table III.6). The 5bp spacing promoters showed

a 4 to 5 fold stronger bound than the 6bp spacing promoters. However, I don't know how trustworthy these differences are since they are really small and the measurements were not taken during the same experiment. Minute changes in temperature and buffer condition could have easily contributed to these differences. Additional testing will be needed in the future to confirm its validity.

4.2 The IκBζ Structure

The IκBζ structure yield a number of novel structures that never been seen in other IκB structures. The three that stood out the most are the capping helix, the elongated AR4 region and the p50 NLS interface. As for the capping helix it's difficult to say if this structure is unique to IκBζ or present in other IκB proteins as well. Argument can be made for both cases. The reason none of the other structures contained this helix was because the constructs they used ended at the beginning of AR1. Crystallographers tend to do that since that's must likely way of making rigid domain without any disordered peptide that could get in the way of crystallization. In our case the region was left on by pure chance and it paid off. What this suggests if the other structures had done the same the capping helix could have been in those structures as well. One of the things we did to explore this idea was using computational software to see if the peptide sequences in those structures could form a helix. The particular software we used was an open source web based program called

Scratch Protein Predictor. As a positive control we first put in the peptide sequence of the observed capping helix from the IκBζ structure. The program predicted an α-helical structure with three complete turns (Fig IV.1B). This is relatively close to the actual structure of α-helical structure of four complete turns (Fig IV. 1A). With reasonable confidence in the program we tried it on the peptide sequences of five other IκB proteins: BCL-3, IκBα, IκBβ, IκBNS and IκBε. All but IκBNS showed random coil structure. The peptide sequence from the IκBNS showed an α-helical structure of two and a half turns (Fig IV. 1C). It's interesting that the only other IκB protein predicted to have a capping structure is IκBNS, a nuclear IκB protein that have been shown to preferentially bind to p50 and down regulates the activation of three pro-inflammatory cytokines, among them is IL-6. This is interesting because this is almost exactly the opposite of what IκBζ does, in particular up regulation of IL-6 through p50. Furthermore, our research has shown the removal of the capping helix disrupts the IκBζ's ability to bind to p50. Its plausible that IκBNS requires the helix for its ability to bind to p50 as well.

The second unique feature seen in our IκBζ structure is its elongated AR4 structure. It's long been known that IκBζ has an exceptionally long peptide sequence right in the AR4 region (Fig I.10). During the early days of our crystallization consideration were made to remove this segment of the AR. This consideration was brought up by an exceptional long peptide in the IκBβ AR3 structure. That peptide was disordered in that crystal structure. Concerned that maybe the case for IκBζ as well and it might hinder it from being crystallized. In the end we decided to try our

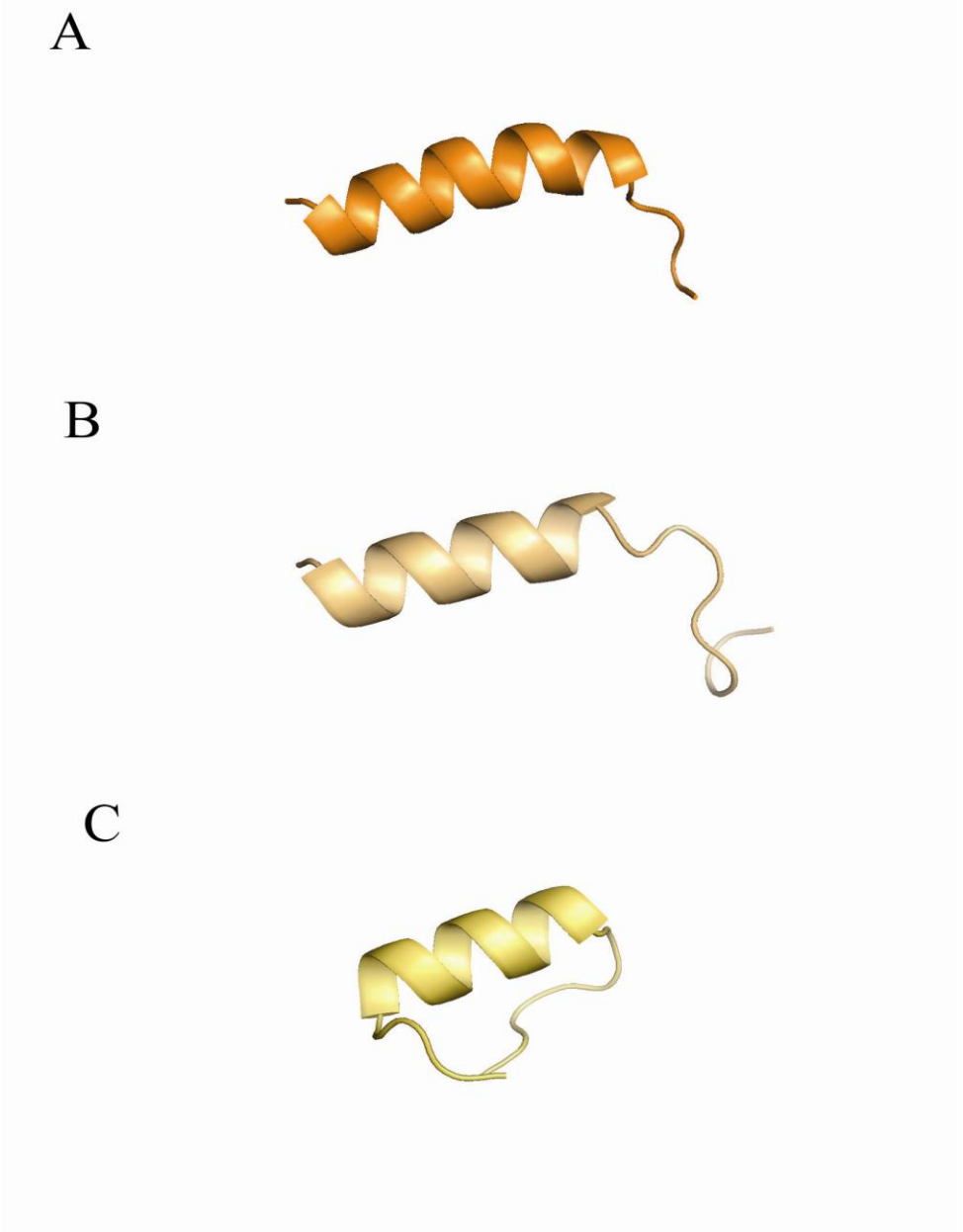

Figure IV.1 A. The actual capping helix on top of AR1 of IkBζ. B. The same peptide but predicted by Scratch Protein Predictor. C. The predicted structure of the capping helix in IκBNS.

luck by keeping it and it paid off. Unlike in IκBβ structure this peptide is ordered and self supported. It doesn't make any significant contact with any part of p50 or parts of IκBζ. It appears to be rigid purely based on its α-helical structure independent of outside support. That is also what makes its function harder to predict. It's unlikely to play role in binding specificity since it doesn't really touch p50. Our biochemical also proved the majority of binding specificity is carried by the NLS region of p50 and not by the DD region (Fig III.26). If its function is not easily seen in the crystal structure maybe because it serves a purpose in regulating the dynamic changes of the protein. Our biochemical results showed IκBζ stability can be easily disturbed by the removal of the capping helix (Fig III.22). This may also imply that replacement of the helix could restore its stability. If this is the case then this intermediate phases of order and disorder could be a mean of regulatory mechanism. It is in these dynamic changes that the elongate AR4 could play a role. The stable helical structure could serve as a "nucleus" where rest of the ARs could gel around. An experimental design that can test this theory is to remove this region from the protein and compare its thermal denaturation CD spectra to that of the wild type. If the theory holds up the mutant should have a lowered melting temperature. What would be even better if IκBζ could be refolded simply with the temperature lowered back down. It might be necessary to play around with the temperature sitting as to find the right temperature where the denaturation process is just beginning while not causing any irreparable damage. If that can be accomplished then the mutant IκBζ should have harder time of folding

itself back. That could either be delayed refolding process or cannot refolded at all. However, unaffected thermal denaturation profile would prove the theory wrong.

Another possible function the elongated AR4 structure could serve is a scaffolding for other transcriptional cofactors to bind. A cell based pull-down assay could verify this theory. Nuclear extract of the LPS induced cells can be incubated with GST tagged wild-type IκBζ or AR4 truncated mutant. It's interaction profile can analysis by SDS PAGE gel and the identity of the bound proteins can be identified by MS. If this theory is correct the mutant should pull down fewer bound proteins than the wild-type. Its relevance can then be tested by a transcription based assay.

Besides IκBζ, IκBNS also has an exceptional long AR4 compared to that of other IκBs (Fig I.10). Once again we used Scratch Protein Predictor to see what possible structure it may forms. As a positive control Scratch successfully predicted the α–helical structure in AR4 based on the amino acid sequence (Figure IV 2B). With the amino acid sequence from IκBNS the program predicted a helical structure similar to that of IκBζ (Figure IV. 2C). It's interesting that one of the helices is longer than the other one. This leaves the two end points on uneven plains which is difficult to imagine how it can be attached to the AR4 of IκBNS without drastic bending of the longer helix. Another explanation that may reconcile this is that prediction is not completely right. I think the most that can be taken from the prediction is the structure is likely to be helical.

The third unique feature in the new IκBζ structure it's interface with the NLS region of p50. From it we able to show its necessity for binding to p50 and its

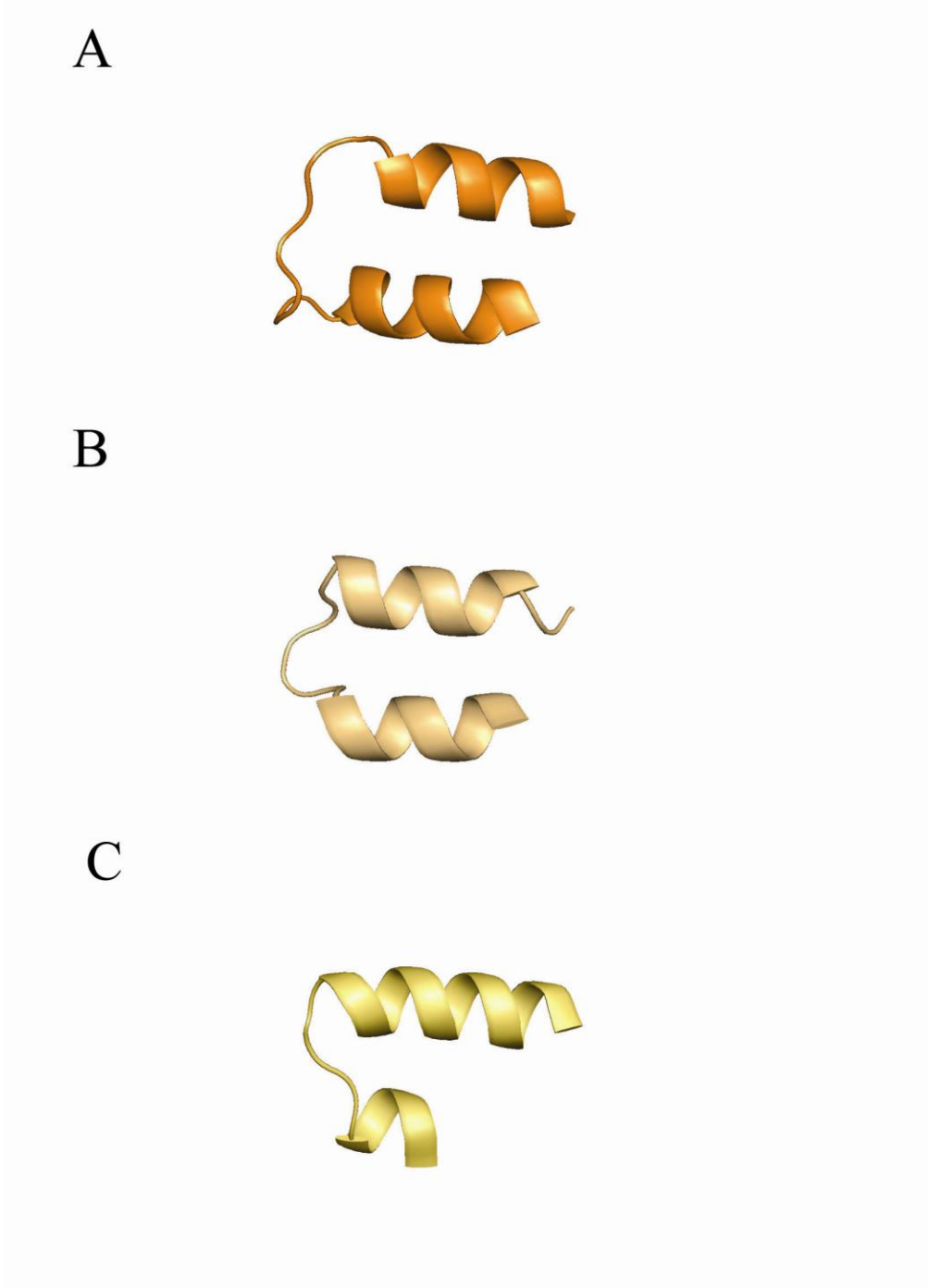

Figure IV.2 A. The actual structure of AR4 structure on IkBζ seen in the crystal structure B. The predicted structure of same region by Scratch Protein Predictor. C. The predicted structure of AR4 region in IκBNS.

majority role it plays in binding specificity. Now that we know these things the next question to consider is what are their implications on other NF-κB/IκB protein interactions? In particular, both BCL-3 and IκBNS have been reported to interact with p50. Are their interactions and recognition also NLS dependent? These questions can easily be address by the same experiment we used for IκBζ and p50 interaction. And if that were the cause that would imply an equilibrium based competitive binding mechanism among p50 and the three nuclear IκB proteins. If this were the case, that would make this area undesirable as a target for drug design. The reason being it's very difficult to target one transcription factor and not affect the other two when they use the same mechanism. One thing we can do is blocking the interaction from the IκBζ side. What I mean by that is to make a non-active version of IκBζ rather than to make an analogy of the NLS peptide. The former idea would only compete away the active IκBζ while leaving BCL-3 and IκBNS alone. The NLS peptide analog would disrupt everything that interact with p50.

4.3 Transcriptional Regulation and IκBζ

In the result section we have demonstrated in the formation of IκBζ/p50/DNA ternary complex on six different promoter sites. These complexes seem to be stable and long lasting. This raise the question if this is how IκBζ activate transcription? Is the formation of this stable ternary complex essential for the activation of the gene

under its regulation? If so this is all it need? This is enough to recruit the general transcription factor to the pre-initiation complex and activate transcription?

One way to assess if the formation of this ternary complex is required for activation is by disrupting its formation. The disruption can be introduced at either between the DNA and p50 or IκBζ and p50. Its effect on transcription can be detected by reporter assay like a luciferase assay with an IL-6 promoter. To disrupt the interaction between p50 and DNA different promoter sequences can be introduced. We actually have a list of them with the affinity already recorded. If the formation of ternary complex is required the promoter with the lower binding affinity should have lower activation. A direct correlation between the different binding affinities and degrees of activation would serve as positive proof. To disrupt the interaction between p50 and IκBζ could be done with NLS peptide analog. A dose dependent decrease of activation would show the importance of ternary complex to activation.

Another phenomenon we observed from the SPR data is that the binding of IκBζ p50 did not alter its natural disassociation at all. This is peculiar since our complied structure of IκBζ on DNA shows it should made DNA contact. This is so it should have some effect. If it doesn't interact with DNA in anyway the physical hindrance should increase p50's disassociation rate. However, if IκBζ interacts with the DNA with some affinity it should decreases its rate of disassociation. No change means it doesn't interact in anyway at all but how can this be? One possibility is the contact bind the DNA just enough to be out of the way while not compromising the binding affinity between the p50 and the DNA. One addition possibility is that IκBζ is

shifted “upward” away from the DNA without causing a change in the binding affinity. One way to test this theory is by using the Froster Resonance Energy Transfer (FRET) method by placing two fluorophores at strategic position to monitor the movement.

Needless to say we still have many unanswered question about IκBζ role and mechanism in gene regulation. To fully understand its transcriptional role would likely to take decades to come. However, it is our hope this is newly solved crystal structure along with its biochemical data included in this dissertation could help point future researchers in the right direction.

References

Adams, P.D., Afonine, P.V., Bunkóczi, G., Chen, V.B., Davis, I.W., Echols, N., Headd, J.J., Hung, L.-W., Kapral, G.J., Grosse-Kunstleve, R.W., et al. (2010). PHENIX: a comprehensive Python-based system for macromolecular structure solution. Acta Crystallogr. D Biol. Crystallogr. *66*, 213–221.

Alkalay, I., Yaron, A., Hatzubai, A., Orian, A., Ciechanover, A., and Ben-Neriah, Y. (1995). Stimulation-dependent I kappa B alpha phosphorylation marks the NF-kappa B inhibitor for degradation via the ubiquitin-proteasome pathway. PNAS *92*, 10599–10603.

Avruch, J., Khokhlatchev, A., Kyriakis, J.M., Luo, Z., Tzivion, G., Vavvas, D., and Zhang, X.F. (2001). Ras activation of the Raf kinase: tyrosine kinase recruitment of the MAP kinase cascade. Recent Prog. Horm. Res. *56*, 127–155.

Baeuerle, P.A. (1991). The inducible transcription activator NF-κB: regulation by distinct protein subunits. Biochimica et Biophysica Acta (BBA) - Reviews on Cancer *1072*, 63–80.

Baeuerle, P.A., and Baltimore, D. (1988a). Activation of DNA-binding activity in an apparently cytoplasmic precursor of the NF-κB transcription factor. Cell *53*, 211–217.

Baeuerle, P.A., and Baltimore, D. (1988b). Activation of DNA-binding activity in an apparently cytoplasmic precursor of the NF-κB transcription factor. Cell *53*, 211–217.

Baeuerle, P.A., and Baltimore, D. (1988c). I kappa B: a specific inhibitor of the NF-kappa B transcription factor. Science *242*, 540–546.

Baeuerle, P.A., and Baltimore, D. (1989). A 65-kappaD subunit of active NF-kappaB is required for inhibition of NF-kappaB by I kappaB. Genes Dev. *3*, 1689–1698.

Barboric, M., Nissen, R.M., Kanazawa, S., Jabrane-Ferrat, N., and Peterlin, B.M. (2001). NF-kappaB binds P-TEFb to stimulate transcriptional elongation by RNA polymerase II. Mol. Cell *8*, 327–337.

Beg, A.A., and Baltimore, D. (1996). An essential role for NF-kappaB in preventing TNF-alpha-induced cell death. Science *274*, 782–784.

Beg, A.A., Ruben, S.M., Scheinman, R.I., Haskill, S., Rosen, C.A., and Baldwin, A.S., Jr (1992). I kappa B interacts with the nuclear localization sequences of the subunits of NF-kappa B: a mechanism for cytoplasmic retention. Genes Dev. *6*, 1899–1913.

Bergqvist, S., Croy, C.H., Kjaergaard, M., Huxford, T., Ghosh, G., and Komives, E.A. (2006). Thermodynamics Reveal that Helix Four in the NLS of NF-κB p65 Anchors IκBα, Forming a Very Stable Complex. Journal of Molecular Biology *360*, 421–434.

Bours, V., Villalobos, J., Burd, P.R., Kelly, K., and Siebenlist, U. (1990). Cloning of a mitogen-inducible gene encoding a κB DNA-binding protein with homology to the rel oncogene and to cell-cycle motifs. , Published Online: 01 November 1990; | Doi:10.1038/348076a0 *348*, 76–80.

Bours, V., Burd, P.R., Brown, K., Villalobos, J., Park, S., Ryseck, R.P., Bravo, R., Kelly, K., and Siebenlist, U. (1992). A novel mitogen-inducible gene product related to p50/p105-NF-kappa B participates in transactivation through a kappa B site. Mol. Cell. Biol. *12*, 685–695.

Braun, A.P., and Schulman, H. (1995). The Multifunctional Calcium/Calmodulin-Dependent Protein Kinase: From Form to Function. Annual Review of Physiology *57*, 417–445.

Brown, K., Gerstberger, S., Carlson, L., Franzoso, G., and Siebenlist, U. (1995). Control of I kappa B-alpha proteolysis by site-specific, signal-induced phosphorylation. Science *267*, 1485–1488.

Bundy, D.L., and McKeithan, T.W. (1997). Diverse effects of BCL3 phosphorylation on its modulation of NF-kappaB p52 homodimer binding to DNA. J. Biol. Chem. *272*, 33132–33139.

Chen, F.E., Huang, D.B., Chen, Y.Q., and Ghosh, G. (1998a). Crystal structure of p50/p65 heterodimer of transcription factor NF-kappaB bound to DNA. Nature *391*, 410–413.

Chen, V.B., Arendall, W.B., 3rd, Headd, J.J., Keedy, D.A., Immormino, R.M., Kapral, G.J., Murray, L.W., Richardson, J.S., and Richardson, D.C. (2010). MolProbity: all-atom structure validation for macromolecular crystallography. Acta Crystallogr. D Biol. Crystallogr. *66*, 12–21.

Chen, Y.Q., Ghosh, S., and Ghosh, G. (1998b). A novel DNA recognition mode by the NF-kappa B p65 homodimer. Nat. Struct. Biol. *5*, 67–73.

Chen, Y.Q., Sengchanthalangsy, L.L., Hackett, A., and Ghosh, G. (2000). NF-kappaB p65 (RelA) homodimer uses distinct mechanisms to recognize DNA targets. Structure *8*, 419–428.

Chen, Z., Hagler, J., Palombella, V.J., Melandri, F., Scherer, D., Ballard, D., and Maniatis, T. (1995). Signal-induced site-specific phosphorylation targets I kappa B alpha to the ubiquitin-proteasome pathway. Genes Dev. *9*, 1586–1597.

Cheng, C.S., Feldman, K.E., Lee, J., Verma, S., Huang, D.-B., Huynh, K., Chang, M., Ponomarenko, J.V., Sun, S.-C., Benedict, C.A., et al. (2011). The specificity of innate immune responses is enforced by repression of interferon response elements by NF-κB p50. Sci Signal *4*, ra11.

Courtois, G., and Gilmore, T.D. (2006). Mutations in the NF-κB signaling pathway: implications for human disease. Oncogene *25*, 6831–6843.

Cowland, J.B., Muta, T., and Borregaard, N. (2006). IL-1beta-specific up-regulation of neutrophil gelatinase-associated lipocalin is controlled by IkappaB-zeta. J. Immunol. *176*, 5559–5566.

Cramer, P., Larson, C.J., Verdine, G.L., and Müller, C.W. (1997). Structure of the human NF-kappaB p52 homodimer-DNA complex at 2.1 A resolution. EMBO J. *16*, 7078–7090.

Davydov, I.V., Krammer, P.H., and Li-Weber, M. (1995). Nuclear factor-IL6 activates the human IL-4 promoter in T cells. J. Immunol. *155*, 5273–5279.

Dechend, R., Hirano, F., Lehmann, K., Heissmeyer, V., Ansieau, S., Wulczyn, F.G., Scheidereit, C., and Leutz, A. (1999). The Bcl-3 oncoprotein acts as a bridging factor between NF-kappaB/Rel and nuclear co-regulators. Oncogene *18*, 3316–3323.

Van Dijk, M., and Bonvin, A.M.J.J. (2009). 3D-DART: a DNA structure modelling server. Nucleic Acids Res. *37*, W235–239.

Van Dijk, T.B., Baltus, B., Raaijmakers, J.A., Lammers, J.W., Koenderman, L., and de Groot, R.P. (1999). A composite C/EBP binding site is essential for the activity of the promoter of the IL-3/IL-5/granulocyte-macrophage colony-stimulating factor receptor beta c gene. J. Immunol. *163*, 2674–2680.

Emsley, P., and Cowtan, K. (2004). Coot: model-building tools for molecular graphics. Acta Crystallogr. D Biol. Crystallogr. *60*, 2126–2132.

Escalante, C.R., Shen, L., Thanos, D., and Aggarwal, A.K. (2002). Structure of NF-kappaB p50/p65 heterodimer bound to the PRDII DNA element from the interferon-beta promoter. Structure *10*, 383–391.

Eto, A., Muta, T., Yamazaki, S., and Takeshige, K. (2003). Essential roles for NF-kappa B and a Toll/IL-1 receptor domain-specific signal(s) in the induction of I kappa B-zeta. Biochem. Biophys. Res. Commun. *301*, 495–501.

Faraj, H.G., and Hoang-Xuan, T. (2001). Chronic cicatrizing conjunctivitis. Curr Opin Ophthalmol *12*, 250–257.

Fiorini, E., Schmitz, I., Marissen, W.E., Osborn, S.L., Touma, M., Sasada, T., Reche, P.A., Tibaldi, E.V., Hussey, R.E., Kruisbeek, A.M., et al. (2002a). Peptide-Induced Negative Selection of Thymocytes Activates Transcription of an NF-κB Inhibitor. Molecular Cell *9*, 637–648.

Fiorini, E., Schmitz, I., Marissen, W.E., Osborn, S.L., Touma, M., Sasada, T., Reche, P.A., Tibaldi, E.V., Hussey, R.E., Kruisbeek, A.M., et al. (2002b). Peptide-Induced Negative Selection of Thymocytes Activates Transcription of an NF-κB Inhibitor. Molecular Cell *9*, 637–648.

Franzoso, G., Bours, V., Park, S., Tomfta-Yamaguchi, M., Kelly, K., and Siebenlist, U. (1992a). The candidate oncoprotein Bcl-3 is an antagonist of pSO/NF-κB-mediated inhibition. , Published Online: 24 September 1992; | Doi:10.1038/359339a0 *359*, 339–342.

Franzoso, G., Bours, V., Park, S., Tomfta-Yamaguchi, M., Kelly, K., and Siebenlist, U. (1992b). The candidate oncoprotein Bcl-3 is an antagonist of pSO/NF-κB-mediated inhibition. , Published Online: 24 September 1992; | Doi:10.1038/359339a0 *359*, 339–342.

Franzoso, G., Carlson, L., Scharton-Kersten, T., Shores, E.W., Epstein, S., Grinberg, A., Tran, T., Shacter, E., Leonardi, A., Anver, M., et al. (1997a). Critical Roles for the Bcl-3 Oncoprotein in T Cell–Mediated Immunity, Splenic Microarchitecture, and Germinal Center Reactions. Immunity *6*, 479–490.

Franzoso, G., Carlson, L., Xing, L., Poljak, L., Shores, E.W., Brown, K.D., Leonardi, A., Tran, T., Boyce, B.F., and Siebenlist, U. (1997b). Requirement for NF-κB in osteoclast and B-cell development. Genes Dev. *11*, 3482–3496.

Fujita, T., Nolan, G.P., Liou, H.C., Scott, M.L., and Baltimore, D. (1993). The candidate proto-oncogene bcl-3 encodes a transcriptional coactivator that activates through NF-kappa B p50 homodimers. Genes Dev. *7*, 1354–1363.

Ghosh, S., and Baltimore, D. (1990). Activation in vitro of NF-κB. , Published Online: 12 April 1990; | Doi:10.1038/344678a0 *344*, 678–682.

Ghosh, S., and Hayden, M.S. (2008). New regulators of NF-κB in inflammation. Nature Reviews Immunology *8*, 837–848.

Ghosh, G., van Duyne, G., Ghosh, S., and Sigler, P.B. (1995). Structure of NF-kappa B p50 homodimer bound to a kappa B site. Nature *373*, 303–310.

Ghosh, G., Wang, V.Y.-F., Huang, D.-B., and Fusco, A. (2012). NF-κB regulation: lessons from structures. Immunological Reviews *246*, 36–58.

Gilmore, T.D. (2006). Introduction to NF-kappaB: players, pathways, perspectives. Oncogene *25*, 6680–6684.

Goodman, R.H., and Smolik, S. (2000). CBP/p300 in cell growth, transformation, and development. Genes Dev. *14*, 1553–1577.

Greenwel, P., Tanaka, S., Penkov, D., Zhang, W., Olive, M., Moll, J., Vinson, C., Di Liberto, M., and Ramirez, F. (2000). Tumor necrosis factor alpha inhibits type I collagen synthesis through repressive CCAAT/enhancer-binding proteins. Mol. Cell. Biol. *20*, 912–918.

Haruta, H., Kato, A., and Todokoro, K. (2001). Isolation of a novel interleukin-1-inducible nuclear protein bearing ankyrin-repeat motifs. J. Biol. Chem. *276*, 12485–12488.

Haskill, S., Beg, A.A., Tompkins, S.M., Morris, J.S., Yurochko, A.D., Sampson-Johannes, A., Mondal, K., Ralph, P., and Baldwin Jr., A.S. (1991). Characterization of an immediate-early gene induced in adherent monocytes that encodes IκB-like activity. Cell *65*, 1281–1289.

Hatada, E.N., Nieters, A., Wulczyn, F.G., Naumann, M., Meyer, R., Nucifora, G., McKeithan, T.W., and Scheidereit, C. (1992). The ankyrin repeat domains of the NF-kappa B precursor p105 and the protooncogene bcl-3 act as specific inhibitors of NF-kappa B DNA binding. PNAS *89*, 2489–2493.

Hirano, F., Chung, M., Tanaka, H., Maruyama, N., Makino, I., Moore, D.D., and Scheidereit, C. (1998). Alternative Splicing Variants of IκBβ Establish Differential NF-κB Signal Responsiveness in Human Cells. Mol. Cell. Biol. *18*, 2596–2607.

Hirotani, T., Lee, P.Y., Kuwata, H., Yamamoto, M., Matsumoto, M., Kawase, I., Akira, S., and Takeda, K. (2005). The Nuclear IκB Protein IκBNS Selectively Inhibits Lipopolysaccharide-Induced IL-6 Production in Macrophages of the Colonic Lamina Propria. J Immunol *174*, 3650–3657.

Hoffmann, A., Levchenko, A., Scott, M.L., and Baltimore, D. (2002). The IκB-NF-κB Signaling Module: Temporal Control and Selective Gene Activation. Science *298*, 1241–1245.

Hoffmann, A., Natoli, G., and Ghosh, G. (2006). Transcriptional regulation via the NF-kappaB signaling module. Oncogene *25*, 6706–6716.

Huang, D.-B., Chen, Y.-Q., Ruetsche, M., Phelps, C.B., and Ghosh, G. (2001). X-Ray Crystal Structure of Proto-Oncogene Product c-Rel Bound to the CD28 Response Element of IL-2. Structure *9*, 669–678.

Huxford, T., Huang, D.B., Malek, S., and Ghosh, G. (1998). The crystal structure of the IkappaBalpha/NF-kappaB complex reveals mechanisms of NF-kappaB inactivation. Cell *95*, 759–770.

Kanarek, N., London, N., Schueler-Furman, O., and Ben-Neriah, Y. (2010). Ubiquitination and Degradation of the Inhibitors of NF-κB. Cold Spring Harb Perspect Biol *2*.

Kannan, Y., Yu, J., Raices, R.M., Seshadri, S., Wei, M., Caligiuri, M.A., and Wewers, M.D. (2011). IκBζ augments IL-12- and IL-18-mediated IFN-γ production in human NK cells. Blood *117*, 2855–2863.

Kawakami, K., Scheidereit, C., and Roeder, R.G. (1988). Identification and purification of a human immunoglobulin-enhancer-binding protein (NF-kappa B) that activates transcription from a human immunodeficiency virus type 1 promoter in vitro. PNAS *85*, 4700–4704.

Keutgens, A., Shostak, K., Close, P., Zhang, X., Hennuy, B., Aussems, M., Chapelle, J.-P., Viatour, P., Gothot, A., Fillet, M., et al. (2010). The Repressing Function of the Oncoprotein BCL-3 Requires CtBP, while Its Polyubiquitination and Degradation Involve the E3 Ligase TBLR1. Mol. Cell. Biol. *30*, 4006–4021.

Kitamura, H., Kanehira, K., Okita, K., Morimatsu, M., and Saito, M. (2000). MAIL, a novel nuclear IκB protein that potentiates LPS-induced IL-6 production. FEBS Letters *485*, 53–56.

Klement, J.F., Rice, N.R., Car, B.D., Abbondanzo, S.J., Powers, G.D., Bhatt, P.H., Chen, C.H., Rosen, C.A., and Stewart, C.L. (1996). IkappaBalpha deficiency results in a sustained NF-kappaB response and severe widespread dermatitis in mice. Mol. Cell. Biol. *16*, 2341–2349.

Kornberg, R.D. (2007). The molecular basis of eukaryotic transcription. Proc. Natl. Acad. Sci. U.S.A. *104*, 12955–12961.

Kracht, M., and Saklatvala, J. (2002). Transcriptional and post-transcriptional control of gene expression in inflammation. Cytokine *20*, 91–106.

Kreisel, D., Sugimoto, S., Tietjens, J., Zhu, J., Yamamoto, S., Krupnick, A.S., Carmody, R.J., and Gelman, A.E. (2011). Bcl3 prevents acute inflammatory lung injury in mice by restraining emergency granulopoiesis. Journal of Clinical Investigation *121*, 265–276.

Kunsch, C., Ruben, S.M., and Rosen, C.A. (1992a). Selection of optimal kappa B/Rel DNA-binding motifs: interaction of both subunits of NF-kappa B with DNA is required for transcriptional activation. Mol. Cell. Biol. *12*, 4412–4421.

Kunsch, C., Ruben, S.M., and Rosen, C.A. (1992b). Selection of optimal kappa B/Rel DNA-binding motifs: interaction of both subunits of NF-kappa B with DNA is required for transcriptional activation. Mol. Cell. Biol. *12*, 4412–4421.

Kuwata, H., Matsumoto, M., Atarashi, K., Morishita, H., Hirotani, T., Koga, R., and Takeda, K. (2006). IκBNS Inhibits Induction of a Subset of Toll-like Receptor-Dependent Genes and Limits Inflammation. Immunity *24*, 41–51.

Lee, J.H., Li, Y.C., Doerre, S., Sista, P., Ballard, D.W., Greene, W.C., and Franza, B.R., Jr (1991). A member of the set of kappa B binding proteins, HIVEN86A, is a product of the human c-rel proto-oncogene. Oncogene *6*, 665–667.

Li, Q., and Verma, I.M. (2002). NF-kappaB regulation in the immune system. Nat. Rev. Immunol. *2*, 725–734.

Li, Z., and Nabel, G.J. (1997). A new member of the I kappaB protein family, I kappaB epsilon, inhibits RelA (p65)-mediated NF-kappaB transcription. Mol. Cell. Biol. *17*, 6184–6190.

Malek, S., Chen, Y., Huxford, T., and Ghosh, G. (2001). IκBβ, but Not IκBα, Functions as a Classical Cytoplasmic Inhibitor of NF-κB Dimers by Masking Both NF-κB Nuclear Localization Sequences in Resting Cells. J. Biol. Chem. *276*, 45225–45235.

Mankan, A.K., Lawless, M.W., Gray, S.G., Kelleher, D., and McManus, R. (2009). NF-kappaB regulation: the nuclear response. J. Cell. Mol. Med. *13*, 631–643.

Matthews, B.W. (1968). Solvent content of protein crystals. J. Mol. Biol. *33*, 491–497.

McCoy, A.J., Grosse-Kunstleve, R.W., Adams, P.D., Winn, M.D., Storoni, L.C., and Read, R.J. (2007). Phaser crystallographic software. J Appl Crystallogr *40*, 658–674.

Mémet, S., Laouini, D., Epinat, J.-C., Whiteside, S.T., Goudeau, B., Philpott, D., Kayal, S., Sansonetti, P.J., Berche, P., Kanellopoulos, J., et al. (1999). IκBε-Deficient Mice: Reduction of One T Cell Precursor Subspecies and Enhanced Ig Isotype Switching and Cytokine Synthesis. J Immunol *163*, 5994–6005.

Mercurio, F., Zhu, H., Murray, B.W., Shevchenko, A., Bennett, B.L., Li, J. wu, Young, D.B., Barbosa, M., Mann, M., Manning, A., et al. (1997). IKK-1 and IKK-2: Cytokine-Activated IκB Kinases Essential for NF-κB Activation. Science *278*, 860–866.

Michel, F., Soler-Lopez, M., Petosa, C., Cramer, P., Siebenlist, U., and Müller, C.W. (2001). Crystal structure of the ankyrin repeat domain of Bcl-3: a unique member of the IkappaB protein family. EMBO J. *20*, 6180–6190.

Motoyama, M., Yamazaki, S., Eto-Kimura, A., Takeshige, K., and Muta, T. (2005). Positive and negative regulation of nuclear factor-kappaB-mediated transcription by IkappaB-zeta, an inducible nuclear protein. J. Biol. Chem. *280*, 7444–7451.

Müller, C.W., and Harrison, S.C. (1995). The structure of the NF-kappa B p50:DNA-complex: a starting point for analyzing the Rel family. FEBS Lett. *369*, 113–117.

Müller, C.W., Rey, F.A., Sodeoka, M., Verdine, G.L., and Harrison, S.C. (1995). Structure of the NF-kappa B p50 homodimer bound to DNA. Nature *373*, 311–317.

Murshudov, G.N., Vagin, A.A., and Dodson, E.J. (1997). Refinement of macromolecular structures by the maximum-likelihood method. Acta Crystallogr. D Biol. Crystallogr. *53*, 240–255.

Natsuka, S., Akira, S., Nishio, Y., Hashimoto, S., Sugita, T., Isshiki, H., and Kishimoto, T. (1992). Macrophage differentiation-specific expression of NF-IL6, a transcription factor for interleukin-6. Blood *79*, 460–466.

Naumann, M., and Scheidereit, C. (1994). Activation of NF-kappa B in vivo is regulated by multiple phosphorylations. EMBO J *13*, 4597–4607.

Nolan, G.P., Ghosh, S., Liou, H.-C., Tempst, P., and Baltimore, D. (1991). DNA binding and IκB inhibition of the cloned p65 subunit of NF-κB, a rel-related polypeptide. Cell *64*, 961–969.

Nolan, G.P., Fujita, T., Bhatia, K., Huppi, C., Liou, H.C., Scott, M.L., and Baltimore, D. (1993). The bcl-3 proto-oncogene encodes a nuclear I kappa B-like molecule that preferentially interacts with NF-kappa B p50 and p52 in a phosphorylation-dependent manner. Mol. Cell. Biol. *13*, 3557–3566.

Ohno, H., Takimoto, G., and McKeithan, T.W. (1990). The candidate proto-oncogene bcl-3 is related to genes implicated in cell lineage determination and cell cycle control. Cell *60*, 991–997.

Otwinowski, Z., and Minor, W. (1997). [20] Processing of X-ray diffraction data collected in oscillation mode. In Methods in Enzymology, J. Charles W. Carter, ed. (Academic Press), pp. 307–326.

Palombella, V.J., Rando, O.J., Goldberg, A.L., and Maniatis, T. (1994). The ubiquitinproteasome pathway is required for processing the NF-κB1 precursor protein and the activation of NF-κB. Cell *78*, 773–785.

Pène, F., Paun, A., Sønder, S.U., Rikhi, N., Wang, H., Claudio, E., and Siebenlist, U. (2011). The IκB Family Member Bcl-3 Coordinates the Pulmonary Defense against Klebsiella pneumoniae Infection. J Immunol *186*, 2412–2421.

Purves, D. (2008). Neuroscience, Fourth Edition (Sinauer Associates, Inc.).

Rao, P., Hayden, M.S., Long, M., Scott, M.L., West, A.P., Zhang, D., Oeckinghaus, A., Lynch, C., Hoffmann, A., Baltimore, D., et al. (2010). IκBβ acts to inhibit and activate gene expression during the inflammatory response. Nature *466*, 1115–1119.

Roeder, R.G. (1996). The role of general initiation factors in transcription by RNA polymerase II. Trends in Biochemical Sciences *21*, 327–335.

Rothwarf, D.M., Zandi, E., Natoli, G., and Karin, M. (1998). IKK-γ is an essential regulatory subunit of the IκB kinase complex. Nature *395*, 297–300.

Ryseck, R.P., Novotny, J., and Bravo, R. (1995). Characterization of elements determining the dimerization properties of RelB and p50. Mol. Cell. Biol. *15*, 3100–3109.

Schmitz, M.L., and Baeuerle, P.A. (1991). The p65 subunit is responsible for the strong transcription activating potential of NF-kappa B. EMBO J *10*, 3805–3817.

Schwarz, E.M., Krimpenfort, P., Berns, A., and Verma, I.M. (1997). Immunological defects in mice with a targeted disruption in Bcl-3. Genes Dev. *11*, 187–197.

Sen, R., and Baltimore, D. (1986a). Multiple nuclear factors interact with the immunoglobulin enhancer sequences. Cell *46*, 705–716.

Sen, R., and Baltimore, D. (1986b). Inducibility of κ immunoglobulin enhancer-binding protein NF-κB by a posttranslational mechanism. Cell *47*, 921–928.

Sen, R., and Baltimore, D. (1986c). Multiple nuclear factors interact with the immunoglobulin enhancer sequences. Cell *46*, 705–716.

Shapiro, V.S., Truitt, K.E., Imboden, J.B., and Weiss, A. (1997). CD28 mediates transcriptional upregulation of the interleukin-2 (IL-2) promoter through a composite element containing the CD28RE and NF-IL-2B AP-1 sites. Mol. Cell. Biol. *17*, 4051–4058.

Shiina, T., Konno, A., Oonuma, T., Kitamura, H., Imaoka, K., Takeda, N., Todokoro, K., and Morimatsu, M. (2004). Targeted disruption of MAIL, a nuclear IkappaB protein, leads to severe atopic dermatitis-like disease. J. Biol. Chem. *279*, 55493–55498.

Simeonidis, S., Liang, S., Chen, G., and Thanos, D. (1997). Cloning and functional characterization of mouse IκBε. PNAS *94*, 14372–14377.

Terwilliger, T.C., Grosse-Kunstleve, R.W., Afonine, P.V., Moriarty, N.W., Zwart, P.H., Hung, L.W., Read, R.J., and Adams, P.D. (2008). Iterative model building, structure refinement and density modification with the PHENIX AutoBuild wizard. Acta Crystallogr. D Biol. Crystallogr. *64*, 61–69.

Thompson, J.E., Phillips, R.J., Erdjument-Bromage, H., Tempst, P., and Ghosh, S. (1995). IκB-β regulates the persistent response in a biphasic activation of NF-κB. Cell *80*, 573–582.

Tran, K., Merika, M., and Thanos, D. (1997a). Distinct functional properties of IkappaB alpha and IkappaB beta. Mol. Cell. Biol. *17*, 5386–5399.

Tran, K., Merika, M., and Thanos, D. (1997b). Distinct functional properties of IkappaB alpha and IkappaB beta. Mol. Cell. Biol. *17*, 5386–5399.

Trinh, D.V., Zhu, N., Farhang, G., Kim, B.J., and Huxford, T. (2008). The Nuclear IκB Protein IκBζ Specifically Binds NF-κB p50 Homodimers and Forms a Ternary Complex on κB DNA. Journal of Molecular Biology *379*, 122–135.

Ueta, M., Hamuro, J., Yamamoto, M., Kaseda, K., Akira, S., and Kinoshita, S. (2005). Spontaneous Ocular Surface Inflammation and Goblet Cell Disappearance in IκBζ Gene-Disrupted Mice. IOVS *46*, 579–588.

Wang, J., Wang, X., Hussain, S., Zheng, Y., Sanjabi, S., Ouaaz, F., and Beg, A.A. (2007). Distinct roles of different NF-kappa B subunits in regulating inflammatory and T cell stimulatory gene expression in dendritic cells. J. Immunol. *178*, 6777–6788.

Watanabe, N., Iwamura, T., Shinoda, T., and Fujita, T. (1997). Regulation of NFKB1 proteins by the candidate oncoprotein BCL-3: generation of NF-κB homodimers from the cytoplasmic pool of p50–p105 and nuclear translocation. The EMBO Journal *16*, 3609–3620.

Whiteside, S.T., Epinat, J.-C., Rice, N.R., and Israël, A. (1997). I kappa B epsilon, a novel member of the IκB family, controls RelA and cRel NF-κB activity. The EMBO Journal *16*, 1413–1426.

Winn, M.D., Ballard, C.C., Cowtan, K.D., Dodson, E.J., Emsley, P., Evans, P.R., Keegan, R.M., Krissinel, E.B., Leslie, A.G.W., McCoy, A., et al. (2011). Overview of the CCP4 suite and current developments. Acta Crystallogr. D Biol. Crystallogr. *67*, 235–242.

Wulczyn, F.G., Naumann, M., and Scheidereit, C. (1992). Candidate proto-oncogene bcl-3 encodes a subunit-specific inhibitor of transcription factor NF-κB. , Published Online: 13 August 1992; | Doi:10.1038/358597a0 *358*, 597–599.

Yamamoto, M., and Takeda, K. (2008). Role of nuclear IkappaB proteins in the regulation of host immune responses. J. Infect. Chemother. *14*, 265–269.

Yamamoto, M., Yamazaki, S., Uematsu, S., Sato, S., Hemmi, H., Hoshino, K., Kaisho, T., Kuwata, H., Takeuchi, O., Takeshige, K., et al. (2004). Regulation of Toll/IL-1-receptor-mediated gene expression by the inducible nuclear protein IkappaBzeta. Nature *430*, 218–222.

Yamaoka, S., Courtois, G., Bessia, C., Whiteside, S.T., Weil, R., Agou, F., Kirk, H.E., Kay, R.J., and Israël, A. (1998). Complementation Cloning of NEMO, a Component of the IκB Kinase Complex Essential for NF-κB Activation. Cell *93*, 1231–1240.

Yamauchi, T. (2005). Neuronal Ca^{2+}/Calmodulin-Dependent Protein Kinase II—Discovery, Progress in a Quarter of a Century, and Perspective: Implication for Learning and Memory. Biological and Pharmaceutical Bulletin *28*, 1342–1354.

Yamauchi, S., Ito, H., and Miyajima, A. (2010a). IκBη, a nuclear IκB protein, positively regulates the NF-κB–mediated expression of proinflammatory cytokines. PNAS *107*, 11924–11929.

Yamauchi, S., Ito, H., and Miyajima, A. (2010b). IκBη, a nuclear IκB protein, positively regulates the NF-κB–mediated expression of proinflammatory cytokines. PNAS *107*, 11924–11929.

Yamazaki, S., Muta, T., and Takeshige, K. (2001). A novel IkappaB protein, IkappaB-zeta, induced by proinflammatory stimuli, negatively regulates nuclear factor-kappaB in the nuclei. J. Biol. Chem. *276*, 27657–27662.

Yamazaki, S., Muta, T., Matsuo, S., and Takeshige, K. (2005). Stimulus-specific induction of a novel nuclear factor-kappaB regulator, IkappaB-zeta, via Toll/Interleukin-1 receptor is mediated by mRNA stabilization. J. Biol. Chem. *280*, 1678–1687.

Yamazaki, S., Matsuo, S., Muta, T., Yamamoto, M., Akira, S., and Takeshige, K. (2008). Gene-specific requirement of a nuclear protein, IkappaB-zeta, for promoter association of inflammatory transcription regulators. J. Biol. Chem. *283*, 32404–32411.

Yan, R., Qureshi, S., Zhong, Z., Wen, Z., and Darnell, J.E., Jr (1995). The genomic structure of the STAT genes: multiple exons in coincident sites in Stat1 and Stat2. Nucleic Acids Res. *23*, 459–463.

Zabel, U., and Baeuerle, P.A. (1990). Purified human IκB can rapidly dissociate the complex of the NF-κB transcription factor with its cognate DNA. Cell *61*, 255–265.

Zandi, E., Rothwarf, D.M., Delhase, M., Hayakawa, M., and Karin, M. (1997). The IκB Kinase Complex (IKK) Contains Two Kinase Subunits, IKKα and IKKβ, Necessary for IκB Phosphorylation and NF-κB Activation. Cell *91*, 243–252.

Zhang, X., Wang, H., Claudio, E., Brown, K., and Siebenlist, U. (2007). A ROLE FOR BCL-3 IN CONTROL OF CENTRAL IMMUNOLOGIC TOLERANCE. Immunity *27*, 438–452.

Zheng, C., Yin, Q., and Wu, H. (2011). Structural studies of NF-κB signaling. Cell Research *21*, 183–195.

Zhong, H., Voll, R.E., and Ghosh, S. (1998). Phosphorylation of NF-kappa B p65 by PKA stimulates transcriptional activity by promoting a novel bivalent interaction with the coactivator CBP/p300. Mol. Cell *1*, 661–671.

Zhong, H., May, M.J., Jimi, E., and Ghosh, S. (2002a). The phosphorylation status of nuclear NF-kappa B determines its association with CBP/p300 or HDAC-1. Mol. Cell *9*, 625–636.

Zhong, H., May, M.J., Jimi, E., and Ghosh, S. (2002b). The phosphorylation status of nuclear NF-kappa B determines its association with CBP/p300 or HDAC-1. Mol. Cell *9*, 625–636.